THE ROLE OF NCK IN BREAST CARCINOMA CELL INVASION AND METASTASIS

A Dissertation

by

DAVID CHRISTOPHER MORRIS

Submitted to the Office of Graduate and Professional Studies of
Texas A&M University
in partial fulfillment of the requirements for the degree of

DOCTOR OF PHILOSOPHY

Chair of Committee,	Gonzalo Rivera
Committee Members,	Robert Burghardt
	Weston Porter
	Ivan Ivanov
Head of Department,	Roger Smith

August 2015

Major Subject: Veterinary Microbiology

ABSTRACT

The high incidence of invasive breast carcinomas, which accounts for about 90% of all breast cancer-related deaths, underscores the need for new and more effective therapeutic approaches to block the development of the malignant phenotype. Changes in the cytoskeletal organization of tumor cells and the physiochemical properties of the extracellular matrix (ECM) are key drivers of invasion and metastasis. Aberrant activation of phosphotyrosine signaling results in the formation of actin-based structures, called invadopodia, known to play an important role in ECM remodeling. We determined the role of Nck, adaptor proteins that link tyrosine phosphorylation with actin dynamics, in mammary carcinoma tumorigenesis and metastatic spread. We hypothesized that Nck-dependent actin remodeling promotes breast cancer invasion and metastasis by promoting the membrane accumulation/activity of MMP14, a key matrix-remodeling protease. To test this hypothesis, we used the highly metastatic MDA-MB-231 breast cancer cell line and a combination of three-dimensional (3D) tissue culture, optical imaging and a xenograft nude mouse model. To determine how Nck promotes invasion and metastasis by altering actin dynamics and membrane localization of MMP14 through regulation of Cdc42 activity we used gelatin degradation in conjunction with immunofluorescence microscopy, fluorescence recovery after photobleaching, total internal fluorescence microscopy and Förster resonance energy transfer.

The results show, for the first time, a requirement for Nck in breast carcinoma growth and invasion in 3D cultures and metastasis *in vivo*. Nck facilitates invasiveness

by promoting invadopodia biogenesis and focalized matrix degradation. Loss of Nck results in decreased MMP14 accumulation at the ventral surface of invasive cells and altered actin dynamics at invadopodia. Loss of Nck also disrupted the localization of active Cdc42, a key regulator of trafficking and polarity. Our results support a model where Nck specifies patterns of Cdc42 activation and the targeted accumulation of MMP14 to facilitate the formation and maturation of invadopodia by integrating extracellular signals that modulate cytoskeletal dynamics.

DEDICATION

To the memory of Patricia Ann Morris

ACKNOWLEDGEMENTS

I would like to thank my committee chair, Dr. Rivera, and my committee members, Dr. Burghardt, Dr. Porter, and Dr. Ivanov, for their guidance and support throughout the course of this research. My thanks also go to Dr. Barhoumi in the College of Veterinary Medicine and Biomedical Sciences, Image Analysis Laboratory for her help and advice with microscopy and image analysis. To Dr. Chaki, Alvin Tang, and Julia Popp of Rivera Lab, I will always be grateful for your advice, support, encouragement, and assistance. Thanks also go to my friends and colleagues and the department faculty and staff for making my time at Texas A&M University a great experience. I also want to extend my gratitude to the Air Force Institute of Technology, Civilian Institution Program and the United States Air Force Academy Department of Biology for providing both the opportunity and funding for my program. This work was also supported by a Texas A&M College of Veterinary Medicine Graduate Student Trainee Research Grant.

Finally, thanks to my family and friends for their continuous encouragement and especially to my wife and kids for their endless patience and love.

The views expressed in this dissertation are those of the author and do not reflect the official policy or position of the United States Air Force, Department of Defense , or the United States Government.

NOMENCLATURE

μm – Micrometer

Arp2/3 – Actin related protein 2/3 complex

ATCC – American Type Culture Collection

BSA – Bovine serum albumin

Cdc42 – Cell division control protein 42

dH_2O – Distilled water

ddH_2O – Deionized distilled water

DPBS – Dulbecco's phosphate buffered saline

ECM – Extracellular matrix

EGF – Epidermal growth factor

EGFR – Epidermal growth factor receptor

EMT – Epithelial to mesenchymal transition

F-actin – Filamentous actin

FBS – Fetal bovine serum

FIJI – FIJI is just ImageJ

FRAP – Fluorescence recovery after photobleaching

FRET – Förster resonance energy transfer

G-actin – Globular actin

GAPDH – Glyceraldehyde 3-phosphate dehydrogenase

kDa – Kilodalton

MMP – Matrix metalloproteinase

MTS – Multicellular tumor spheroid

Nck – Non-catalytic region of tyrosine kinase adaptor protein

N-WASp – Neuronal Wiskott - Aldrich syndrome protein

Pen/Strep – Penicillin and streptomycin

PFA – Paraformaldehyde

$PI(3,4,5)P_3$ – Phosphatidylinositol (3,4,5)-trisphosphate

$PI(4,5)P_2$ – Phosphatidylinositol (4,5)-bisphosphate

ROI – Region of interest

RTK – Receptor tyrosine kinase

TIRF – Total internal reflection fluorescence microscopy

TABLE OF CONTENTS

Page

LIST OF FIGURES

Page

CHAPTER I

INTRODUCTION

An Overview of Cancer Biology

According to the National Cancer Institute (1) the term cancer is used to describe more than 100 different types of disease. In stark contrast to the diversity of disease types, cancer can be characterized by two major traits including: unrestrained tumor cell proliferation, and altered tissue architecture (2, 3). To more precisely define the hallmarks of cancer, Hanahan and Weinberg proposed that tumor cells develop enabling mechanisms to evade apoptosis, proliferate autonomously, promote angiogenesis, undergo self-regeneration, invade local tissues, and metastasize (4). In addition, cancer cells frequently thrive by evading immune surveillance and reprogramming cellular energetics (5).

It is widely accepted that cancer cells evolve from normal cells through a process of transformation induced by the accumulation of multiple mutations. Knudson's two hit hypothesis, based on a statistical analysis of retinoblastoma, provided the first direct evidence that cancer results from as few as two mutations; either inherited through germinal cells or acquired by somatic cells (6). Mutations responsible for cancer can be caused by a number of different factors including chemical carcinogens, radiation, and faulty cellular mechanisms of DNA copying/repair.

Mutations result in gain (hyperactivation) or loss (inactivation) of protein function. Protein hyperactivation drives signaling mechanisms beyond homeostasis and

makes cells susceptible to oncogenic transformation. The genes affected by these mutations are typically referred to as proto-oncogenes. Protein inactivation disrupts the normal control mechanisms that balance the activating effects of proto-oncogenes. These genes are referred to as tumor suppressor genes. In addition to mutations to specific genes, gene amplification and translocation can result in altered protein levels or an altered protein and thus protein function. Gene amplification increases the number of gene copies and ultimately results in overexpression of the protein product. The result of gene translocation is dependent on the expression profile of the location of translocation and typically results in overexpression of proto-oncogenes (7).

In addition to mutations, cells can also undergo epigenetic changes that influence gene expression leading to aberrant cell behavior. Epigenetic changes affect the profile of gene expression without alterations in the DNA sequence in both development and disease (8). DNA methylation and histone modification are classic examples of epigenetic changes that can be inherited or directly influenced by environmental factors (2). Thus, the combined accumulation of mutations and epigenetic changes are likely to overcome cellular mechanisms of homeostasis and drive the progressive acquisition of the hallmarks of cancer.

Cancers can be categorized according to the tissue of origin. Thus, cancers originating from epithelial cells are designated as carcinomas. They can be further categorized based on the origin of epithelial cells; squamous cell carcinomas originate from protective epithelial layers, while adenocarcinomas originate from secretory epithelia. Given their protective and secretory functions, epithelial cells typically

undergo rapid proliferation; therefore, epithelia are more likely to undergo oncogenic transformation. Leukemia and lymphomas, cancers of white blood cells, result from excessive production of cells in the bone marrow and lymph nodes, respectively. Neuroectodermal tumors, on the other hand, derive from the cells of the central and peripheral nervous system (7).

Breast Cancer is a Significant Worldwide Health Concern

Breast cancer or breast adenocarcinoma is the second most common cancer and the most common type of cancer in women worldwide (9). In 2012 there were approximately 1.67 million cases of breast cancer diagnosed worldwide, accounting for about 25% of all cancers (9). In addition, an estimated 522,000 women died from breast cancer in 2012 (9).

For women in the United States, the most commonly diagnosed cancer and the second most frequent cause of cancer related death is breast cancer (10). Over 230,000 new breast cancer cases and 40,000 deaths related to breast cancer are estimated for the year 2015 (10). In addition, approximately 2,300 men will be diagnosed with breast cancer in 2015 (10). Early detection and advancements in treatment of breast cancer have improved the overall 5-year relative survival rate to nearly 90%; however, once metastases arise, the 5-year relative survival rate sharply decreases to only 25% (10). Metastasis, therefore, accounts for greater than 90% of deaths due to breast cancer (10, 11).

According to the National Cancer Institute, there are currently six standard types of treatment for breast cancer: surgery, sentinel lymph node biopsy with surgery,

radiation therapy, chemotherapy, hormone therapy, and targeted therapy. The most common treatment is surgical removal of the affected breast tissue and any affected local lymph nodes. In some circumstances, a sentinel lymph node biopsy is performed prior to surgery to determine if the tumor has spread. Surgery may be limited to the primary tumor or may be as extensive as a radical mastectomy, with the ultimate goal of removing all cancerous cells associated with the primary tumor and any affected local lymph nodes. Radiation therapy using x-rays or radioactive material is used to kill or prevent further growth of cancerous cells. Chemotherapy is a general term that represents more than 28 drugs that slow proliferation or kill cancerous cells. Chemotherapeutic agents can be administered locally or systemically and are often used to treat metastatic cancer. Hormone therapy works by interfering with the production of hormones or their actions to prevent hormone-induced cancer growth. Targeted therapies, on the other hand, are used to treat specific molecular targets that are overexpressed or hyperactivated in types of cancer (12). For example, a number of antibodies and antibody-drug combinations are available to treat HER2-positive breast cancer (13). Even with targeted therapies, beneficial effects are limited to increasing survival rates. Unfortunately, available therapeutic options are ineffective to prevent metastatic breast cancer progression. Treatments are frequently tailored to the needs of individual patients by combining any of the six standard therapeutic methods outlined above.

Cancer Invasion and Metastasis

Invasion and metastasis are complex, multi-step processes that involve breaching of basement membranes by cancer cells, invasion through the local extracellular matrix (ECM), and access to blood/lymphatic vessels (14). Cancer cells enter the vasculature, a process known as intravasation, to subsequently transit to local lymph nodes and eventually spread to distal organs (14). As tumor cells disseminate from the primary tumor, they are likely to escape the circulatory system by extravasation (14) and infiltrate distal tissues. Tumor cells with competence to adjust to the local environment may, after variable latency, colonize the organ and develop metastases (14).

Epithelial to Mesenchymal Transition (EMT)

Transformed epithelial cells exhibit "plasticity" or the ability to change their morphology and mode of motility to disseminate and colonize distant tissues during metastasis. During cancer progression, epithelial cells lose their typical apical-basal polarity and undergo a series of morphological and biochemical changes collectively known as epithelial to mesenchymal transition (EMT) (15). For example, EMT involves changes in cell-cell and cell-ECM adhesion, cytoskeletal remodeling, increased motility, and activation of a transcription program supporting acquisition and maintenance of the mesenchymal phenotype (16). Cues from the microenvironment ECM fibrils and soluble factors, in combination with the accumulation of genetic and epigenetic changes, promote EMT (17). The resulting signaling activation triggers changes in cell morphology, motility, and the expression of key transcription factors including: Slug, Snail and Twist. These transcription factors act by decreasing the expression of epithelial

markers, namely E-cadherin, and increasing expression of mesenchymal markers such as vimentin (15, 18).

Role of Extracellular Matrix (ECM) Remodeling in Tumor Progression

Reciprocal cell-ECM interactions are essential in both tissue homeostasis and disease progression. Key features of the extracellular matrix (ECM) that modulate the migration of mesenchymal and tumor cells are its chemical composition, stiffness, topography, and ligand density (19). Mesenchymal and tumor cells, on the other hand, are capable of altering (remodeling) the ECM through a variety of mechanisms including synthesis/deposition and/or degradation of matrix components as well as alignment and crosslinking of matrix fibrils (20).

Three major classes of proteases employed in the ECM remodeling are the Zinc-dependent metalloproteases, the cathepsin cysteine proteases, and serine proteases (20, 21). Although multiple secreted or membrane-associated proteases are capable of altering/degrading the ECM, the matrix metalloproteinases (MMPs) are key modifiers of the ECM during tumor progression (20, 22). MMPs are zinc-dependent protein hydrolases essential for tissue remodeling during both disease and development (23, 24). MMP activity results in degradation/modification of the ECM and, consequently, exposure of cryptic binding sites in ECM proteins and changes in the bioavailability of extracellular signaling molecules (25). Matrix metalloproteinase 14 (MT1-MMP/MMP14), in particular, is thought to play a central role in invasion and metastasis (26). MMP14 is one of the key membrane-tethered metalloenzymes required for collagenolysis and tumor cell intravasation (27, 28). Evidence suggests that MMP14

accumulates and/or is differentially activated at invadosomes (29). In addition, MMP14 activates MMP2 and MMP9, two secreted MMPs known to promote remodeling of the ECM and facilitate tumor cell invasion (29). The levels and activities of MMPs are tightly regulated through biosynthesis and post-translational modifications, including activation by furin-like proteases (20, 30). Of significance, the trafficking through the endocytic/recycling pathways is considered an important mechanism regulating the enrichment of MMP14 at sites of matrix degradation in tumor cells (29, 31)

Tumor Cell Migration

Cell migration is an essential process involved in organogenesis, tissue repair, and disease progression. Various modalities of cell movement, including single and multicellular migration, as well as expansive growth are recognized (32).

Single cells migrating through amoeboid movement do not require strong cell-substratum adhesion or protease-dependent ECM remodeling. Mesenchymal migration, on the other hand, is a mechanism of single cell migration that involves the formation of polarized membrane protrusions, substantial cell-ECM adhesion, and active protease-dependent ECM remodeling (32-34). Depending on the elastic properties of the matrix, lobopodial and lamellipodial modes of single cell migration have been described in three-dimensional environments (35). Importantly, cells exhibit plasticity in their migration behavior, i.e. are capable of alternating between mechanisms of cell movement in order to adapt to the prevalent microenvironment (34).

Collective cell migration includes multicellular streaming, characterized by differentiation of path-generating leader and follower cells. Sheet migration, on the other

hand, is another modality of collective invasion that relies on the maintenance of cell-cell junctions (32).

Expansive growth refers to an expanding tumor mass resulting from proliferating tumor cells pressing out on a permissive ECM in the absence of active cell migration (32). The diverse mechanisms of migration/invasion require cytoskeletal remodeling, and in the case of the most aggressive cancers, ECM remodeling by MMPs appears to be required.

Actin Dynamics Determine Cell Morphology and Motility

The actin cytoskeleton determines cell morphology and enables motility. Globular actin (G-actin) is an abundant cellular protein with structural polarity that assembles into polar, double-stranded helical filaments (F-actin) presenting a slow-growing pointed end and a fast-growing barbed end (2, 36). Actin monomers being incorporated into the polymers are loaded with ATP, which is hydrolyzed soon after polymerization (2). The spontaneous nucleation of actin is not thermodynamically favorable (37, 38). However, the presence of polymerization machineries allows cells to overcome the energetic barrier of actin nucleation. Once actin nucleation is initiated, the abundantly present actin monomers are added to barbed ends of an elongating actin filament at a rate limited only by its diffusion constant (36, 39). Therefore, the nucleation of actin is tightly regulated within the cells (40).

Cellular Machineries of Actin Polymerization

Two major contributors to F-actin nucleation/elongation are the Arp 2/3 complex and formins (36, 40). The Arp 2/3 complex is an intrinsically inactive complex

of seven polypeptides that form an anchor on existing (mother) actin filaments and promote actin nucleation and elongation of daughter filaments. The resulting filament network displays a y-branched geometry in which mother/daughter filaments are typically arranged at a 70^{o} angle (40-43).

Unlike the Arp2/3 complex, formins are a large family of proteins (15 members in humans) that use conserved domains to form homodimers that polymerize linear actin (40, 44). Thus, a "lasso" shaped domain (FH2) engages the barbed end of actin filaments while a second polyproline-rich domain (FH1) binds multiple profilin-actin complexes (activated building blocks) and positions them at the growing end of the filament facilitating processive polymerization (40, 45). Formins also protect the barbed ends of actin filaments from capping proteins during elongation, but the underlying mechanism remains to be elucidated (40, 46). In addition, Spire and Cordon-blue are actin nucleation factors that use multiple WH2 domains, G-actin binding modules, to promote polymerization of unbranched filaments (47, 48). Of significance, the linear actin filaments generated by formins and Spire play an important role in tumor cell invasiveness (49-51).

It is now recognized that the concerted action of the various actin nucleation/polymerization machineries are important for the dynamic organization of the actin cytoskeleton. Thus, the cooperation of multiple actin nucleators are required for the assembly and remodeling of F-actin structures contributing to cell shape and locomotion, including lamellipodia, filopodia, invadosomes, as well as tension-bearing actin cables and cortical actin networks (52).

Actin Dynamics Power Tumor Cell Invasion

Actin dynamics play a central role in invasion of tumor cells, a critical step leading to metastasis. More than 160 actin-binding proteins have been discovered and classified according to their role in the regulation of actin dynamics including nucleation/polymerization, nucleation-promoting, filament severing, capping and stabilization, and G-actin buffering (37, 53). Many of the molecules that drive cytoskeletal dynamics in response to extracellular cues are upregulated or activated in invasive tumor cells.

A Key Role for Arp2/3-dependent Actin Polymerization in Tumor Cell Invasion

Regulation of Arp2/3 by nucleation promoting factors

The assembly of a branched actin network by the Arp2/3 complex is critically important in the generation of protrusive structures that enable cell migration/invasion (54-56). Because the Arp2/3 complex is intrinsically inactive (40), the activity of nucleation promoting factors, and particularly the Wiskott-Aldrich syndrome protein (WASp) family, is required for the formation of branched actin networks. Members of the WASp family act as scaffold proteins that integrate signals from extracellular stimuli and modulate the activity of downstream effectors that, regulate actin dynamics (57).

The WASp protein, expressed in hematopoietic cells, was first identified as the causative agent of Wiskott-Aldrich syndrome, a rare X-linked recessive disease characterized by eczema, thrombocytopenia, and immunodeficiency (58). The closely related N-WASp (neuronal WASp) was subsequently discovered and found to be expressed in many tissue types (57, 59).

WASp proteins belong to the class I nucleation promoting factors that possess conserved C-terminal VCA domain consisting of three short conserved motifs including verprolin homology (V), connecting (C) and acidic (A) regions (40, 60). The VCA "output" domain mediates interactions with G-actin and the Arp2/3 complex, thus bringing together building blocks and the builder for effective nucleation of daughter actin filaments (40). In addition, N-terminal domains including WASp homology 1 (WH1) or Ena/VASP homology 1 (EVH1) domain, a basic region, a GTPase binding (GBD) or Cdc42 and Rac interactive binding (CRIB) domain, and a proline-rich region, provide interaction sites that enable regulation of N-WASp activity (57, 60). The WH1 domain binds members of the WASp-interacting protein (WIP) family, scaffolds that appear to suppress the activity of N-WASp and assist with binding adaptor proteins such as Nck (57). The basic region just upstream of the GBD can bind phosphatidylinositol (4,5)-bisphosphate or PI(4,5)P_2, while the GBD domain binds the small GTPase Cdc42 (57, 61). The proline-rich region of N-WASp acts as a binding site for SH3 domain-containing proteins such as Nck or Grb2 (57, 61). The intramolecular interaction between the VCA and GBD/basic regions results in a folded, auto-inhibited confirmation of N-WASp that prevents exposure of the VCA region and its interaction with Arp2/3 complex and G-actin (57, 61). Thus interactions of the WASp/N-WASp regulatory domains with upstream signals disrupts the intramolecular interaction between the VCA and the basic region/GBD domains, allowing the unfolding of WASp/N-WASp and exposure of the VCA domain for G-actin and Arp2/3 complex binding (57, 61). It is now well established that N-WASp-stimulated actin polymerization by the Arp2/3 complex is

critically involved in tumor cell invasiveness through the regulation of invadosome biogenesis (56, 62-64). In addition, a recent report provides evidence that N-WASp is involved in the delivery and anchoring of MMP14 at invadopodia (65).

WASH is another member of the WASp family of nucleation promoting factors that is involved in regulation of tumor cell invasion (66). WASH also possesses a VCA region that mediates interaction with G-actin and the Arp2/3 complex but its N-terminal region differs from that of WASp/N-WASp. Thus, the N-terminal WASH homology domain 1 (WHD1) facilitates the assembly of a five-member WASH complex that regulates the nucleation-promoting activity of the WASH protein and targets it to the endosomes compartment (67, 68). The WASH proteins stimulate actin polymerization through activation of the Arp2/3 complex in lamellipodia and filopodia (66). In addition, recent evidence suggests that WASH interaction with the exocyst complex on late endosomes is required for MMP14-dependent ECM remodeling (66, 69). Collectively, these findings suggest that WASH plays an important role in regulating F-actin dynamics to promote the trafficking and targeted delivery of MMP14 to invasive structures.

Regulation of Arp2/3 by cortactin

Cortactin is an actin regulatory protein consisting of a N-terminal acidic domain followed by tandem F-actin binding repeats and a regulatory C-terminus that includes a proline-rich segment, and one SH3 domain. By virtue of its N-terminal acidic region, cortactin binds Arp2/3 complex and acts as a nucleation promoting factor. Cortactin may also help stabilize actin filaments and enhance N-WASp-stimulated actin polymerization

(70). Importantly, cortactin acts as signaling hub by integrating signals from tyrosine and serine/threonine kinases, interacting with a number of SH3 binding partners, and undergoing posttranslational modifications including acetylation and phosphorylation (70, 71). Cortactin is known to play an important role in cancer cell invasion. In particular, the formation of cellular invasive structures requires tyrosine phosphorylation of cortactin and the subsequent activation of N-WASp/Arp2/3-dependent actin polymerization through the adaptor Nck (63, 72). Cortactin has also been linked to pH dependent invasion and secretion of MMPs (MMP2, 9 and 14) (73, 74).

Invadosomes

A variety of cancer cells form specialized F-actin based structures, collectively termed invadosomes, that in conjunction with other cytoskeletal structures such as lamellipodia and lobopodia enable tumor cell invasion and metastasis (35, 75, 76). Invadosomes are enriched in proteases that by promoting remodeling of the ECM facilitate migration/invasion of tumor cells (28).

The two primary structures that make up the invadosomes are invadopodia and podosomes. The term invadopodia was coined by Wen-Tien Chen in 1989 when he described the membrane protrusions found in Rous sarcoma virus (RSV) -transformed fibroblasts that were capable of localized ECM degradation (77). Previously, David-Pfeuty and Singer had identified altered localization of cytoskeletal proteins in RSV transformed fibroblasts (78). This was followed by Tarone et al. discovering that these sites formed cell-to-ECM adhesions that resembled cellular feet, leading them to describe them as podosomes (79). Thus, the terms invadopodia and podosome were

initially used to describe the same structures identified in RSV-transformed fibroblasts. Currently, podosome and invadopodia are used, respectively, to refer to the actin-based invasive structures formed in normal cells and in tumor/Src-transformed cells (28).

Podosomes and invadopodia share a similar overall architecture, but present differences in morphology and molecular composition (28, 76). Important morphological differences include: i) the presence of a prominent vinculin-containing ring surrounding the actin core in podosomes but not in invadopodia; ii) number and location: tumor cells typically form fewer than ten invadopodia that localize in proximity to the nucleus. Normal cells, in contrast, display a large (greater than one hundred) number of podosomes that localize in the proximity of the cell's edge); iii) size and clustering: invadopodia are usually found as single entities of 0.5-2 μm in diameter whereas podosomes tend to cluster/form arrays of larger size; and iv) lifetime: invadopodia persist for over an hour whereas podosomes have a lifetime of only a few minutes (21, 28, 80). At the molecular level, Nck1 and Grb2 localize specifically to invadopodia and podosomes, respectively (81). Despite characterized differences, the degrading capacity of these structures enables cell migration through dense ECM, and for breast cancer cells, enables invasion and metastasis.

Key Signaling Mechanisms Linking Actin Dynamics and Tumor Cell Invasion

Tumor cell invasion requires coordinated cytoskeletal rearrangement in response to cellular stimuli. Stimulation of cell surface receptors results in activation of intracellular signaling pathways that lead to localized actin polymerization. Multiple signaling pathways contribute to the spatial and temporal regulation of actin dynamics

during invasion. Within these signaling pathways, Rho GTPases, phosphoinositides and tyrosine phosphorylation provide critical links enabling coordinated actin rearrangement necessary for tumor cell invasion.

Rho GTPases

The Rho GTPases are well characterized regulators of the actin cytoskeleton that function as convergence nodes, integrating and coordinating signaling cascades activated by multiple cell surface receptors. These small proteins are enzymes that hydrolyze guanine-triphosphate (GTP) to guanine-diphosphate (GDP). The binding of GTP or GDP results in alternation between two conformational states that allow the Rho GTPases to function as molecular switches, i.e., the GTP-bound active and the GDP-bound inactive states (82). The transitions between active/inactive states are regulated by about 85 guanine exchange factors (GEFs) and 80 GTPase activating proteins (GAPs) (83). Whereas GEFs activate Rho GTPases by facilitating the exchange of GDP for GTP, GAPs promote their inactivation by accelerating their GTPase activity (83). In addition, three guanine nucleotide dissociation inhibitors (GDIs) prevent spontaneous activation by sequestering the Rho GTPases in the cytoplasm (82, 83).

Key processes regulated by Rho GTPases through cytoskeletal remodeling include cell polarization, migration, intracellular trafficking, and proliferation (82). Twenty-two Rho GTPases have been identified; however, RhoA, Rac1 and Cdc42 are the most extensively involved in regulation of cytoskeletal dynamics (82, 83). Of particular interest is Cdc42, a key GTPase that controls cell polarity and directional migration (82, 84). Key downstream targets of Cdc42, WASp/N-WASp, and

diaphanous-related formins (83) are critical in invadosomes biogenesis. A role for Cdc42 in invadopodia formation was first established in human melanoma cells (85), subsequently asserted in mammary adenocarcinoma cells (56, 86), and more recently, pancreatic tumor cells (87).

Phosphoinositides

Another regulator of actin dynamics is a family of phosphorylated amphipathic lipids (phosphatidylinositol) called the phosphoinositides (PI). Although phosphoinositides constitute only a small fraction of the total membrane phospholipids (i.e., $<1/6^{th}$), their diversity and subcellular distribution contributes to organelle membrane differentiation and spatiotemporally-regulated signaling (88). Two of the seven phosphoinositide species, phosphatidylinositol (4,5)-bisphosphate ($PI(4,5)P_2$) and phosphatidylinositol (3,4,5)-trisphosphate ($PI(3,4,5)P_3$) are enriched at the plasma membrane and have prominent roles in modulating actin dynamics (89). The relatively more abundant $PI(4,5)P_2$ contributes to regulation of actin dynamics in endocytic processes, membrane ruffling, cell adhesion and migration, and invadosome formation (88, 89). The much less abundant $PI(3,4,5)P_3$, on the other hand, is increased in response to growth factor stimulation to promote cellular responses that depend on actin dynamics, including macropinocytosis, phagocytosis, and chemotactic migration (88). Both $PI(4,5)P_2$ and $PI(3,4,5)P_3$ regulate actin dynamics through actin binding proteins, localization of scaffolding proteins and activation of the Rho GTPases (89). It has been shown that disruption of phosphoinositide metabolism alters the formation/function of invadosomes (90-92). A recent investigation suggests that the balance between $PI(4,5)P_2$

and PI(3,4,5)P_3 is regulated by the inositol phosphate SHIP-2 during invadopodia maturation (93).

Tyrosine Phosphorylation

Tyrosine phosphorylation, the addition of a phosphate group to particular tyrosine residues in substrates of tyrosine kinases, is an important signal transduction mechanism that regulates many cellular processes including proliferation, differentiation, metabolism, transcriptional activation, immune defense, adhesion and cytoskeletal dynamics (94). The tyrosine phosphorylation signaling mechanism relies on a three part toolkit: tyrosine kinases (writers), phosphotyrosine phosphatases (erasers), and phosphotyrosine peptide recognition domains (readers) such as the Src Homology (SH)2 and phosphotyrosine binding (PTB) domains present in a number of effector proteins (95). Because cues from the microenvironment, including growth factors and the ECM, modulate cytoskeletal dynamics through activation of tyrosine phosphorylation, it is not surprising that dysregulation of such signaling mechanisms contribute to cancer progression, invasion and metastatic spread. Dysregulation of receptor tyrosine kinases (RTK) including, among others, epidermal growth factor receptor (EGFR) and hepatocyte growth factor receptor (c-Met), promotes uncontrolled cell proliferation, tumor angiogenesis, and metastasis (96, 97). In addition, the non-receptor tyrosine kinase Src is known to act as a common downstream node cooperating with activated RTK in tumorigenesis and metastasis (98). Src phosphorylates key cytoskeletal effectors including cortactin, Tks5 and N-WASp (75, 99). Phosphorylated cortactin initiates invadopodia formation by engaging Nck through its SH2 domain. The

cortactin-Nck complex, in turn, drives activation of the N-WASp-Arp-2/3 pathway of actin polymerization that is required for invadopodia biogenesis (63, 72). Activation of this pathway is reinforced by Src dependent phosphorylation of Tks5 (99, 100).

The discoidin domain receptors (DDR), receptor tyrosine kinases activated upon engagement of collagen fibrils, are known to facilitate tumor invasion through cooperation with MMPs, though the specific nature of the interaction remains to be elucidated (101-104). Interestingly, a recent report showed that DDR1 induces linear invadosome assembly, independently of its inherent kinase activity, through activation of the Rho GTPase Cdc42 (86). Since activated DDRs interact with Nck (101), it is possible that these adaptors provide a link between collagen signaling and N-WASp/Arp2/3 actin remodeling.

Nck

The non-catalytic region of tyrosine kinase Nck1 and Nck2 (collectively referred to as Nck) are a pair of SH2/SH3 domain-containing adaptor proteins that link cell surface signaling to actin dynamics (105, 106). Nck consists of a single C-terminal SH2 domain and three N-terminal SH3 domains (107). SH2 and SH3 domains have no inherent enzymatic activity and serve as protein interaction modules that facilitate the formation of signaling ensembles (107). The SH2 domain binds phosphorylated tyrosine residues in a sequence-specific context to perform the “reader” function in phosphotyrosine signaling (95). The SH3 domain interacts with proline-rich binding sites of a number of downstream effectors that include members of the WASp family (108).

First identified in melanoma, Nck are 47 kDa proteins that share 68% homology (105, 106). Nck1 and Nck2 display significant overlap in expression patterns during development and are thought to have redundant functions, with few identified exceptions (109-111). Inactivation of both Nck1 and Nck2 causes embryonic death in mice and defects in motility and actin polymerization in cultured embryonic fibroblasts (109). The Nck adaptors are also required for the development of the glomerular filtration barrier by linking nephrin phosphorylation to actin dynamics in podocytes (112). Similarly, a role for Nck in mammary gland development downstream of activated DDRs has been proposed (113, 114). Findings from a recent study show lethality associated with ablation of Nck in the mouse endothelium (115). Conceivably, Nck signaling may also contribute to tumor angiogenesis.

Several pathogens are known to manipulate actin dynamics through Nck binding. For example, vaccinia virus induces actin comets through activation of the Nck/N-WASp/Arp2/3 pathway; such comets propel the viral particles for productive pathogen dissemination (116, 117). Enteropathogenic *Escherichia coli*, on the other hand, activate N-WASp/Arp2/3-dependent actin polymerization through translocation of virulence factors (118). One such factor, the intimin receptor (Tir), undergoes phosphorylation by host tyrosine kinases and subsequently recruits Nck to induce the formation of actin pedestals (118).

It is known that maximum stimulation of the nucleation promoting activity of N-WASp requires the coincidence of multiple signals. Pioneer studies by Rohatgi et al. demonstrated synergistic activation of N-WASp by converging signals from $PI(4,5)P_2$

and Cdc42 (119) or $PI(4,5)P_2$ and Nck SH3 domains (120). Clustering of membrane-targeted SH3 domains induce efficient activation of N-WASp dependent actin polymerization and the formation of actin comets (121, 122). In addition, a reciprocal interaction of Nck and $PI(4,5)P_2$ was shown to enhance localized actin polymerization in living cells (123). By combining experimentation with computational modeling, it was shown that full activation of localized actin polymerization in cells requires a 4:2:1 stoichiometry within the Nck/N-WASp/Arp2/3 complex (124). Such models also underscore a critical role for WASp-interacting protein (WIP), another scaffold recently shown to provide a key linkage between N-WASp and Nck (125).

Evidence suggests that Nck plays a role in cancer through modulation of tumor cell proliferation, invasion, and metastasis. For example, work from Condeelis et al. described a critical role for Nck1 in EGF stimulated invadopodia formation and invasion. Findings from *in vitro* studies from this group suggest that EGF stimulation of invasive breast carcinoma cells induces Src-mediated phosphorylation of cortactin and the subsequent recruitment of Nck1 to stimulate focalized actin polymerization through the N-WASp/Arp2/3 complex (56, 72). The silencing of Nck2 was reported to impair cell adhesion/spreading thus precluding further analysis (56). In addition, Nck1 and Grb2 were identified as unique markers to distinguish invadopodia from podosomes (81).

The existing literature also suggests relationships between the scaffolding protein Tks5/Fish and Nck in invadosome biogenesis. Tks5, a substrate of the non-receptor tyrosine kinase Src, is required for invadopodia formation (99, 126, 127). Integrin

engagement stimulates Src-dependent phosphorylation of Tks5 and the recruitment of Nck *in vitro*. The Tks5/Nck complex, in turn, stimulates N-WASp/Arp2/3-dependent actin polymerization and ECM remodeling (100). Collectively, these studies suggest a critical role for Nck in invadosome formation downstream of RTK activation and/or integrin engagement (56, 100).

Activation of EGF in pancreatic cancer cell lines promotes formation of a complex between p130Cas and Nck that leads to activation of Ras-associated protein 1 (Rap1) (128). This study showed that EGF-mediated Rap1 activation was required for metastasis but not primary tumor growth (128). Of note, overexpression of Nck2 in melanoma cells resulted in larger tumors in mice (129). Thus, the role played by Nck in tumor progression and metastasis remains largely undetermined.

Summary

Reciprocal interactions between cancer cells and their microenvironment set in motion changes in the cytoskeletal architecture and remodeling of the ECM that enable tumor cell invasion and metastasis. Invasion of tumor cells is facilitated by enhanced cell motility and the formation of actin-based cellular structures, collectively termed invadosomes, which remodel the ECM (130). The formation of invadosomes involves localized actin polymerization stimulated primarily by the actin-related protein (Arp) 2/3 complex. Whereas the activity of the Arp2/3 complex is highly increased by the nucleation promoting factor neural Wiskott-Aldrich Syndrome protein (N-WASp), actin filament (F-actin) stabilization is enhanced by the actin binding protein cortactin (130). Nck adaptors, containing SH2/SH3 domains, link tyrosine phosphorylation induced by

extracellular signals with cytoskeletal dynamics (105, 106). Recent findings suggest that cortactin recruits Nck to promote localized actin assembly through the N-WASp/Arp2/3 pathway (72). Thus, the cortactin-Nck complex is critically involved in actin polymerization during invadosome biogenesis, localized ECM remodeling, and tumor cell invasion *in vitro* (72).

Remodeling of the ECM is greatly dependent on the activity of matrix metalloproteases (MMPs) (22, 25). Although the activities of multiple MMPs contribute to the development of a tumor microenvironment, MMP14 is of particular importance in tumor cell invasion and metastasis (29, 131). Loss of MMP14, but not other type I collagenolytic metalloenzymes, decreases the invasive capacity of cancer cells (26). MMP14 also activates MMP2 and MMP9, two secreted MMPs known to promote remodeling of the ECM (29).

Components of the cytoskeletal network are required for structural formation, delivery, and anchoring of ECM degrading MMPs at invadosomes. For example, N-WASp is required for invadosome formation and anchors MMP14 to the F-actin scaffold of invadosomes in breast cancer cells (56, 65). In addition, the cytoskeletal network is critical for cell motility and invasion. These findings support a hypothesis that a functional relationship exists between intracellular trafficking and localization of MMP14; however, the role of Nck in the trafficking of MMP14 and targeted delivery to invadosomes remains undetermined (31). More importantly, the functional significance of Nck signaling in tumor progression and metastasis has not been elucidated.

CHAPTER II

NCK IS REQUIRED FOR BREAST CARCINOMA GROWTH, INVASION AND METASTASIS

Introduction

Cancer invasion and metastasis is a multi-step process that requires tumor cells to breach the basement membrane and invade through the adjacent ECM. Subsequently, tumor cells reach the local blood and/or lymphatic vessels, a process called intravasation, to spread to distal tissues/organs where they potentially develop into secondary tumors (14). Tumor progression results in loss of the architectural organization of affected tissues and neovascularization (5). At the cellular level, an important step in the metastatic process involves the epithelial-to-mesenchymal transition (EMT), a combination of functional and morphological changes that results in an altered pattern of protein expression, increased cellular motility, and the development of invasive/matrix remodeling capacity (15).

Remodeling the ECM requires the activity of matrix modifying enzymes that alter the structural, biochemical and biomechanical properties of the matrix (20). Metalloproteinases, including the related families of MMPs (matrix metalloproteinases) and ADAMs (A Disintegrin And Metalloproteinases), facilitate normal and tumor cell invasion, activate tumor-associated inflammation, and stimulate angiogenesis (25). Overall, the activity of the metalloproteinases results in the degradation of protein components of the extracellular matrix, the shedding of the ectodomain of several cell

surface-associated molecules, and modification of the activity and bioavailability of extracellular signaling molecules (25). There are 23 MMPs that are expressed in human tissues; however, MMP14 is critically involved in ECM remodeling, invasion and metastasis (20, 25, 26). In addition to degrading multiple components of the extracellular matrix, MMP14 also activates MMP2 and MMP9, two secreted MMPs that contribute to invasion and metastasis (29).

Actin dynamics play a central role in the EMT transition. For example, actin dynamics underlie the formation of transient membrane protrusion including lamellipodia and invadopodia that facilitate tumor cell migration and invasion. Thus, regulation of actin dynamics by extracellular signals is paramount in cancer progression. This research focuses on the role of Nck adaptors, known to link signals that activate tyrosine phosphorylation with actin dynamics (105, 106), in breast carcinoma growth, invasion, and metastasis. Previous work relying on 2D models *in vitro* suggests that Nck is an important mediator of matrix degradation and transwell invasion (72, 100). However, how Nck regulates breast carcinoma cell behavior in three-dimensional environments *in vitro* as well as tumor growth, invasion, and metastasis remains poorly understood.

We hypothesized that Nck-dependent actin remodeling promotes breast carcinoma invasion and metastasis. To test this hypothesis we combined analysis of breast carcinoma cell growth/invasion in 3D collagen matrices with assessment of tumorigenesis and metastasis in a model of xenogeneic transplantation of human breast

carcinoma cells in immunodeficient mice. Here we determine the role of Nck in breast carcinoma invasion and metastasis.

Materials and Methods

Cell Culture

MDA-MB-231 (CRM-HTB-26) and 293T (CRL-3216) were purchased from American Type Culture Collection (ATCC) and cultured in DMEM high glucose (HyClone) without sodium pyruvate (MDA-MB-231) or with sodium pyruvate (293T) supplemented with 1% penicillin/streptomycin and 10% fetal bovine serum (FBS) (Gemini), at 37^{o}C in an atmosphere with 5% CO_2. MDA-MB-231s were sub-cultured every 4-5 days at ~5x10^3 cells/cm^2 and 293T were sub-cultured every 4-5 days at ~2x10^4 cells/cm^2. For sub-culture, cells were washed twice with warm DPBS and incubated with 0.05% Trypsin/0.53 mM ethylenediaminetetraacetic acid (EDTA) in Hank's balanced salt solution (HBSS) without sodium bicarbonate (Cellgro®) for 5 minutes at room temperature (MDA-MB-231) or 1 minute at 37^{o}C (293T). Trypsin was neutralized using complete growth media and cells were centrifuged at 800 rpm for 3 minutes then re-suspended in complete media, counted by hemocytometer and plated in plastic tissue culture plates.

MDA-MB-231 is a triple negative (estrogen receptor negative, progesterone receptor negative and human epidermal growth factor receptor 2 negative), claudin-low cell line that was derived in 1973 from a pleural effusion in a 51 year old, white female (132, 133). This cell line has been used extensively for breast cancer research and has been shown to be both tumorigenic and metastatic in the nude mouse model (132, 134).

Cryopreservation

Cells were grown for 3-4 days then sub-cultured. After centrifugation at 800 rpm for 3 minutes cells were re-suspended in 90% FBS/ 10% DMSO and 500 μL aliquots distributed in cryopreservation vials. Vials were placed in a Mr. Frosty™ freezing container and placed at -80°C for 24 hours. After 24 hours, the vials were stored in liquid nitrogen vapor phase.

Plasmids and Viral Transduction

Virus was produced as previously described with minor modification (135, 136). A detailed description of the protocol for viral transduction can be found in Appendix P and Appendix Q. Briefly, virus were produced in 293T cells by calcium precipitation with pSuper.puro/hygro carrying oligonucleotide sequences (shRNA) either non-targeting (shScr) (scrambled sequence - Oligo2, Dharmacon non-targeting siRNA SMARTPool), targeting human MMP14 (shMMP14) (Oligo3, Dharmacon MMP14 siRNA SMARTPool) or targeting human Nck1 or Nck2 (shNck) (137) for protein knockdown. Plasmids were co-transfected with pHCMV-G and pMD.gag.pol plasmids and incubated with chloroquine (25 μM) for 4-6 hours, then media was exchanged and virus collected 20-48 hours later and either spun at 3500 rpm for 10 minutes and distributed in 1 mL aliquots for storage at -80°C or filter sterilized with a 0.22 μm syringe filter and used immediately. MDA-MB-231 were infected in the presence of 8 μg/mL polybrene and selected for 2-3 days in the presence of 1 μg/mL puromycin and/or 800 μg/mL hygromycin.

siRNA Transfection

siRNA transfections were carried out according to the manufacturers protocol (Dharmacon). The transfection of siRNA for all experiments was carried out with the standard conditions of 50 nM siRNA for MMP14, Nck1 and Nck2 and 25 nM scrambled siRNA. For 3D spheroid assays DharmaFECT 4 transfection reagent was used at 1 μL/mL on $5x10^4$ cells in a 35-millimeter dish. For transwell invasion assays DharmaFECT 4 transfection reagent was used at 3 μL/mL on $30x10^4$ cells in a 35-millimeter dish. Transfection reagent and siRNA were incubated in separate tubes containing serum-free and antibiotic-free media for 5 minutes. The tubes were then combined and incubated for 20 minutes before the entire contents of the tube was added to a plate containing the appropriate volume (1.6 mL for 35-millimeter dish) of antibiotic free complete media and incubated for six hours. For 3D spheroid assays, after 6 hours the cells were lifted, counted and placed into 10X spheroid formation matrix. For transwell invasion assays, media was exchanged with fresh complete media after 6 hours and allowed to grow for 48 hours. At 48 hours cells were starved overnight prior to starting the invasion assay.

Transwell Invasion Assay

Transwell invasion assays were conducted as described by the manufacturer (Corning) with minor modifications [Appendix G]. Briefly, individual cell invasion was measured using control and growth factor reduced Matrigel-coated invasion chambers (Corning BioCoat™, 354578 and 354483). MDA-MB-231 cells were starved overnight in starvation media (0.2% FBS) and a total of $5x10^4$ cells in starvation media were

seeded in the upper chamber and allowed to migrate (5 hours) and invade (18 hours), towards the lower chamber containing starvation media with 10 ng/mL EGF as a chemoattractant. After 5 or 18 hours incubation at 37^{o}C with 5% CO_2, cells on the underside of the filter were fixed with 3.7% paraformaldehyde (Electron Microscopy Science) and cells on the upper side of the filter were removed using a cotton swab. NucBlue® Live ReadyProbes® Reagent was diluted 2 drops in 1 mL DPBS and 100 μL used to stain fixed cells. Images of nuclei were captured using an Olympus IX70 inverted microscope equipped with an Olympus Plan-Apo 10X/0.30 numerical aperture objective, a Spot RT3 Camera (7.4 μm x 7.4 μm pixel size) and Spot software. Percent invasion was calculated as previously described: number of cells invaded divided by number of cells migrated, then the result multiplied by 100 (138).

3D Growth Assay

3D growth assays were conducted as described by the manufacturer (Trevigen) with minor modification [Appendix M]. Briefly, MDA-MB-231 cells expressing short hairpin (sh) RNAs encoding non-targeting sequences (shScr) or sequences Nck (shNck) were subjected to spheroid formation in 3D culture qualified 96-well spheroid formation plate (Trevigen) in the presence of 10X spheroid formation matrix diluted to 1X in complete media for 3 days, then 50 μL complete media was added and cell imaged every 24 hours for 6 days. To determine cell count after spheroid formation, spheroids were disaggregated using Trypsin/EDTA and counted using a hemocytometer. To determine changes in growth, images were acquired using an Olympus IX70 inverted microscope equipped with an Olympus UPlan-Fluorite 4X/0.13 numerical aperture objective, a Spot

RT3 Camera (7.4 μm x 7.4 μm pixel size) and Spot software. FIJI is just ImageJ (FIJI) was used to determine spheroid area and exported to Excel or Minitab for analysis.

3D Spheroid Invasion Assay: Laminin-rich Matrix

3D Spheroid invasion assays in laminin-rich matrix were conducted as described by the manufacturer (Trevigen) with modifications [Appendix H]. Briefly, MDA-MB-231 cells were transiently transfected with small interference (si) RNA oligonucleotides encoding non-targeting sequences (siScr) or sequences targeting MMP14 (siMMP14), or Nck (siNck) cells subjected to spheroid formation in 3D culture qualified 96-well spheroid formation plate (Trevigen) in the presence of 10X spheroid formation matrix diluted to 1X in complete media and then embedded in laminin-rich matrix (Invasion Matrix Trevigen) and allowed to invade in the presence of EGF (5 ng/ml) used as a chemoattractant in serum-reduced media. A total of $3x10^3$ cells were seeded and incubated for 2 days (spheroid formation), then imaged every 24 hours.

3D Spheroid Invasion Assay: Collagen I

The 3D spheroid invasion assay in collagen I was adapted from manufacturer's literature (Trevigen/Corning), and previously described protocols [Appendix I] (139, 140). Briefly, MDA-MB-231 cells expressing short hairpin (sh) RNAs encoding non-targeting sequences (shScr) or sequences targeting MMP14 (shMMP14), or Nck (shNck) were subjected to spheroid formation in 3D culture qualified 96-well spheroid formation plate (Trevigen) in the presence of 10X spheroid formation matrix diluted to 1X in complete media. Formed spheroids were then embedded in 2 mg/ml acid-extracted type I rat tail collagen polymerized at 37^{o}C and allowed to invade in the presence of EGF (5

ng/ml) used as a chemoattractant in serum-reduced media (2% FBS). A total of $3x10^3$ cells were seeded and incubated for 3 days (spheroid formation), then imaged every 24 hours.

Quantification of 3D Invasion

Images were captured on an Olympus IX70 inverted microscope equipped with an Olympus UPlan-Fluorite 4X/0.13 numerical aperture objective, a Spot RT3 Camera (7.4 μm x 7.4 μm pixel size) and Spot software. Invasion distance was determined as previously described (141). Briefly, the extreme diameter of each spheroid was measured using FIJI at four different angles and the average diameter calculated in Microsoft Excel. The average diameter for time zero was then subtracted from each time point to determine the average invasion distance.

Xenograft Studies

Xenograft studies were performed as previously described with modification (142). A detailed protocol can be found in Appendix N. Briefly for xenograft studies, MDA-MB-231 cells ($2x10^6$) were injected subcutaneously into the flanks of 6-9 week old nude mice (Jackson Laboratory NU/J 002019) in 75% growth factor reduced Matrigel (BD Biosciences, 9.9 mg/mL). Tumors were grown for 9 weeks and measured weekly using calipers starting after 1 week. Volumes were calculated as previously described (143). Xenograft tumors were harvested, weighed and snap-frozen in liquid nitrogen then stored at -80^{o}C for DNA/RNA purification or fixed in 4% paraformaldehyde and paraffin embedded for immunohistochemistry. Lungs and liver were harvested and portions snap-frozen in liquid nitrogen then stored at -80^{o}C for

DNA/RNA purification or fixed in 4% paraformaldehyde and paraffin embedded for immunohistochemistry. Animal experiments were accomplished according to protocols approved by the Texas A&M Animal Care and Use Committee (AUP 2014-0194).

RNA Isolation and Reverse Transcription

RNA isolation from tissues was performed using the manufacturer's protocol provided with the Direct-zol™ RNA MiniPrep with TRI-Reagent® kit (Zymo Research R2052). From the isolated total RNA 2 μg was subjected to reverse transcription into cDNA using the manufacturer's protocol with the iScript™ cDNA Synthesis Kit (Bio-Rad 170-8990).

Quantitative Real-time PCR (qPCR)

Q-PCR was performed as previously described (142, 144). A detailed protocol can be found in Appendix N. Briefly, q-PCR was performed on a Bio-Rad CFX384 Real-Time PCR detection systems using FastStart Universal SYBR Green Master (Rox) mix (Roche). Primers (Integrated DNA Technologies) for human glyceraldehyde 3-phosphate dehydrogenase (GAPDH) were used to detect lung metastasis: forward primer 5'-CCA GGT GGT CTC CTC TGA CTT C-3'; reverse primer 5'-CCA GGT GGT GAG GGC AAT G-3'. Mouse β-actin (forward primer 5'-GTT TGA GAC CTT CAA CAC CCC-3'; reverse primer 5'-GTG GCC ATC TCT TGC TCG AAG TC-3') was used as a normalizing gene and data was analyzed by the $\Delta\Delta C_T$ method (145, 146).

Western Blotting

Western blotting was performed as described by the manufacturer (Bio-Rad) and as previously described (137). A detailed protocol for western blotting can be found in

Appendix L. Briefly, lysates were prepared for western blot by first washing adherent cultures twice with cold DPBS then harvesting with ice-cold kinase lysis buffer (25 mM Tris, pH 7.4, 150 mM NaCl, 5 mM EDTA, 10% glycerol, 1% Triton X-100, 10 mM β-glycerophosphate, 1 mM sodium orthovanadate, 10 mM sodium pyrophosphate, 10 μg/L aprotinin and 1 mM phenylmethylsulfonyl fluoride) and the cells collected using a cell scraper. Lysates were vortexed briefly and incubated on ice for 15-30 minutes, then centrifuged at max speed for 10 minutes in a refrigerated centrifuge. Cleared lysate was transferred to a fresh tube and stored at -80^{o}C or protein concentration immediately quantified using a Bradford Assay (Bio-Rad). For western blotting, sodium dodecyl sulfate-polyacrylamide gel electrophoresis (SDS-PAGE) was performed on equal amounts of protein prior to transfer to nitrocellulose membranes and blocking with non-fat dry milk (NFDM). Blots were probed with primary antibody in blocking solution overnight at 4^{o}C then washed 5 times for 5 minutes in tris-buffered saline and Tween 20 (TBST). Blots were incubated with secondary antibody in blocking solution for 1 hour at room temperature then washed 5 times for 5 minutes in TBST. Washed membranes were then incubated with enhanced chemiluminescence substrate (Western Lightening® Plus-ECL NEL103001) for 1 minute before imaging on ImageQuant™ LAS 4000 mini documentation system. Anti-Nck antibody (Millipore, 06-288) was diluted 1:4000 in 3% NFDM, anti-MMP14 antibody (Millipore, MAB3328) was diluted 1:2000 in 1% NFDM and anti-GAPDH antibody (Invitrogen, 43700) was diluted 1:10,000 in 1% NFDM. For secondary antibodies goat anti-mouse IgG-HRP (Santa Cruz Biotechnology, sc-2055) was diluted 1:10,000 in 1% NFDM and goat anti-rabbit IgG-HRP (Santa Cruz

Biotechnology, sc-2030) was diluted 1:10,000 in 3% NFDM. Images were analyzed using FIJI software.

Statistics

When comparing multiple groups with normal distributions ANOVA with a Tukey post-hoc was used. If data did not approximate a normal distribution a Mann-Whitney non-parametric analysis was performed or when applicable data was log transformed. Growth curves were analyzed using a general linear model to determine interaction between time and treatment, followed by a Tukey post-hoc analysis. For data depicted as a box and whisker plot the bottom and top of the boxes are the first and third quartile, respectively, whereas the band inside is the middle quartile (median). The ends of the whiskers extend to the lowest and highest values excluding outliers. Grubbs outlier test was used to identify and remove outliers. Significant values where a specific p-value is not listed indicate a p-value < 0.05.

Results

Nck is Required for Individual Cell Invasion Through Matrigel

Previous work demonstrated that Nck1 is required for matrix proteolysis and FBS-stimulated invasion of breast carcinoma cells (72). Here, we hypothesized that Nck is required for EGF-stimulated proteolytic invasion through a laminin-rich basement membrane (Matrigel). To test this hypothesis we determined migration and invasion of isolated/single MDA-MB-231 cells in the presence of 10 ng/mL EGF. Figure 2.1A shows the experimental set-up for the transwell invasion assay. Percent invasion, calculated as the number of cells invading divided by the number of cells migrating, was

used to compare cells transfected with siRNA oligonucleotides encoding non-targeting, scrambled sequences (siScr), or sequences targeting MMP14 (siMMP14) or both Nck1 and Nck2 (siNck) (138). We found that loss of Nck reduced the percent of cell invasion significantly below that of the scrambled control (siScr) and proteolysis dependent (siMMP14) populations (Figure 2.1 A). To further test the role of Nck in invasion, we performed an experiment using cells stably expressing shRNAs encoding non-targeting sequences, or sequences targeting MMP14, or both Nck1 and Nck2. We found that silencing MMP14 and Nck significantly reduced invasion below the scrambled control; however, we were unable to detect a significant difference between the MMP14 and Nck silenced populations (Appendix A). Using siRNA it was also observed that the Nck silenced population of cells migrated significantly ($p<0.05$) faster than the siScr and siMMP14 population (data not shown), a finding suggesting that the loss of Nck may increase the sensitivity to EGF-induced chemotaxis through a yet undetermined mechanism. Figure 2.1B shows the morphology and density of cells after 5 hours of migration and 18 hours of invasion. Silencing of target proteins was confirmed by western blotting (Figure 2.1C).

Loss of Nck Reduces Multicellular Tumor Spheroid (MTS) Growth

We assessed the growth of MTSs in complete media for 5 days by measuring spheroid area. Identical seeding densities were used for spheroid formation and after three days, the initial spheroid areas were measured and tracked for five additional days (Figure 2.2A-B). Loss of Nck resulted in significantly smaller ($p<0.05$) spheroids that the scrambled controls (Figure 2.2C). In addition to overall MTS area, we determined

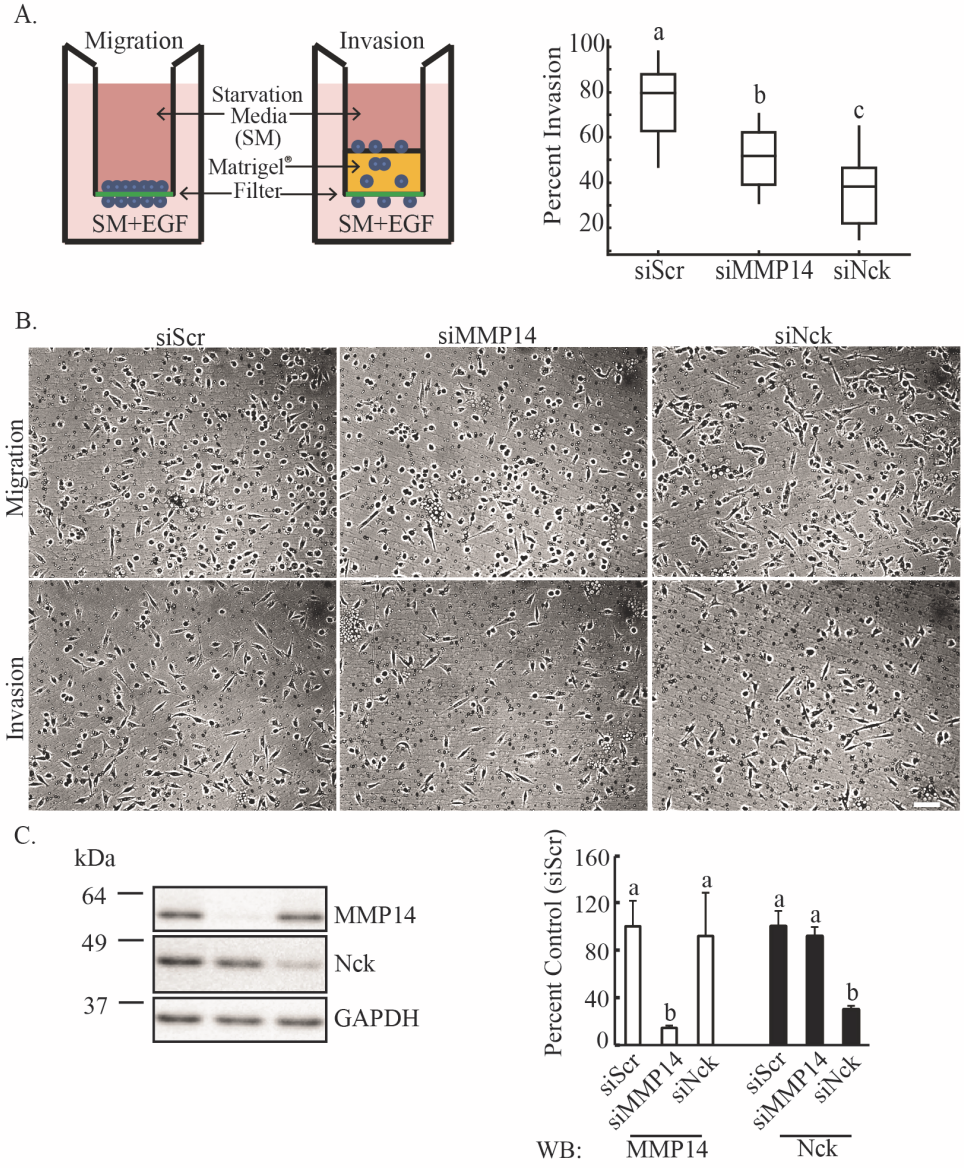

Figure 2.1. Loss of Nck decreases individual mammary carcinoma cell invasion. MDA-MB-231 cells were transiently transfected with small interference (si) RNA oligonucleotides encoding non-targeting sequences (siScr) or sequences targeting MMP14 (siMMP14) or both Nck1 and Nck2 (siNck). **A)** Cells were subjected to migration or invasion assays using BD BioCoat™ Invasion Chambers (left) supplied with 8 µm PET filters uncoated or coated with a laminin-rich matrix (Matrigel) in the presence of EGF (10 ng/ml) used as a chemoattractant. A total of $5x10^4$ cells were seeded and incubated for 5 (migration) or 18 (invasion) hours. Box and whisker plot (right) showing cell invasiveness calculated as percent invasion (invaded cells / migrated cells * 100). Results shown summarize data from three independent experiments performed in triplicate. Different letters indicate a significant difference ($p<0.05$). **B)** Representative photomicrographs showing the bottom surface of filters with cells that migrated or invaded after incubation. Scale bar represents 100 microns. **C)** Representative western blot (left) and quantitative analysis (right, mean ± s.d.) showing the efficacy of protein silencing using siRNA oligonucleotides. Within each group, means with a different letters indicate statistical differences ($p<0.05$).

the change in area as an indicator of growth rate. Based on changes in MTS area, the loss of Nck significantly decreased growth rate ($p<0.05$) relative to scrambled controls.Of note, the growth rates of spheroids formed by scrambled control versus parental/untreated cells were not significantly different ($p>0.05$).

To determine if there was an interaction between cell area and time we applied a general linear model to the data and found a significant interaction only at day 0. Since there was not a significant interaction for the remainder of the time points we reanalyzed the data only looking at the main effects, treatment (Untreated, shScr, shNck) and time. We found that each had a significant ($p<0.001$) effect on spheroid area according to the model. Based on the findings from the general linear model we subjected each time point to one-way ANOVA analysis.

We also analyzed the change in spheroid area using a general linear model to determine if there was an interaction between treatment (untreated, shNck and shNck) and time. The model did not indicate any significant interactions between treatment and time though each main effect resulted in a significant difference ($p<0.001$). Since there was no interaction between treatment and time based on the general linear model, we analyzed each time point using ANOVA analysis.

In spite of similar cell seeding densities, spheroids formed following 72 hours of incubation were significantly smaller ($p<0.05$) in the Nck silenced versus control (Scr) condition. Such difference in area could be attributed to multiple factors including changes in proliferation, volume, and compaction of cell. Thus, we ascertained if the differences in spheroid area were the result of proliferation or migration defect during

spheroid formation, i.e. the initial 72 hours following seeding. The number of cells counted with a hemocytometer following spheroid disaggregation did not differ ($p>0.05$) between the Scr versus Nck-silenced condition (Figure 2.2A). The results suggest that the loss of Nck does not alter proliferation/viability or efficiency of cell aggregation during spheroid formation.

Loss of Nck Reduces Growth-factor Induced Multicellular Tumor Spheroid Invasion in 3D Laminin-rich Matrices

Based on our findings that Nck is required for individual cell migration in response to EGF in the transwell invasion assay, we hypothesized that the loss of Nck would also decrease invasion in 3D cultures of MTS in a laminin-rich matrix. To test this prediction, we used a commercially available kit (Trevigen) following the recommended experimental procedure with slight modifications as detailed in Materials and Methods. The assays use a proprietary invasion matrix with properties similar to those of Matrigel. Using parental MDA-MB-231 cells, we first determined that 5 ng/mL of EGF constitutes a physiologically relevant dose capable of stimulating invasion (Appendix B). Then, we formed spheroids of Scr control, MMP14-, and Nck-silenced cells and allowed them to invade in the presence of 5 ng/mL EGF for three days. The results show that Nck silencing significantly ($p<0.05$) reduced invasion distance by greater than 30% relative to scrambled controls as early as day 1 (Appendix C) and the decreased invasion was maintained through day 3 (Figure 2.3). Consistent with the

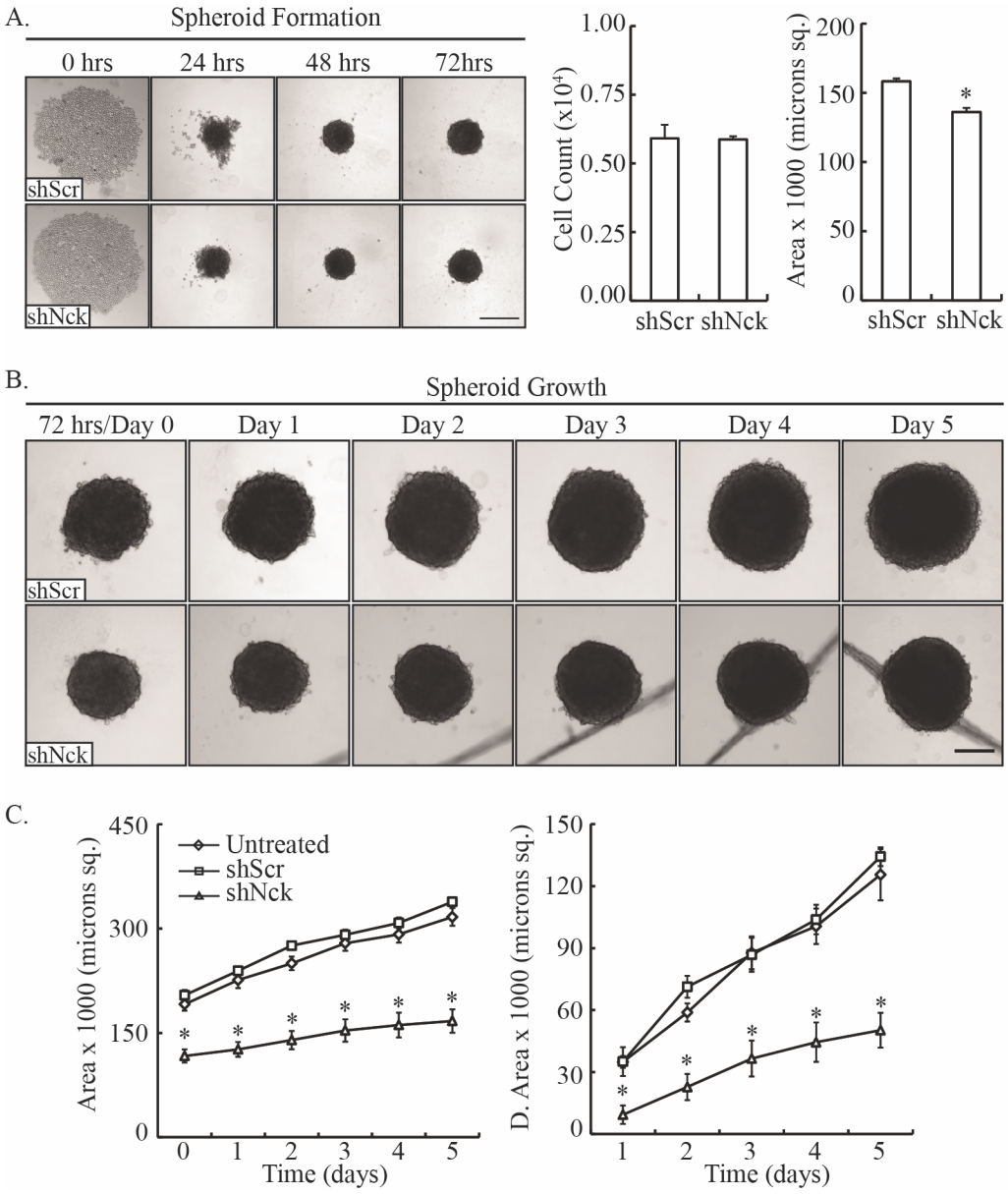

Figure 2.2. Loss of Nck reduces growth of mammary carcinoma cell multicellular tumor spheroids in laminin-rich matrices. MDA-MB-231 cells expressing short hairpin (sh) RNAs encoding non-targeting sequences (shScr) or sequences targeting Nck (shNck) were subjected to a spheroid growth assay. **A)** Representative photomicrographs of spheroid formation (left). Bar graph depicting total cell number (center) and area (right) per spheroid (mean ± s.e.m.) measured at 72 hours. Results from two independent experiments, total 15 spheroids. Scale bar equals 500 microns. **B)** Representative photomicrographs of spheroid growth. Scale bar equals 250 microns. **C)** Total spheroid area (left) and change in spheroid area (right) from day 0-5 after spheroid formation (mean ± s.e.m.) D. Area represents differential area (Day X – Day 0). Results summarize data from two independent experiments; each consisted of three spheroids per condition. * indicates p-value < 0.05.

results from growth profiling experiments the Nck silenced spheroids were slightly smaller ($p<0.05$) than the scrambled controls at day 0 (Figure 2.3B).

We found that mammary carcinoma cells cultured in 3D laminin-rich matrices (Figure 2.3A, insets) invade through a collective streaming-like mechanism (32). Cells located at the invasive front (leader cells) in control (Scr) and MMP14-silenced spheroids exhibited a mesenchymal phenotype characterized by elongated invasive protrusions that extended into the matrix. In contrast, streams of mostly rounded cells lacking leader cell differentiation or displaying leader cells with less pronounced protrusions were observed in Nck-silenced spheroids (Figure 2.3A). Silencing MMP14, on the other hand, had no effect on invasion distance. This finding suggests that the invasion defect of siNck cells in 3D laminin-rich matrices is independent of matrix degradation by MMP14. However, our results showed negligible invasion when parental cells were incubated in the presence of GM6001, a broad-spectrum MMP inhibitor. Together; these results suggest that although MMP14 activity might be dispensable, the overall MMP activity is still required for carcinoma cell invasion in 3D laminin-rich matrices (Figure 2.4).

The siRNA silencing methodology employed for MTS assays deviated slightly from the manufacturers established protocol (see Materials and Methods); however, we confirmed efficacious silencing of target by western blotting in each independent experiment (Figure 2.3C). We also tested potential effects of the transfection reagent and the scrambled siRNA oligonucleotide in carcinoma cell invasion. We found that the transfection reagent alone did not significantly decrease invasion distance; however,

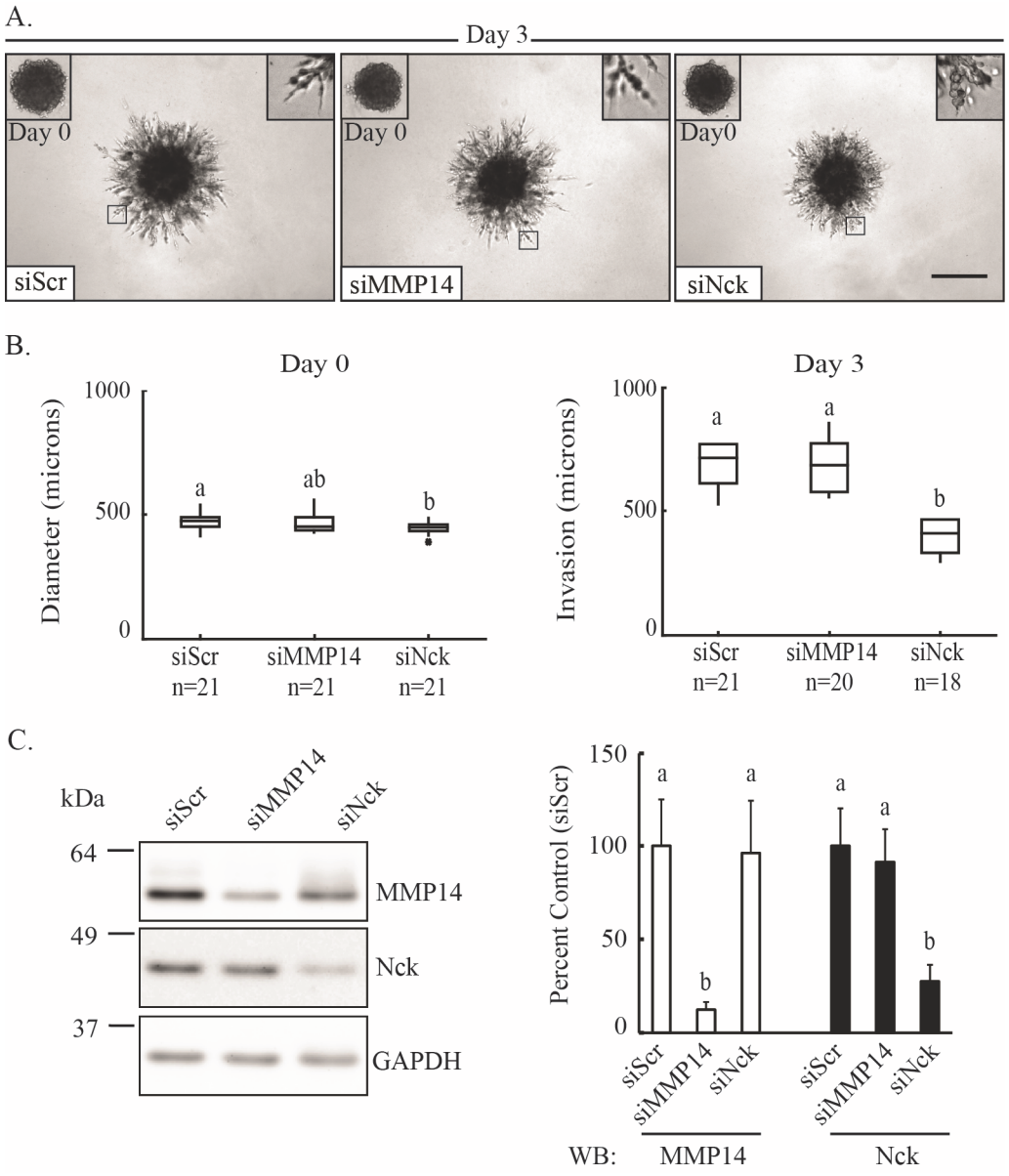

Figure 2.3. Loss of Nck reduces invasion of mammary carcinoma cells in 3D laminin-rich matrices. MDA-MB-231 cells were transiently transfected with small interference (si) RNA oligonucleotides encoding non-targeting sequences (siScr) or sequences targeting MMP14 (siMMP14) or Nck (siNck). Subsequently, cells were subjected to a spheroid invasion assay using laminin-rich matrix (Trevigen) in the presence of EGF (5 ng/mL). **A)** Representative photomicrographs of spheroids at day 0 (left insets) and day 3 of invasion. Boxed areas were magnified to show morphology of invading cells (right insets). Scale bar equals 500 microns. **B)** Box and whisker plots showing average spheroid diameter at day 0 (left) and invasion distance at day 3 (right). Results shown summarize data from four independent experiments (n=total number of spheroids examined) **C)** Representative western blot (left) and quantitative analysis (mean ± s.d., right) showing the efficacy of protein silencing using siRNA oligonucleotides. Cells were grown in 2D culture for 96 hours for western blot analysis. Within each group, means with a different letters indicate a significant difference ($p<0.05$).

transfection of the scrambled siRNA resulted in a slight, but significant decrease in invasion at day 3, but not at day 1 or day 2 (Figure 2.4). We also confirmed that the DMSO carrier for GM6001 did not influence invasion behavior of MDA-MB-231 (Appendix D).

Loss of Nck Reduces Growth Factor Induced Multicellular Tumor Spheroid Invasion in 3D Collagen I

Fibrillar collagen, a major constituent of the breast tissue microenvironment (147), is known to play a major role in the mechanical properties of the mammary gland (148). Based on our previous findings that loss of Nck reduces invasion in laminin-rich matrices, we hypothesized that the loss of Nck would also reduce invasion in dense collagen I matrices. To test this prediction, we prepared MTSs using cells stably expressing non-targeting shRNAs or shRNA targeting MMP14, or Nck1 and Nck2. Spheroids were subsequently embedded in 2 mg/mL acid-extracted rat-tail collagen type I polymerized at 37^{o}C/ pH7.4, a procedure that increases the density of the meshwork and decreases the diameter of individual fibers (149). We determined that silencing of Nck or MMP14 significantly ($p<0.05$) reduces invasion distances nearly 40% and 25%, respectively, compared to scrambled controls (Figure 2.5). We also observed that loss of Nck resulted in significantly ($p<0.05$) smaller spheroid size at day 0 (Figure 2.5B). In addition, breast carcinoma cells appear to use a mix of mesenchymal and amoeboid mechanisms of migration. Whereas invading cells in Scr spheroids displayed a typical mesenchymal morphology, invading cells in MMP14-silenced spheroids exhibited a more rounded, amoeboid appearance. Invading cells in the Nck-silenced spheroids, on

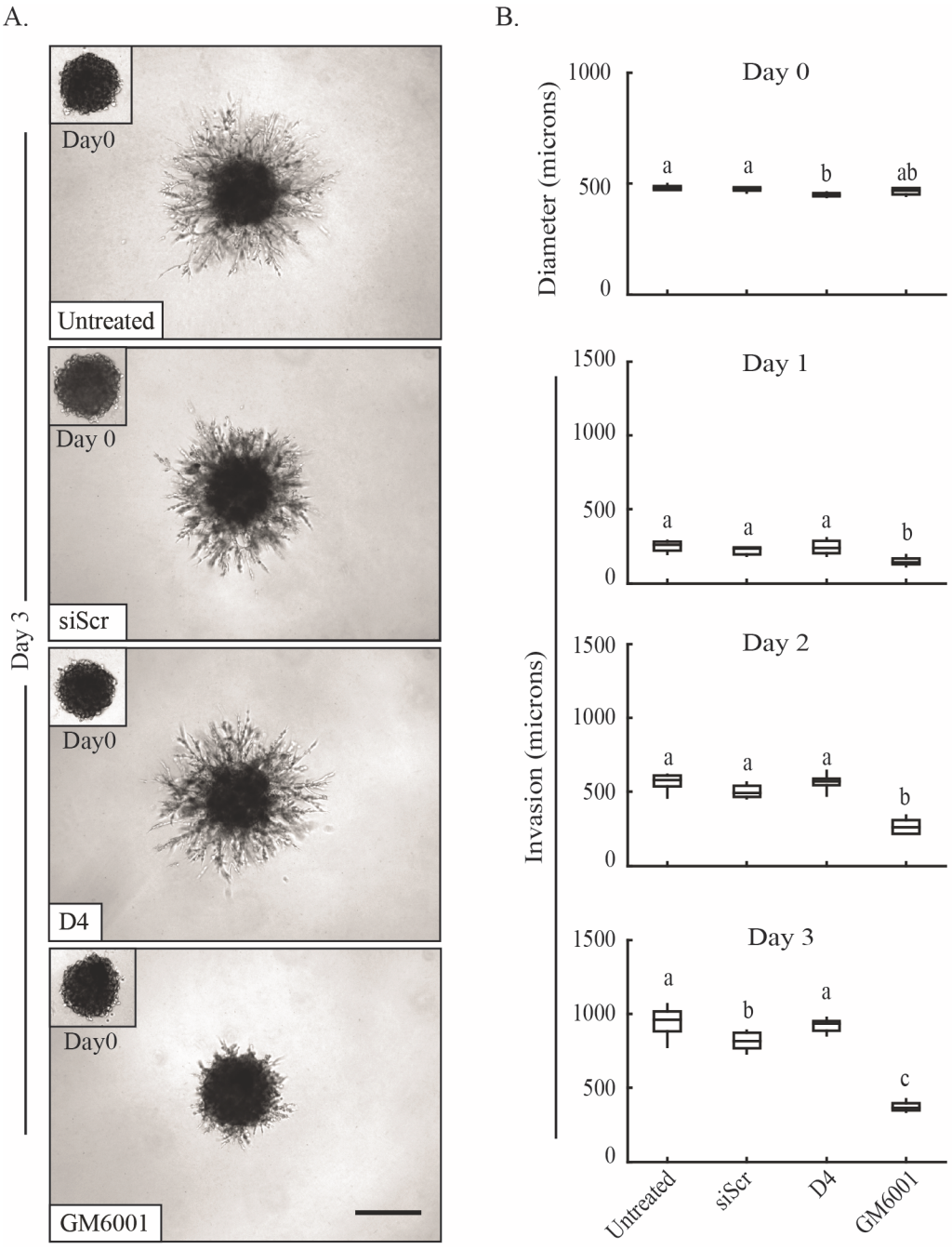

Figure 2.4. Invasion in 3D laminin-rich matrices requires MMPs and is not inhibited by the siRNA transfection reagent. MDA-MB-231 cells were left untreated or transiently transfected with small interference (si) RNA oligonucleotides encoding non-targeting sequences (siScr) or sequences targeting MMP14 (siMMP14) or Nck (siNck). Alternatively, cells were exposed to DharmaFECT4 transfection reagent alone (D4), or the broad-spectrum metalloproteinase inhibitor (GM6001). **A)** Representative photomicrographs of spheroids cultured in the presence of EGF (5 ng/mL) and allowed to invade for 0 (insets) or 3 days. Scale bar equals 500 microns. **B)** Box and whisker plots showing spheroid diameter at day 0 and invasion distance at days 1-3. Different letters represent statistically different values ($p<0.05$).

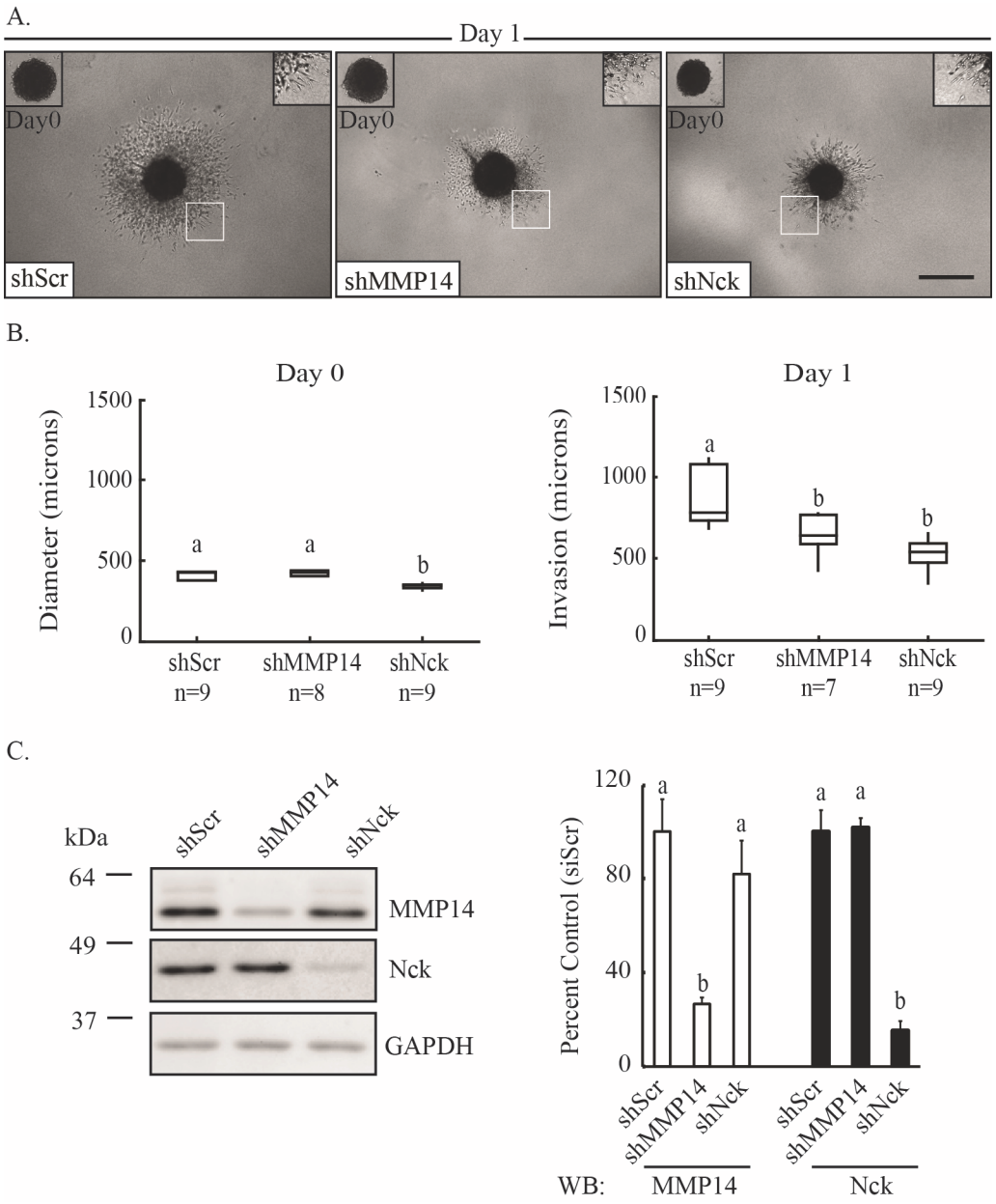

Figure 2.5. Loss of Nck reduces invasion of mammary carcinoma cells in 3D collagen matrices. MDA-MB-231 cells expressing short hairpin (sh) RNAs encoding non-targeting sequences (shScr) or sequences targeting MMP14 (shMMP14) or Nck (shNck) were subjected to a spheroid formation assay in a collagen I matrix in the presence of EGF (5 ng/mL). **A)** Representative photomicrographs of spheroids at day 0 (insets) and day 1 of invasion. Results shown summarize data from three independent experiments performed in triplicate. Scale bar equals 500 microns. **B)** Box and whisker plot showing spheroid diameter at day 0 (left) and invasion distance at day 1 (right). **C)** Representative western blot (left) and quantitative analysis (right) showing the efficacy of protein silencing using shRNAs. Cells were grown in 2D culture for western blot analysis. Different letters represent statistically different values ($p<0.05$).

the other hand, exhibited a mixed phenotype (Figure 2.5A, inset) (32). We confirmed efficacy of target protein knockdown through western blot (Figure 2.5C).

Loss of Nck in MDA-MB-231 Xenografts Reduces Primary Tumor Growth and Metastasis

Results from experiments in 3D matrices prompted us to test the role of Nck in tumorigenesis and metastasis. Breast carcinoma cells stably expressing non-targeting versus Nck-targeting shRNAs were injected bilaterally into the flanks of nude mice and tumor size was monitored for nine weeks. No differences were observed in primary tumor initiation; however, the results show a significant reduction ($p<0.05$) in tumor xenograft growth in mice injected with Nck-silenced versus control cells (Figure 2.6). In both control and Nck-silenced groups, we observed that 7 of 7 mice developed primary tumors in 12 (shNck) or 13 (shScr) of 14 injection sites. One mouse from shScr and two mice from shNck group failed to develop bi-lateral tumors. We tracked tumor volume weekly over the duration of the study and found that mice injected with the shNck cell population had significantly ($p<0.05$) smaller tumors after 6 weeks post injection (Figure 2.6B). To confirm that this analysis was appropriate we applied a general linear model to our data to determine if there was a significant interaction between time and treatment. We found no significant interaction between time and treatment; however, we determined each main effect was statistically significant ($p<0.001$). In addition, tumor mass was measured at experiment termination and the shNck tumors weighed ($p<0.071$) less than the control tumors (Figure 2.6B). Images of visible tumors were taken at two weeks and again at eight weeks as a visual reference for the difference in size between

the two groups (Figure 2.6C). The levels of Nck protein in both cell populations were confirmed by western blotting (Figure 2.6D).

The cell line and experimental model selected for the *in vivo* assay were also capable of producing micrometastases in distal organs, the lungs being a primary site for colonization. Lung samples were processed and subjected to real-time PCR to detect human-specific GAPDH gene expression, which has been previously shown as an indicator of human cells in mouse lung tissue due to metastasis (150). We confirmed the specificity of the probes used in this study by testing them against human breast cancer cDNA and mouse tissue cDNA (Figure 2.7). We observed that 4 of 7 mice injected with shScr cells had greater than 6-fold increase in expression of human GAPDH in the lung tissue while there were none in the shNck injected group (Figure 2.7). A conservative threshold of 6-fold was selected based on potential bias introduced when using only a single reference gene (151). In addition, the average fold change, calculated using the $\Delta\Delta C_T$ method (145), of human GAPDH in the lung tissue for the scrambled group was greater than 40 fold higher than shNck group, with a considerable trend towards significance ($p= 0.0552$). Together these results strongly suggest a role for Nck as a regulator of breast carcinoma growth, invasion and metastasis.

Discussion

Results from this study show that Nck signaling contributes significantly to breast cancer progression. More specifically, this study highlights the contribution of Nck to key hallmarks of the malignant phenotype including: i) growth of primary tumors, and ii) invasion and metastatic dissemination. These novel findings support the

A.

Subcutaneous Tumors			
Cell Line MDA-MB-231	Number of Cells Injected	Mice with Primary Tumors	Number of Primary Tumors
shScr	$2X10^6$	7/7	13/14
shNck	$2X10^6$	7/7	12/14

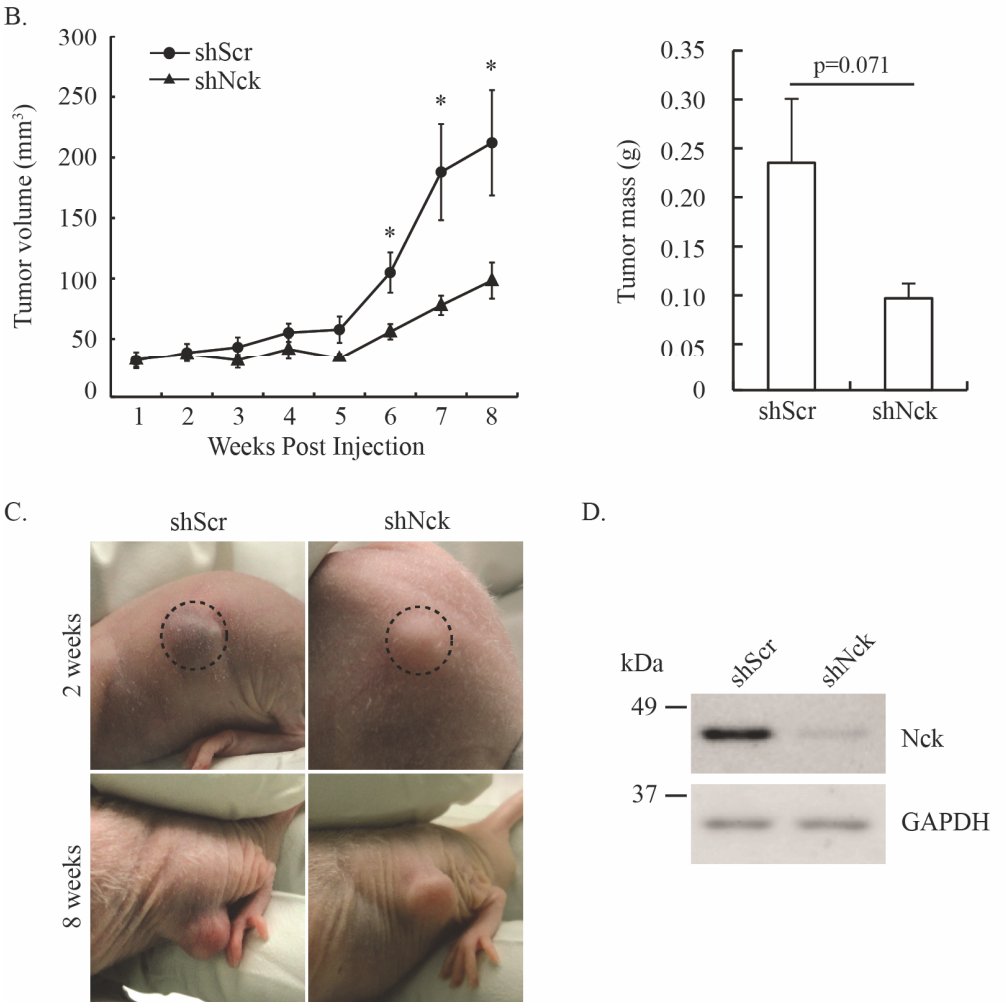

Figure 2.6. Loss of Nck reduces primary tumor growth. Six to nine week old nude mice (NU/J) received subcutaneous, bilateral flank injections of MDA-MB-231 cells expressing short hairpin (sh) RNAs encoding non-targeting sequences (shScr) or sequences targeting Nck (shNck). **A)** Summary of xenograft tumor development 9 weeks post-injection. **B)** Analysis of xenograft tumor growth (left) and mass (right). Tumor volume was assessed weekly using a caliper and tumor mass was determined after dissection at sacrifice 9 weeks post-injection. Values represent means ± s.e.m. Statistical differences are indicated ($p<0.05$). **C)** Representative images of tumors at 2 and 8 weeks post injection. Dotted circle highlights early tumor location. **D)** Western blot showing Nck levels in cells from same populations injected into mice. GAPDH levels were used to monitor equal loading.

A.

Tumor Metastasis	
Cell Line MDA-MB-231	Human GAPDH Positive Lungs / Total Lungs Analyzed
shScr	4/7
shNck	0/7

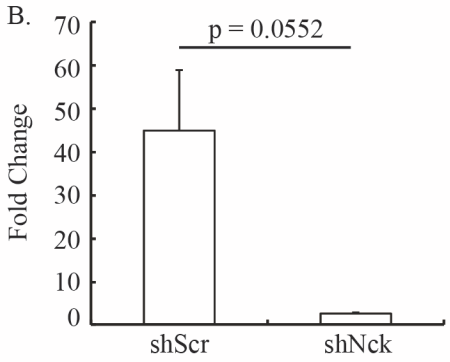

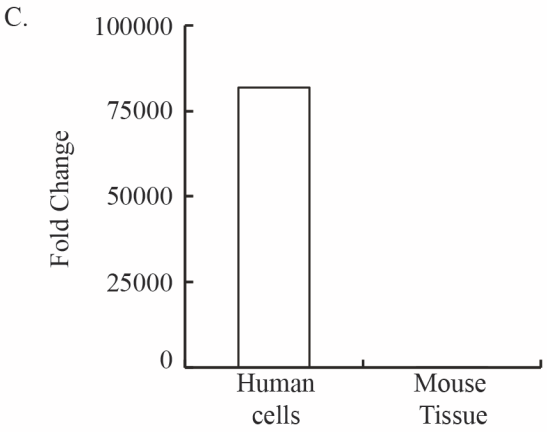

Figure 2.7. Loss of Nck reduces breast carcinoma metastasis. MDA-MB-231 micrometastases in lungs were detected 9 weeks after tumor cell injection by quantitative (q) PCR. **A)** Proportion of animals with lung metastases was determined by q-PCR amplification of human GAPDH. Positive samples were determined based on greater than 6-fold increase in human GAPDH expression level in the lungs. **B)** Human GAPDH fold change was quantified to determine extent of lung metastasis. **C)** Human GAPDH fold change was quantified in human cells and mouse tissue to determine human GAPDH probe specificity. Fold change was calculated using the $\Delta\Delta C_T$ method.

hypothesis that Nck adaptors constitute an important signaling node integrating microenvironmental cues promoting tumorigenesis and metastasis. This study validates Nck as a target of intervention in aggressive breast cancer and paves the way for future research to develop new therapeutics that specifically disable interactions of Nck with key binding partners involved in mammary carcinogenesis.

Previous studies using 2D *in vitro* cultures highlighted a role for Nck, alone or in cooperation with Src, in invadosome formation, matrix degradation, and serum-stimulated transwell invasion (72, 100). Because activation of signaling through the EGFR drives epithelial-to-mesenchymal transition and promotes breast cancer metastasis (152), we specifically focused on how Nck signaling modulates the behavior of mammary carcinoma cells in response to EGF. We postulated that Nck-dependent actin remodeling facilitates EGF-stimulated invasion through a mechanism that involves increased motility and matrix remodeling by MMP14. Using EGF as a chemoattractant in a transwell system we determined that Nck depletion not only reduces the invasion index, a ratio between cell invasion and cell migration, but it does to a larger extent than MMP14 deficiency. This observation supports the notion that Nck promotes invasiveness of mammary carcinoma cells through a complex, multi-layered mechanism of regulation that involves the fine-tuning of MMP14 levels/activity at the cell surface. Interestingly, Nck depletion resulted in a slight but significant increase in chemotaxis toward EGF (data not shown). The seemingly increased sensitivity to EGF resulting from Nck silencing is interesting in the light of recent findings showing that secreted

factors released by cells deficient in Arp2/3, an actin nucleation/polymerization complex activated downstream of Nck, alter EGF chemotaxis in a nonautonomous manner (153).

Multicellular tumor spheroids in 3D culture provide an important model to investigate tumor biology that more closely mimics the *in vivo* environment (154, 155). The present study shows, for the first time, a requirement for Nck in breast carcinoma invasion in both 3D laminin-rich and collagen I matrices. During the course of these studies we observed, surprisingly, that invasion in 3D laminin-rich matrices is unaffected by MMP14 silencing, although MMP14 is required for individual/single cell invasion through such matrices. Interestingly, breast carcinoma cells displayed a rounded morphology and appeared to migrate using a multicellular streaming mode of migration in 3D laminin-rich matrices. In addition, although the overall MMP activity is required for breast carcinoma cell invasion in 3D laminin-rich matrices (Figure 2.4), MMP14 is dispensable. Together, these results suggest that there are important differences in mechanisms driving individual versus multicellular/collective cell invasion. The strong inhibitory effect of Nck silencing in invasion in 3D laminin-rich matrices, on the other hand, points to an important role of these adaptors in regulating invasiveness through actin remodeling/cell motility independently of the surface expression/activity of MMP14.

A major component of the breast microenvironment is fibrillar collagen; it is known that cross-linked collagen contributes to ECM stiffening and acts synergistically with growth factor signaling to increase invasion and metastasis (20, 147, 156). Therefore, for our 3D invasion studies we chose acid-extracted collagen, a preparation

suitable for enzymatic cross-linking (140). It has been shown that highly cross-linked collagen I more closely resembles the tissue ECM and provides an environment conducive to testing MMP14-dependent carcinoma cell invasion (26). Using this model, we determined that loss of Nck decreases mammary carcinoma cell invasion to a greater extent than MMP14 silencing. Since invasion through collagen-rich matrices requires both the accumulation/activation of MMP14 at the cell surface and actin remodeling/increased cell motility, we speculate that a combination of both processes underlies decreased invasiveness resulting from abrogation of Nck signaling.

Although the loss of Nck did not alter tumor initiation, tumor growth was reduced by Nck depletion. Likewise, similar numbers of cells in shScr versus shNck spheroids suggests that spheroid formation in 3D laminin-rich matrices was not compromised by Nck depletion. However, the growth rate of Nck-deficient spheroids versus control/Scr was significantly reduced over a period of 5 days following spheroid formation. Of interest, a recent study demonstrated a role for Nck in regulating gene expression by acting as a scaffold for the assembly of the cytoplasmic capping complex (157), a cellular ensemble known to modulate mRNA stability. In contrast, growth of primary mammary tumors was not affected by silencing of N-WASp (64); an Arp2/3-nucleation promoting factor directly activated by Nck. Ascertaining the role of Nck in tumor cell viability/proliferation and underlying mechanisms of regulation, i.e. cytoskeletal dependence, warrants further investigation. The hypothesis that Nck promotes tumor growth through stimulation of tumor angiogenesis is currently being tested.

In sum, using a combination of *in vitro* and *in vivo* models, we show here that Nck signaling enables breast carcinoma tumorigenesis and metastasis. The present results lay the groundwork for future research to identify new therapies that, by specifically disabling Nck-dependent interaction, may provide alternative treatment for patients with malignant breast cancer.

CHAPTER III

REGULATION OF ACTIN DYNAMICS AND MEMBRANE LOCALIZATION OF MMP14 BY NCK ENABLES BREAST CARCINOMA CELL INVASION

Introduction

Breast carcinoma invasion and metastasis requires reciprocal interactions between tumor cells and their microenvironment. Changes in tissue architecture brought about by these interactions are the result of both cytoskeletal rearrangements in tumor cells and remodeling of the ECM. Invadosomes are actin-based cellular structures enriched with MMPs that play a direct role in remodeling the extracellular matrix (130). In cancer cells, invadosomes are specifically termed invadopodia, while in non-cancer cells related structures are referred to as podosomes (28). Although invadopodia were initially described in 2D cultures, recent findings suggest that related invasive structures are also found in tissues. For example, a role for invadopodia *in vivo* has been linked to invasion of basement membrane by transformed epithelial cells in the digestive tract of *D. rerio* (158); intravasation, extravasation and lung metastasis of mammary cells (64, 159), and breaching of the basement membrane and invasion by anchor cells in *C. elegans* (160, 161). Together, these findings highlight invadopodia as important organelles used by malignant tumor cells in invasion and metastasis.

The formation of invadopodia involves localized actin polymerization stimulated primarily by the Arp2/3 complex. Activity of the Arp2/3 complex is greatly enhanced by the nucleation promoting factor N-WASp (130). Regulatory domains and motifs located

in the N-terminal region of N-WASP enable protein-protein and lipid-protein interactions that alter the molecular conformation of N-WASp and modulate the activity of the Arp2/3 complex (61). The adaptor Nck, consisting of three N-terminal SH3 domains and one C-terminal SH2 domain, has been shown to bind through its SH3 domains a proline-rich segment of N-WASp (120). Similarly, the inositol phospholipid PI(4,5)P2 and the small GTPase Cdc42, respectively, interact with the basic region and CDC42/Rac interactive binding (CRIB) domain in N-WASp (162). These interactions act cooperatively to disrupt intramolecular interactions that hold N-WASp in an auto-inhibited conformation. The relief of auto-inhibition results in exposure of the VCA "output" region of N-WASp which becomes available to engage actin monomers and the Arp2/3 complex (163).

Remodeling of the ECM is dependent on focalized activity of MMPs (22, 25). It has been shown that MMP14 plays a central role in matrix degradation at invadopodia; whereas its inactivation decreases the invasive capacity of cancer cells, the loss of other type I collagenolytic metalloenzymes has little effect (26, 29, 131). MMP14 also acts indirectly to degrade the ECM by activating two secreted MMPs, MMP2 and MMP9 (29). It has been suggested that intracellular trafficking is a key mechanism regulating the cell surface levels/activity of MMP14 (29, 164).

Another important layer of regulation in breast carcinoma cell invasion is provided by the activation of tyrosine phosphorylation, in particular activation of the EGF receptor (EGFR) and Src (165). Tyrosine phosphorylation of scaffold proteins such as cortactin and Tks5 by EGFR/Src generates docking sites for Nck, which is recruited

through its SH2 domain. The resulting signaling complex drives activation of N-WASp/Arp2/3-dependent actin polymerization, invadopodia formation, and localized matrix degradation (72, 100). However, the exact contribution of Nck to actin dynamics at invadopodia and membrane localization/activity of MMP14 remains poorly understood.

We hypothesized that Nck promotes invasion and metastasis by altering actin dynamics and membrane localization of MMP14 through spatiotemporal regulation of Cdc42 activation.

Materials and Methods

Cell Culture

MDA-MB-231 (CRM-HTB-26) and 293T (CRL-3216) were purchased from American Type Culture Collection (ATCC) and cultured in DMEM high glucose (HyClone) without sodium pyruvate (MDA-MB-231) or with sodium pyruvate (293T) supplemented with 1% penicillin/streptomycin and 10% fetal bovine serum (FBS) (Gemini), at 37^{o}C in an atmosphere with 5% CO_2. MDA-MB-231 were sub-cultured every 4-5 days at ~5x10^3 cells/cm^2 and 293T were sub-cultured every 4-5 days at ~2x10^4 cells/cm^2. For sub-culture, cells were washed twice with warm DPBS and incubated with 0.05% Trypsin/0.53 mM EDTA in HBSS without sodium bicarbonate (Cellgro®) for 5 minutes at room temperature (MDA-MB-231) or 1 minute at 37^{o}C (293T). Trypsin was neutralized using complete growth media and cell were centrifuged at 800 rpm for 3 minutes then re-suspended in complete media, counted by hemocytometer and plated in plastic tissue culture plates

Antibodies

Western blot: anti-Nck antibody (Millipore, 06-288) was diluted 1:4000 in 3% NFDM, anti-GFP antibody was diluted 1:4000 in 3% NFDM, anti-MMP14 antibody (Millipore, MAB3328) was diluted 1:2000 in 1% NFDM and anti-GAPDH antibody (Invitrogen, 43700) was diluted 1:10,000 in 1% NFDM. For secondary antibodies goat anti-mouse IgG-HRP (Santa Cruz Biotechnology, sc-2055) and goat anti-rabbit IgG-HRP (Santa Cruz Biotechnology, sc-2030) were diluted 1:10,000 in NFDM at the same concentration used for probing with primary antibody. Fluorescent Gelatin Degradation: Texas Red®-X Phalloidin 1:200 (Life Technologies T7471), anti-cortactin 1:200 (Millipore #05-180), anti-MMP14 antibody 1:100 (Millipore, MAB3328), Alexa Fluor® 647Goat Anti-Mouse IgG (H+L) 1:500 (Life Technologies A-21235), NucBlue® Live ReadyProbes® Reagent (Life Technologies R37605).

siRNA Transfection

siRNA transfections were carried out according to the manufacturers protocol (Dharmacon). The transfection of siRNA for all experiments was carried out with the standard conditions of 50 nM siRNA for MT1-MMP, Nck1 and Nck2 and 25 nM scrambled siRNA. For MDA-MB-231 cells DharmaFECT 4 transfection reagent was used at multiple concentrations based on cell seeding density: $20x10^4$ cells in a 35-millimeter dish use 2.5 μL/mL DharmaFECT 4 and $30x10^4$ cells in a 35-millimeter dish use 3 μL/mL DharmaFECT 4. The general protocol involved incubating siRNA and transfection reagent in separate tubes containing serum-free and antibiotic-free media for 5 minutes. The tubes were then combined and incubated for 20 minutes before the entire

contents of the tube was added to a plate containing the appropriate volume (1.6 mL for 35-millimeter dish) of antibiotic free complete media and incubated for six hours. After six hours the media was replaced with fresh complete media. Experiments were started between 48 and 72 hours post transfection with siRNA based on specific assay.

Plasmids and Viral Transduction

Virus was produced as previously described with minor modification (135, 136). A detailed description of the protocol for viral transduction can be found in Appendix P and Appendix Q. Briefly, virus were produced in 293T cells by calcium precipitation with pSuper.puro/hygro carrying oligonucleotide sequences (shRNA) either non-targeting (shScr) (scrambled sequence - Oligo2, Dharmacon non-targeting siRNA SMARTPool) or targeting human Nck1 or Nck2 (shNck) (137) for protein knockdown. For expression, pMSCV carrying cDNA for actin-EYFP or LifeAct EYFP was used. We also used the Raichu Cdc42 Förster resonance energy transfer (FRET) probe (166). Plasmids were co-transfected with pHCMV-G and pMD.gag.pol plasmids and incubated with chloroquine (25 μM) for 4-6 hours, then media was exchanged and virus collected 20-48 hours later and either spun at 3500 rpm for 10 minutes and distributed in 1 mL aliquots for storage at -80^{o}C or filter sterilized with a 0.22 μm syringe filter and used immediately. MDA-MB-231 were infected in the presence of 8 μg/mL polybrene and selected for 2-3 days in the presence of 1 μg/mL puromycin and/or 800 μg/mL hygromycin. Lipofectamine 2000 was used according to the manufacturer's protocols (see Appendix J) to transiently express pcDNA3.1 MT1-MMP mCh (167).

Western Blotting

Western blotting was performed as described by the manufacturer (Bio-Rad) and as previously described (137). A detailed protocol for western blotting can be found in Appendix L. Briefly, lysates were prepared for western blot by first washing adherent cultures twice with cold DPBS then harvesting with ice-cold kinase lysis buffer (25 mM Tris, pH 7.4, 150 mM NaCl, 5 mM EDTA, 10% glycerol, 1% Triton X-100, 10 mM β-glycerophosphate, 1 mM sodium orthovanadate, 10 mM sodium pyrophosphate, 10 μg/L aprotinin and 1 mM phenylmethylsulfonyl fluoride) and the cells collected using a cell scraper. Lysates were vortexed briefly and incubated on ice for 15-30 minutes, then centrifuged at max speed for 10 minutes in a refrigerated centrifuge. Cleared lysate was transferred to a fresh tube and stored at -80^{o}C or protein concentration immediately quantified using a Bradford Assay (Bio-Rad). For western blotting, sodium dodecyl sulfate-polyacrylamide gel electrophoresis (SDS-PAGE) was performed on equal amounts of protein prior to transfer to nitrocellulose membranes and blocking with non-fat dry milk (NFDM). Blots were probed with primary antibody in blocking solution overnight at 4^{o}C then washed 5 times for 5 minutes in TBST. Blots were incubated with secondary antibody in blocking solution for 1 hour at room temperature then washed 5 times for 5 minutes in TBST. Washed membranes were then incubated with enhanced chemiluminescence substrate (Western Lightening® Plus-ECL NEL103001) for 1 minute before imaging on ImageQuant™ LAS 4000 mini documentation system. Images were analyzed using FIJI software.

Fluorescent Gelatin Degradation Assay

Fluorescent gelatin degradation was performed as described previously (168). A detailed protocol can be found in Appendix F. In brief, MDA-MB-231 cells were transiently transfected with small interference (si) RNA oligonucleotides encoding non-targeting sequences (siScr) or sequences targeting MMP14 (siMMP14), or Nck (siNck). A total of $7.5x10^4$ cells were allowed to degrade 0.2% Alexa-488 conjugated gelatin for 6 hours at 37^oC in an atmosphere of 5% CO_2 then fixed with 3.7% PFA/5% sucrose. For labeling of actin and cortactin, cells were permeabilized with 0.2% Triton X-100, blocked with 2% BSA and stained with Texas Red®-X phalloidin and/or immunolabeled with anti-cortactin. For labeling of actin and MMP14, non-permeabilized cells were blocked in 2.5% human serum/5% goat serum and then stained with Texas Red®-X phalloidin and immunolabeled with anti-MMP14. Cells were imaged using a Zeiss LSM780 confocal microscope equipped with a Plan-Apo 40X/1.40NA oil objective or an Olympus IX70 inverted microscope equipped with an Olympus Plan-Apo 60X/1.40NA oil objective, a Spot RT3 Camera (7.4 μm x 7.4 μm pixel size) and Spot software. Image analysis was performed using FIJI as previously described (169, 170). FIJI was used for image presentation by first background subtracting each channel using rolling ball method with a radius of 50 pixels, followed by filtering gelatin channel using Gaussian Blur with a sigma (radius) of 1.0.

Fluorescence Recovery After Photobleaching (FRAP)

FRAP was previously described with some modifications as detailed in Appendix K (171, 172). Briefly, FRAP was performed with the following settings:

image acquisition pixel dwell time 0.79 μs/pixel, resolution 512 x 512 pixels, 2.4% 514 nm laser power; photobleaching pixel dwell time 90 μs/pixel, region of interest 166 x 164 pixels, 100% 514 nm laser power. After collection of pre-bleach images, the region of interest was photobleached and recovery was measured from six sequential scans beginning immediately after photobleaching and then at 1.94 second intervals. FRAP data was collected from at least 30 images and 3-15 actin puncta per image from two culture dishes per experimental group. The rate constant (k) was estimated for fluorescence recovery by fitting data to the following equation: $FI = A\ (1\text{-}e^{-kt}) + B$, where FI represents the percent fluorescence intensity at a given time, A represents the percent fluorescence recovery of the bleached structure at equilibrium and B represents percent fluorescence intensity immediately after photobleaching. Data from at least 80 actin-EYFP puncta from each experimental group were pooled for regression analysis (GraphPad Software) to extrapolate fluorescence recovery as a function of time.

Cdc42 Activity FRET

A detailed protocol is available in Appendix T. Briefly, time-series images were acquired of MDA-MB-231 cells expressing scrambled or Nck shRNA and the Raichu/Cdc42 single chain FRET probe every minute for 60 minutes using a Zeiss LSM780 confocal microscope equipped with a Plan-Apo 40X/1.40NA oil objective. Ratio maps for visualization of Cdc42 activity were generated using Biosensor Processing Software 2.1 in MATLAB (173). Image processing for analysis was performed by first processing the CFP channel stack and FRET channel stack using a 3x3 median filter. Then, the median filtered stacks were used to create a ratio stack of

the FRET channel divided by the CFP channel. Analysis area was limited to individual cells using regions of interest and the average FRET ratio over one hour was determined.

Total Internal Reflection Fluorescence Microscopy (TIRF)

A detailed protocol is available in Appendix O. Briefly, shScr and shNck MDA-MB-231 cell populations were transiently transfected using Lipofectamine 2000 with pcDNA3.1 MT1-mCh (167) (see Appendix J for detailed protocol). Cells were incubated for one hour with transfection reagent and plasmid then fresh complete media without antibiotic was added. The cells were incubated overnight. The following day, approximately 20 hours before TIRF imaging the cells were lifted and plated on fibronectin coated 35-millimeter MatTek dishes. For fibronectin coating, 1 mL fibronectin (10 μg/mL) was added directly to the glass bottom of the MatTek dish and incubated at room temperature for 1 hour. After 1 hour the fibronectin was removed and replaced with 200 μL of phenol-red free complete media for ~15 minutes while the cells were lifted and counted. Approximately $4X10^4$ cells were plated in 200 μL phenol-red free complete media and allowed to adhere for 1 hour. After 1 hour, 2 mL of phenol-red free complete media was added to each MatTek dish and the cells incubated at 37°C in normal growth conditions overnight. One hour before imaging media was exchanged to remove any non-adherent cells and to add phenol-red free complete media with 25 mM HEPES for imaging. Imaging was performed on a Zeiss Axio Observer Z1 TIRF 3 microscope, equipped with a plan-apochromat 100X/1.46NA oil objective and a Roper S/W PVCAM. Samples were placed on the microscope stage at 37°C with 5% CO_2 and allowed to equilibrate for a minimum of 15 minutes before imaging. Samples were kept

on the stage for approximately 1 hour 30 minutes total time for equilibration and imaging. The TIRF angle was set at 74^{o} and images were acquired every 3 seconds for a total of 5 minutes.

To quantify MMP14 mobility we calculated the "displacement index" DI as previously described (174, 175). The DI was calculated by dividing the total area of MMP14 mCherry present during the 5 minute time-lapse (as a result of a maximum projection) by the area of MMP14 mCherry in the first image.

Statistics

When comparing multiple groups with normal distributions ANOVA with a Tukey post-hoc was used. If data did not approximate a normal distribution a Mann-Whitney non-parametric analysis was performed or when applicable data was log transformed followed by ANOVA or a student's t-test. For data depicted as box and whisker plots the bottom and top of the boxes are the first and third quartile, respectively, whereas the band inside is the middle quartile (median). The ends of the whiskers extend to the lowest and highest values excluding outliers. Grubbs outlier test was used to identify and remove outliers. Significant values where a specific p-value is not listed indicate a p-value < 0.05.

Results

RNAi Silencing was Specific and Effective in Targeting Nck1 and Nck2

We used a commercial siRNA silencing system manufactured by Dharmacon. Due to the sequence homology between Nck1 and Nck2, we performed experiments to confirm the specificity of each individual siRNA nucleotide or SMARTPool (which

contains four different oligonucleotides against a specific target). Due to the cross-reactivity of available anti-Nck antibodies (i.e., no discrimination of Nck1 versus Nck2), we tested the efficacy and specificity of SMARTPool siRNAs in cells expressing fluorescently-tagged hNck proteins. This allowed us to express each Nck protein independently and assess specificity of the siRNAs. SMARTPool siRNAs for Nck1 showed specific silencing of Nck1 reducing hNck1-enhanced yellow fluorescent protein (EYFP) expression by ~70%, while only a minor change of <8% was observed in hNck2-mCherry (mCh) (Figure 3.1A). SMARTPool siRNAs for Nck2 showed specific silencing of Nck2 reducing hNck2-mCh expression by ~65%, while only a minor change of <5% was observed in hNck1-EYFP (Figure 3.1B). We compared individual targeting of Nck1 and Nck2 to combined targeting with the two SMARTPool siRNAs and observed a similar decrease in protein levels. When silencing Nck we also observed that MMP14 expression levels remained relatively constant.

We also tested the four individual siRNAs that constitute the SMARTPools to refine our silencing methodology and evaluate the effectiveness of each individual siRNA nucleotide. We found that siNck1 Oligo #1 outperformed the other four siRNAs including the SMARTPool; however, all individual oligos reduced protein expression by greater than 50% (Figure 3.2A). For Nck2, Oligos #1, 2 and 4 reduced protein expression greater than 70% and exceeded the performance of the SMARTPool, while Oligo #3 performed poorly only reducing protein expression by ~20% (Figure 3.2B). The MMP14 protein expression level in the siNck1 experiment was approximately the same as the untreated control, while there was some variability in the siNck2 data.

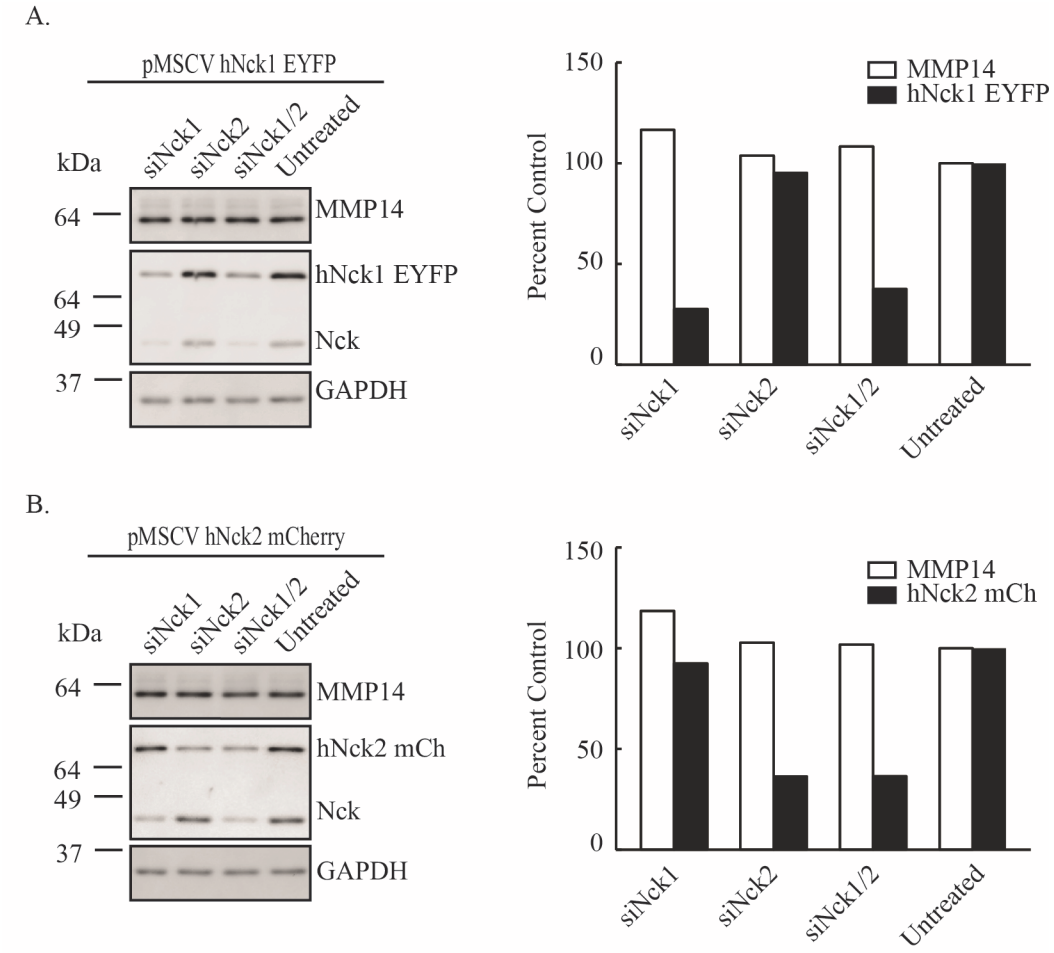

Figure 3.1. Nck 1 and Nck 2 SMARTPool siRNAs specifically reduce target protein levels. MDA-MB-231 cell lines expressing human Nck1 or human Nck2 fusion proteins were treated with 50 nM individual SMARTPool siRNAs targeting Nck1, Nck2 or Nck1 and Nck2 for 72 hours. **A-B)** Representative western blot (left) and quantitative analysis (right) showing the efficacy of human Nck1 (A) or Nck2 (B) silencing using siRNA oligonucleotides. Levels of MMP14 were determined to rule out a potential off target effect of Nck SMARTPool siRNAs and GAPDH was used to monitor equal loading.

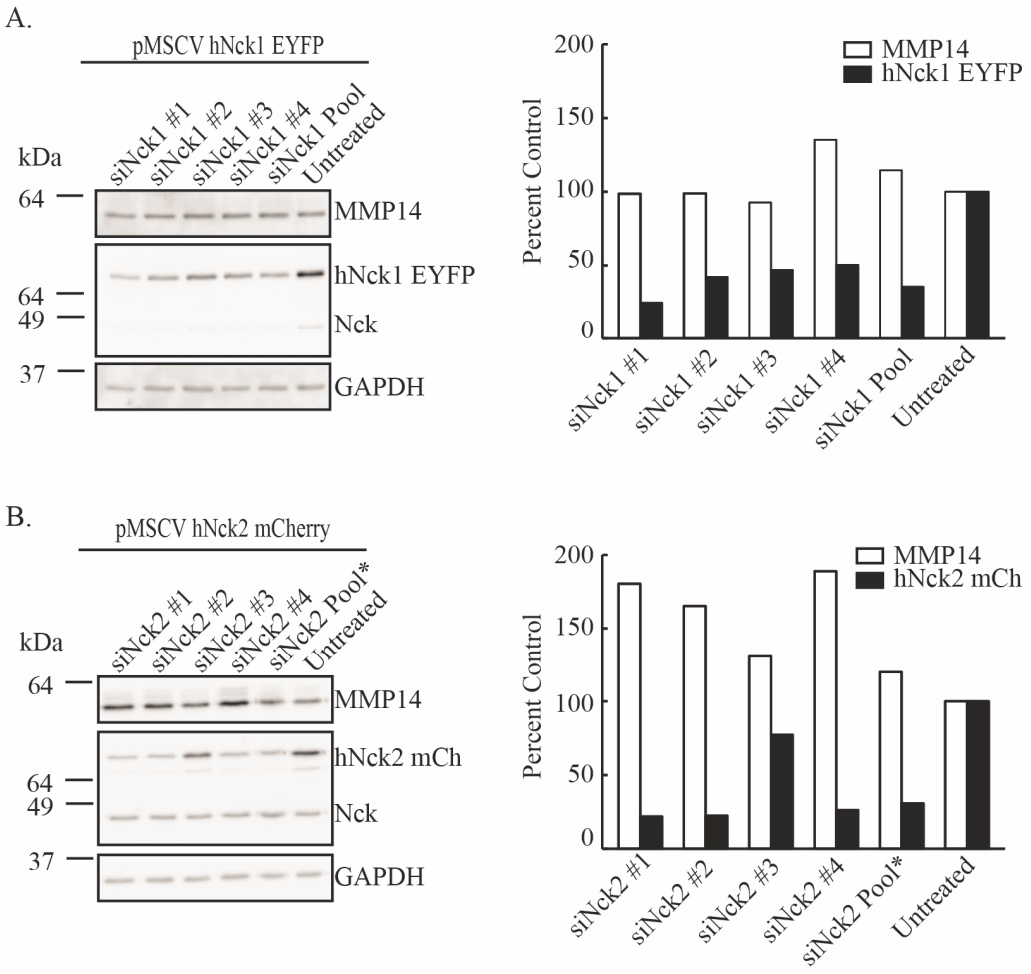

Figure 3.2 Nck 1 and Nck 2 individual siRNA oligonucleotides effectively reduce target protein levels. MDA-MB-231 cell lines expressing human Nck1 or human Nck2 fusion proteins were treated with 50 nM individual oligonucleotide siRNAs targeting Nck1 or Nck2 for 72 hours. **A-B)** Representative western blot (left) and quantitative analysis (right) showing the efficacy of human Nck1 (A) or Nck2 (B) silencing. * Cell line expressing hNck2-mCh fusion protein and exogenous hNck1. Levels of MMP14 were determined to rule out a potential off target effect of Nck SMARTPool siRNAs and GAPDH was used to monitor equal loading.

Silencing Nck Does Not Alter Overall MMP14 Protein Levels

Based on our findings that loss of Nck reduced MDA-MB-231 invasion and metastasis, we ascertained if Nck silencing alters the cellular levels of MMP14, a key MMP previously shown to facilitate invasion and metastasis (26). We found that efficacious silencing of Nck, by either siRNA transfection or shRNA expression, does not significantly alter ($p<0.05$) the overall cellular levels of MMP14 (Figure 3.3). In addition, we confirmed that efficacious silencing of MMP14 by either siRNA transfection or shRNA expression does not alter the overall cellular levels of Nck (Figure 3.3).

MDA-MB-231 Gelatin Degrading Properties are Dependent on Culture Density

Because Nck silencing decreases invasion and metastasis of breast carcinoma cells without altering the total cellular levels of MMP14, we hypothesized that Nck depletion alters the subcellular distribution of MMP14 and/or its activity at the membrane, and particularly, at invadopodia. To begin to test this hypothesis, we resorted to an established assay of focalized degradation of a fluorescent matrix (168) that estimates membrane-associated proteolysis, and therefore, allowed us to make inferences on the activity of MMP14 at the cell's surface. To validate this approach, the effect of MMP14 silencing on fluorescent matrix degradation was assessed in parallel. Figure 3.4A shows how cells plated on fluorescent gelatin form invasive structures (invadopodia) that are enriched in MMPs, protrude into the matrix, and as a result of focalized degradation leave dark, non-fluorescent spots. This allows quantification of the areas of degradation for comparative analysis.

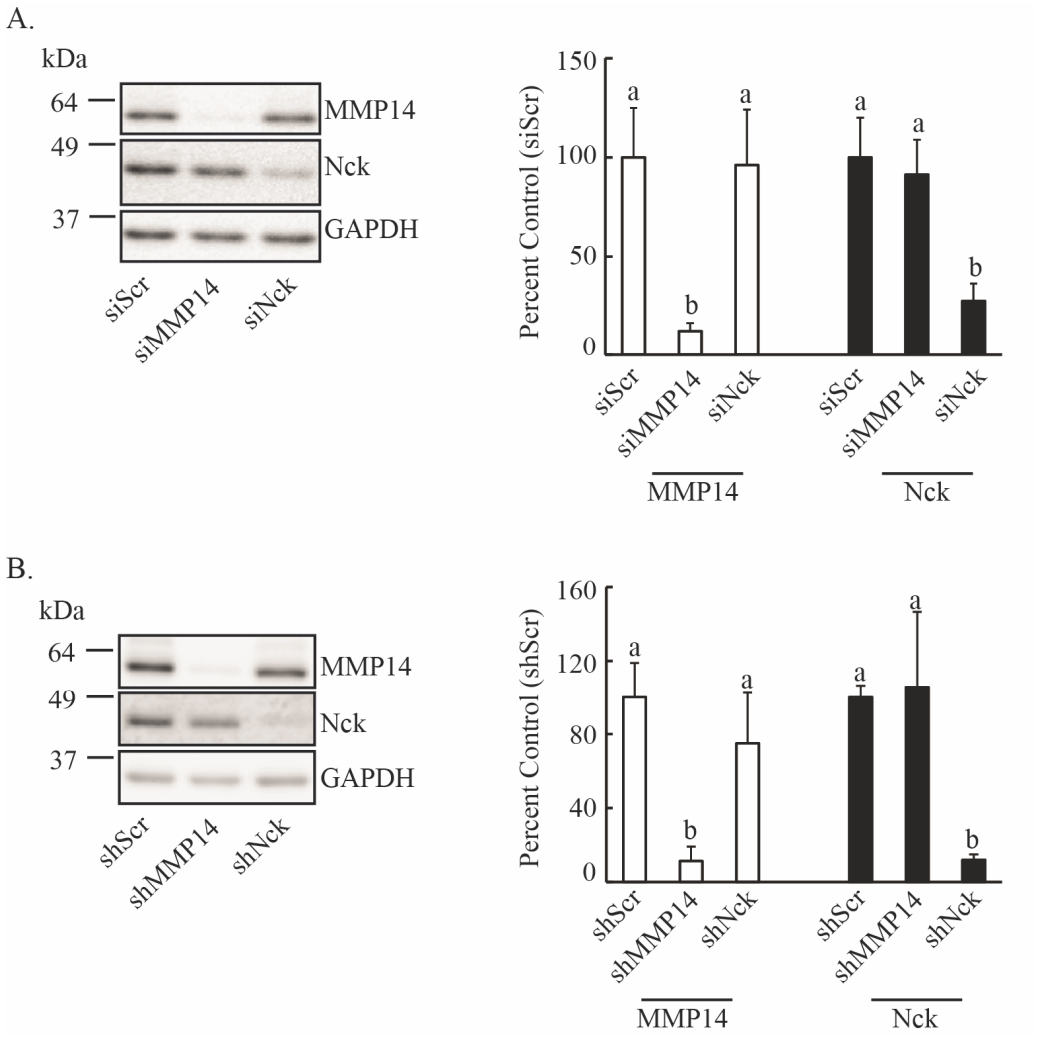

Figure 3.3. Silencing of Nck does not alter total MMP14 levels in mammary carcinoma cells. **A-B)** Representative western blots (left panels) and analysis of protein levels (right panels) showing efficacy of protein silencing in MDA-MB-231 cells transiently transfected with small interference (si) RNA oligonucleotides (top) or stably expressing short hairpin (sh) RNAs (bottom) encoding non-targeting sequences (Scr) or sequences targeting MMP14 or Nck. Protein levels (mean ± SD), expressed as percent of Scr control, include three independent experiments. Different letters represent statistically different values ($p<0.05$). GAPDH was used as a loading control and for normalization of protein levels.

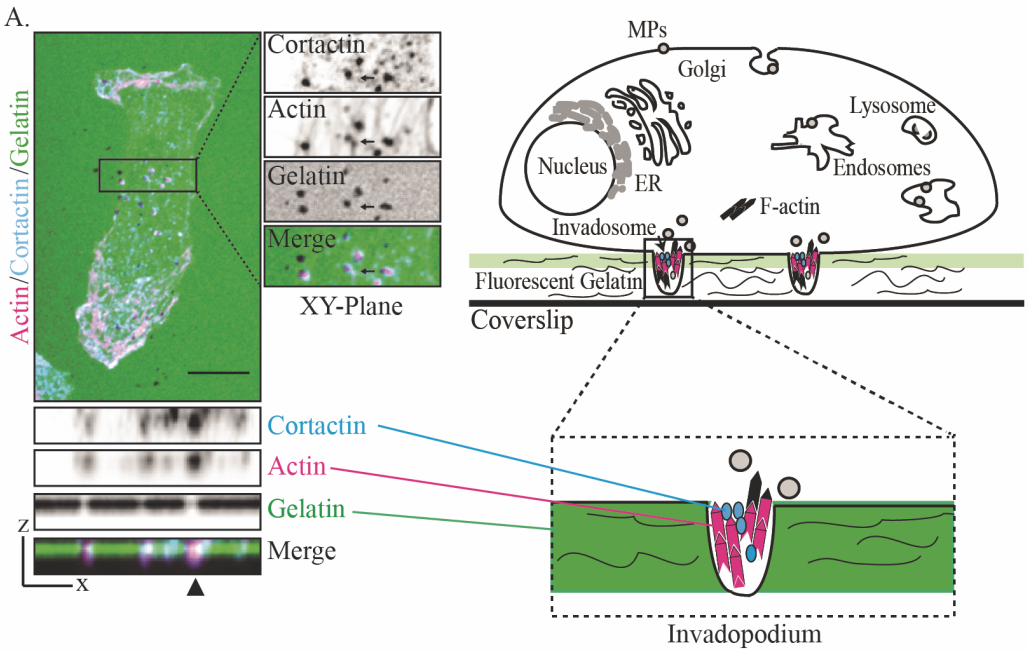

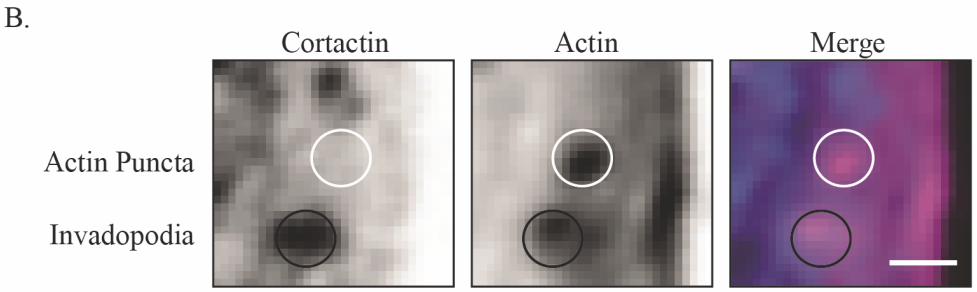

Figure 3.4. Structural analysis of invadopodia by confocal imaging. **A)** Mammary carcinoma cells form invadopodia, actin-rich subcellular structures capable of matrix remodeling/degradation. Single plane confocal images showing actin organization and matrix degradation by MDA-MB-231 cells (left) and graphical representation (right) depicting the structure of an invadopodium and the experimental setup. This assayed allowed the determination of number of actin puncta/invadopodia per cell, area of actin puncta/invadopodia per cell, area of degradation, and the actin/cortactin ratio at invadopodia. Scale bar equals 10 microns. **B)** A region of interest from a confocal image showing an invadopodium and an actin puncta. Structures showing colocalization of F-actin and cortactin were defined as invadopodia. Scale bar equals 1 micron.

When MDA-MB-231 cells were cultured at "high density" (cells initiated in culture at $3.3x10^4$ cells/cm^2) and grown for 2-3 days we observed decreased capacity to degrade fluorescent gelatin when compared to cells cultured at "low density" (cells initiated in culture at $5.4x10^3$ cells/cm^2) (Figure 3.5). Even though both populations were seeded at $6.0x10^3$ cells/cm^2 on fluorescent gelatin and grown for 6 hours, when pre-cultured at high density only 16.5% of the siScr population and 16% of the siNck population degraded gelatin. When pre-cultured at low density, greater than 50% of the siScr population actively degraded gelatin while 36% of the Nck population was active. The pre-culture density had a similar impact on gelatin degrading capacity of MMP14-silenced cells, although as expected, these cells were considerable less active.

Loss of Nck Reduces Matrix Degradation by Breast Carcinoma Cells

Since gelatin degradation requires the focalized activity of MMPs at invadopodia (Figure 3.4), we determined whether Nck modulates the gelatin degrading capacity of MDA-MB-231. The results show that Nck silencing decreases the percent of actively degrading cells in the population (Figure 3.6). In addition, we performed an alternate analysis on only the subset of cells actively degrading matrix and determined there was a decrease in the degradation index (Figure 3.6B). We also ascertained the involvement of MMP14 dependent proteolysis in gelatin degradation. The data showed a significant decrease in both the percent of active degrading cells and the degradation index as a result of MMP14 silencing (Figure 3.6). Efficient silencing of target proteins was confirmed by western blot (Figure 3.6C). These results expand findings from previous work on the role of Nck in localized matrix degradation (72) and suggest that reduced

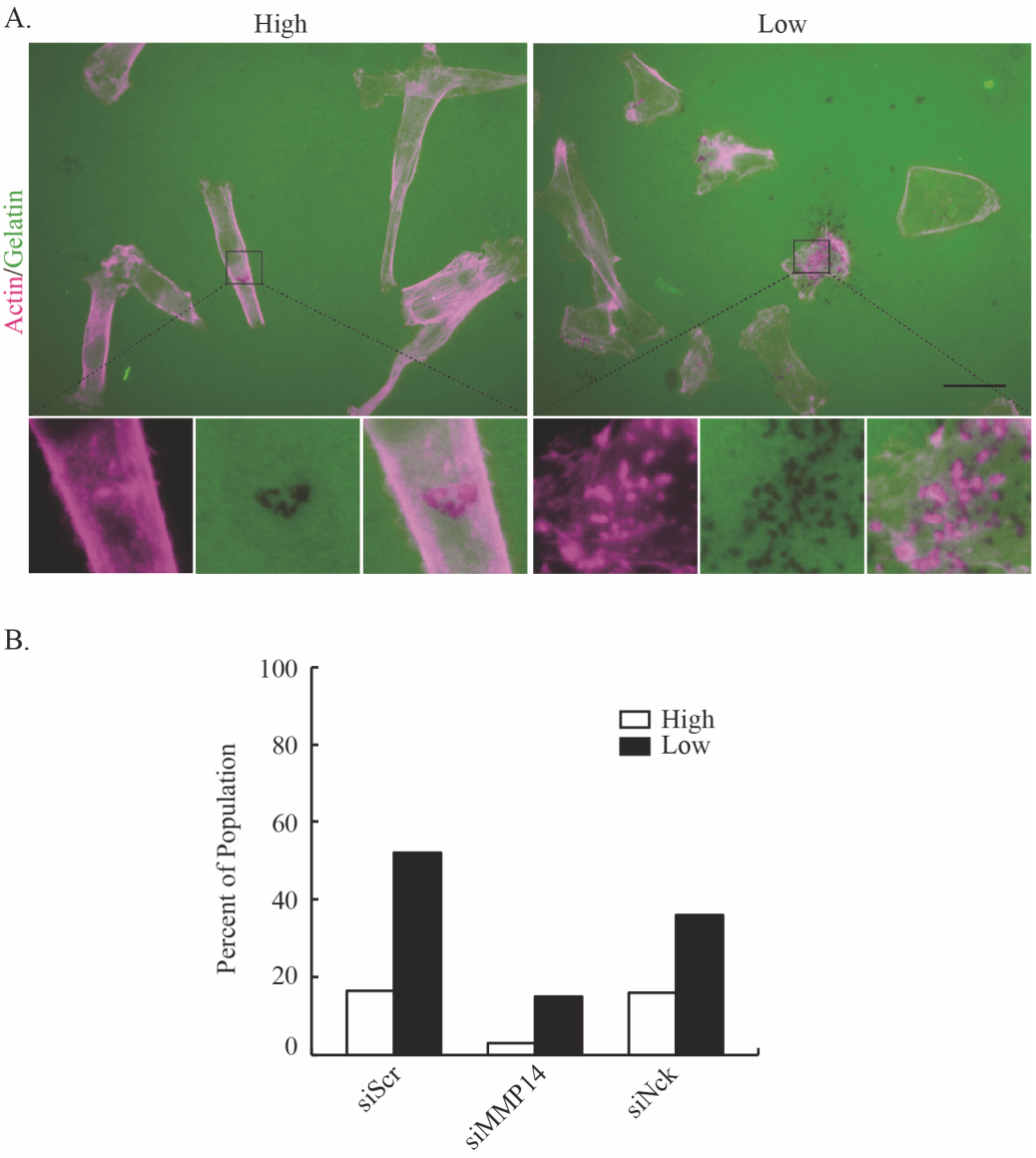

Figure 3.5. Culture density affects matrix remodeling by mammary carcinoma cells. MDA-MB-231 cells were transiently transfected with small interference (si) RNA oligonucleotides encoding non-targeting sequences (siScr) or sequences targeting MMP14 (siMMP14) or Nck (siNck). After transfection, cells were cultured at high ($3.3x10^4$ cells/cm^2) or low ($5.4x10^3$ cells/cm^2) densities for 2-3 days. Subsequently, cells from both populations were seeded at the same density ($6.0x10^3$ cells/cm^2) on fluorescent gelatin-coated coverslips and incubated for 6 hours before fixation and staining with fluorescent phalloidin to visualize cytoskeletal F-actin. **A)** Representative immunofluorescence images depicting fields of degrading cells and specific areas of degradation. Inset highlights specific regions of degradation. Scale bar represents 20 microns. **B)** Bar graph depicting percentage of cells actively degrading the fluorescent matrix (siScr n=60, siMMP14 n=30, siNck n=133).

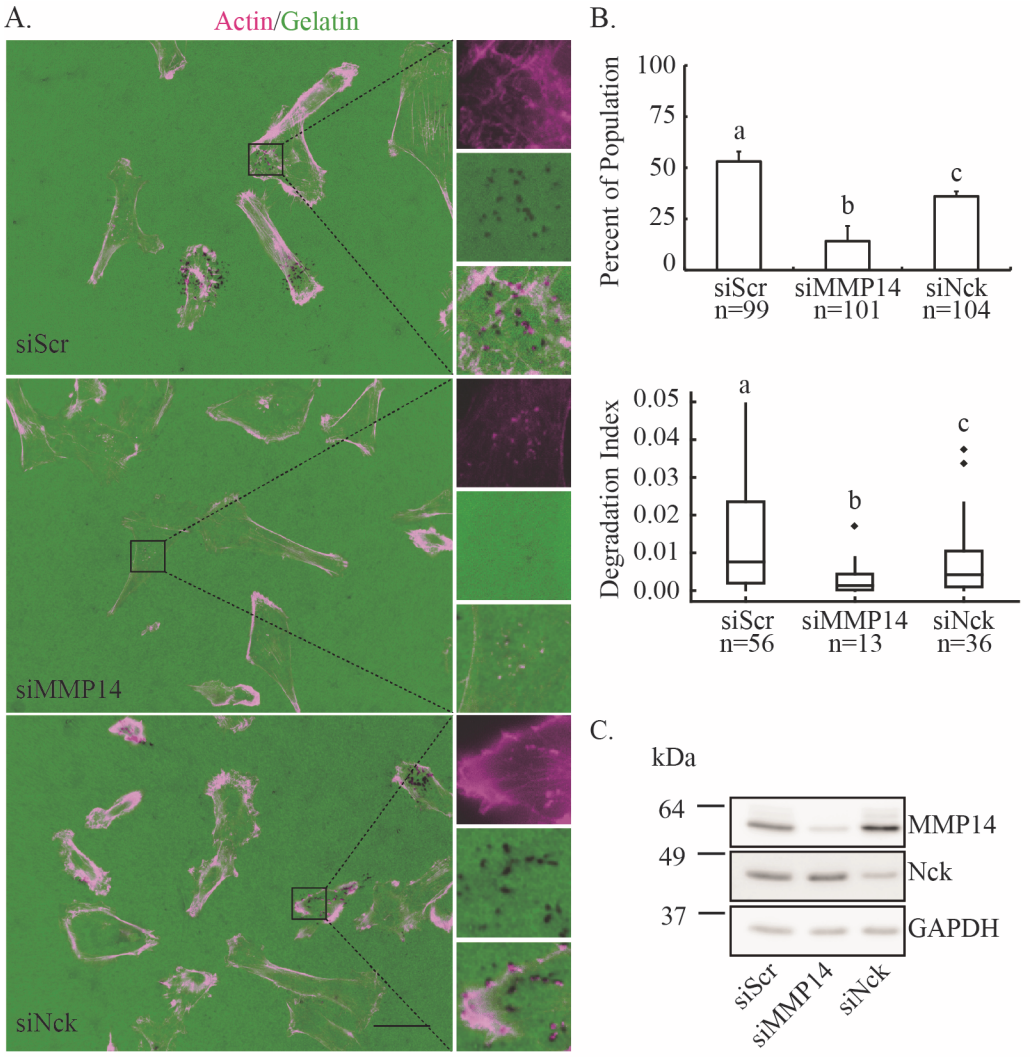

Figure 3.6. Loss of Nck decreases matrix degradation by mammary carcinoma cells. MDA-MB-231 cells were transiently transfected with small interference (si) RNA oligonucleotides encoding non-targeting sequences (siScr) or sequences targeting MMP14 (siMMP14) or Nck (siNck). Subsequently, cells were seeded on fluorescent gelatin-coated coverslips and incubated for 6 hours before fixation and staining with fluorescent phalloidin to visualize cytoskeletal F-actin. **A)** Representative confocal images depicting fields of degrading cells (left). Boxed areas were magnified and single channel/merge images are displayed (right). Scale bar represents 20 microns. **B)** Percentage (mean ± SD) of active cells (top, degrading cells) and degradation index (bottom, degradation area per active cell / cell area). Different letters represent statistically different values ($p<0.05$). Results shown summarize data from three independent experiments. **C)** Representative western blot showing the efficacy of protein silencing using siRNA oligonucleotides.

matrix remodeling resulting from Nck abrogation is due, at least in part, by decreased accumulation/activity of MMP14 at the cell surface.

Loss of Nck Reduces the Number of Actin Puncta and Invadopodia Formed by Breast Carcinoma Cells

We hypothesized that disruption of invadopodia formation contributes to decreased matrix degradation. Thus, we performed a detailed quantitative image analysis of invadopodia formation by MDA-MB-231 cells plated on fluorescent gelatin and subjected to F-actin staining and endogenous cortactin immunolabeling (Figure 3.4). We defined invadopodia as the colocalization of actin and cortactin (Figure 3.4B). We intentionally excluded degradation as a third marker for invadopodia to include invadopodia pre-cursors as well as mature invadopodia (176, 177). Therefore, our analysis differentiates invadopodia (colocalization of F-actin and cortactin) from actin puncta (focalized F-actin without cortactin accumulation). The results show that silencing Nck or MMP14 decreased ($p<0.05$) both the size and number of actin puncta and invadopodia formed by MDA-MB-231 (Figure 3.7). In both Nck- and MMP14-silenced populations, actin puncta and invadopodia were approximately 20-25% smaller when compared to similar structures in the scrambled control population. In addition, the distribution of cells according to the number of actin puncta or invadopodia per cell was altered in Nck- and MMP14-silenced populations versus the scrambled control. Remarkably, only 10-20% of the cells in the Nck or MMP14 silenced populations had greater than 20 puncta or invadopodia per cell, while more than 60-70% of the cells in the scrambled population had greater than 20 puncta or invadopodia per cell.

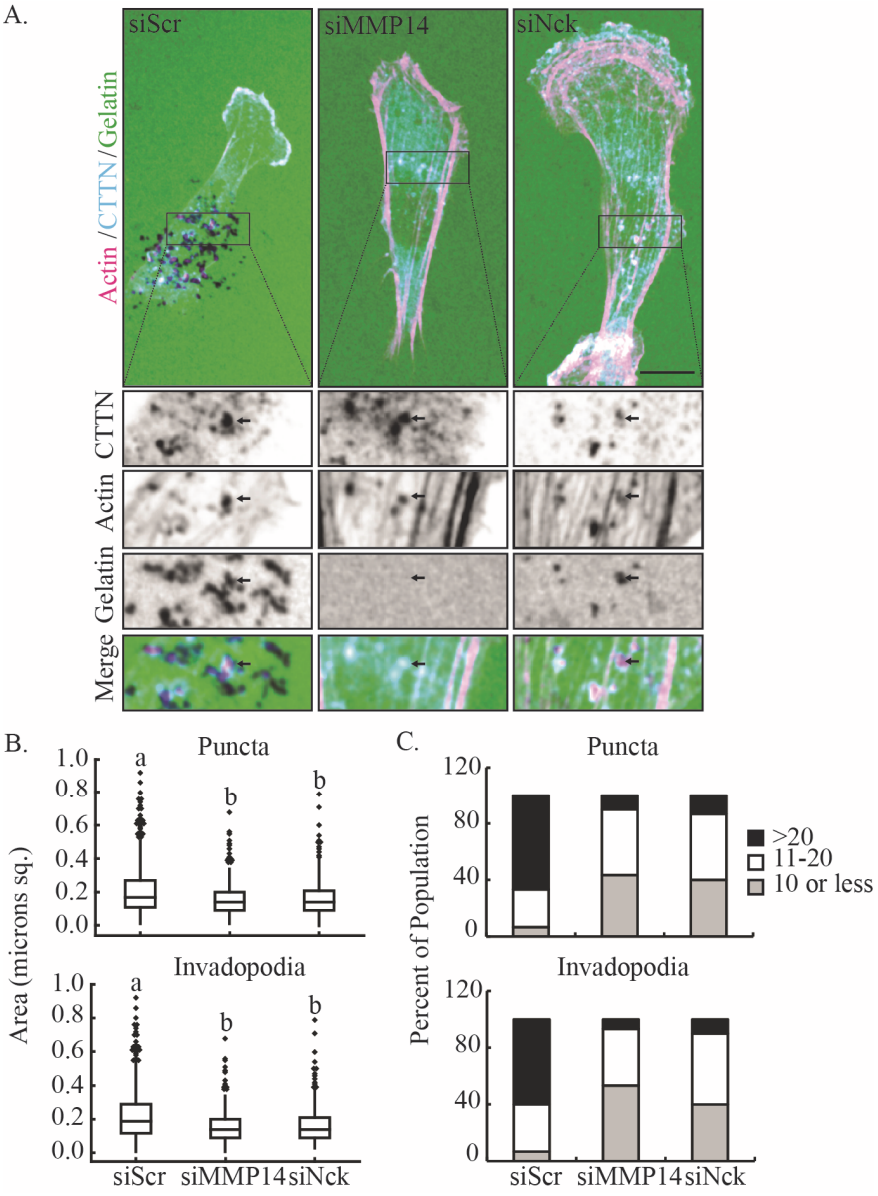

Figure 3.7. Loss of Nck reduces the number and size of actin puncta and invadopodia. MDA-MB-231 cells were transiently transfected with small interference (si) RNA oligonucleotides encoding non-targeting sequences (siScr) or sequences targeting MMP14 (siMMP14) or Nck (siNck). Cells were seeded on coverslips coated with fluorescent gelatin, incubated for 6 hours, and subsequently stained with an anti-cortactin (CTTN) antibody and fluorescent phalloidin (F-actin). **A)** Representative confocal images of MDA-MB-231 cells depicting overlays of actin, cortactin and gelatin. Boxed areas were magnified and single channels/merge images in the X/Y planes are displayed. Scale bar equals 10 microns. **B)** Area of actin puncta and invadopodia. Different letters represent statistically different values ($p<0.001$). **C)** Distribution of cells as a function of the number of actin puncta/invadopodia displayed. Invadopodia were defined as colocalization of actin puncta with cortactin. Three independent experiments were performed. A minimum of 30 cells/condition and a range of 313-715 actin puncta/invadopodia were analyzed.

These results, showing that silencing of Nck or MMP14 decrease invadopodia/actin puncta formation to a similar extent, support the hypothesis that the reduction in fluorescent matrix remodeling caused by Nck silencing is due, at least in part, to decreased MMP14 accumulation/activity at the plasma membrane.

Loss of Nck Reduces the Ratio of F-actin to Cortactin in Invadopodia

Based on our observations that invadopodia size was decreased when Nck was silenced and previous findings that cortactin phosphorylation is linked to Nck-stimulated actin polymerization (72, 178); we hypothesized that Nck silencing alters the ratio of F-actin to cortactin in invadopodia. To test this predication, we analyzed invadopodia formed by MDA-MB-231 cells plated on fluorescent gelatin and determined, indeed, there was a significant ($p<0.001$) decrease (~25%) in the ratio of F-actin to cortactin in Nck- and MMP14-silenced cells versus scrambled controls (Figure 3.8).

Loss of Nck Alters Actin Dynamics at Actin Puncta

Fluorescence recovery after photobleaching (FRAP) microscopy allows the determination of the rate constant for actin diffusion into the local area of actin structures. This relates to actin polymerization through the availability of actin monomers for polymerization into the filamentous structures. We performed FRAP microscopy with MDA-MB-231 stably expressing actin-EYFP cultured on fibronectin coated MatTek dishes. We found through transient silencing of Nck that the rate of actin-EYFP recovery at actin puncta was decreased relative to scrambled controls (Figure 3.9). Representative images and a graphical plot of the photobleaching process

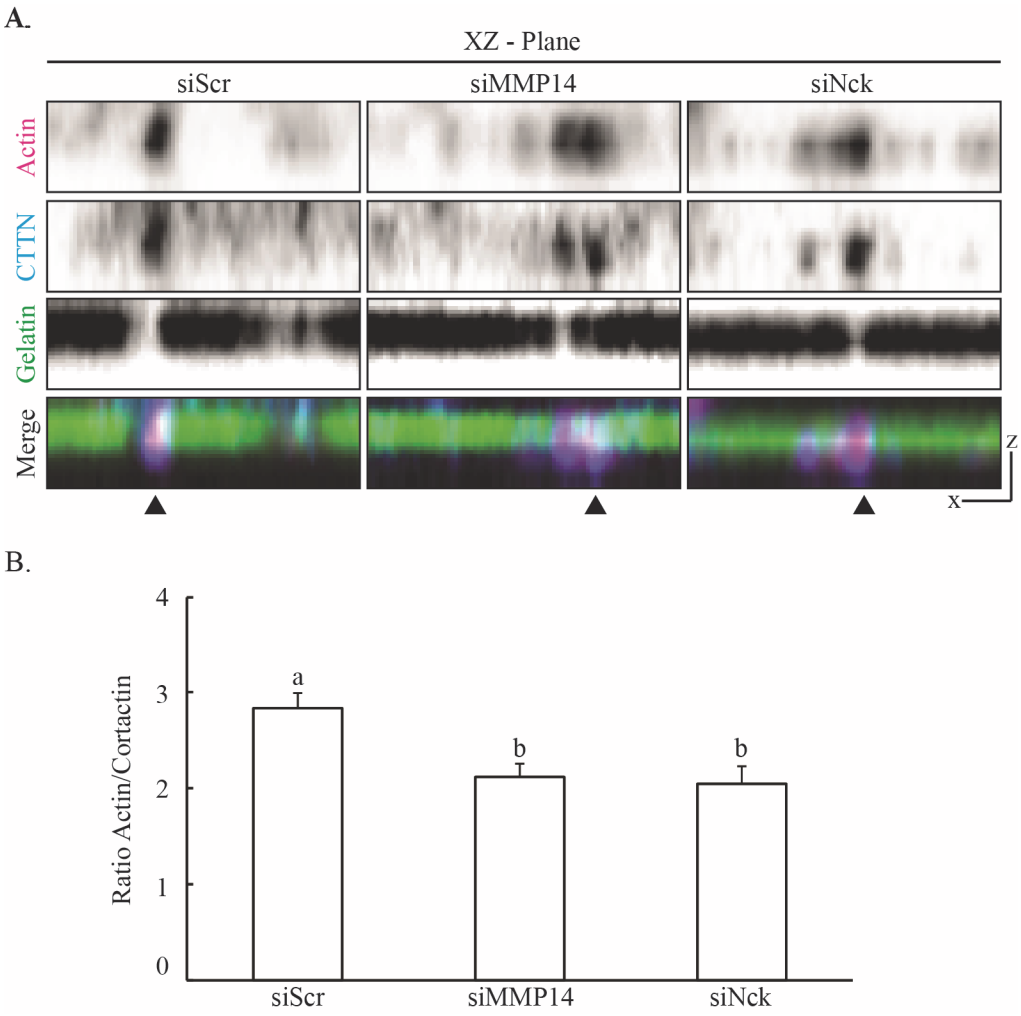

Figure 3.8. Loss of Nck reduces the ratio of F-actin to cortactin accumulation in invadopodia. MDA-MB-231 cells were transiently transfected with small interference (si) RNA oligonucleotides encoding non-targeting sequences (siScr) or sequences targeting MMP14 (siMMP14) or Nck (siNck). Cells were seeded on coverslips coated with fluorescently-labeled gelatin, incubated for 6 hours, and subsequently stained with anti-cortactin (CTTN) and fluorescent phalloidin (F-actin). **A)** Representative XZ projection from confocal images showing actin, cortactin and gelatin. **B)** Ratio of F-actin to cortactin area at invadopodia (mean ± s.e.m.). Invadopodia were defined as colocalization of F-actin clusters with cortactin. Different letters represent statistically different values ($p<0.001$). Data extracted from a minimum of 30 cells/condition and a range of 313-667 invadopodia from three independent experiments.

and subsequent recovery of signal in the region of invasive structures are depicted in Figure 3.9 A and B. We calculated the rate constant for recovery using the equation $FI=A\ (1 - e^{-kt}) + B$ as previously described (171). Figure 3.9B (left) represents how each component was determined from the fluorescent intensity recovery curves. Figure 3.9B, right shows that the recovery rate for shScr was significantly faster ($p<0.001$) than shNck.

Loss of Nck Decreases Localization of MMP14 at the Ventral Cell Surface

Based on our findings that gelatin degradation was reduced but total cellular MMP14 levels remained unchanged in Nck silenced cells, we hypothesized that Nck plays a role in the membrane targeting/accumulation and mobility of MMP14. To determine whether loss of Nck altered localization of MMP14 at the ventral cell surface, we performed time-lapse TIRF imaging of breast carcinoma cells co-expressing Life-Act EYFP, an F-actin probe (179), and MMP14 mCherry. To quantify the localization of MMP14 at the ventral surface we used a previously described method for determination of the "displacement index" (174, 175). The displacement index (DI), an estimate of MMP14 mobility, was calculated as the total area of MMP14 over the entire time-lapse divided by the area of MMP14 in the initial frame of the series. Based on this methodology, the silencing of Nck resulted in greater than 60% decrease of MMP14 mobility at the ventral surface (Figure 3.10).

As a complementary approach, we plated siRNA treated cells on fluorescent gelatin and performed quantitative imaging of fluorescently labeled actin and

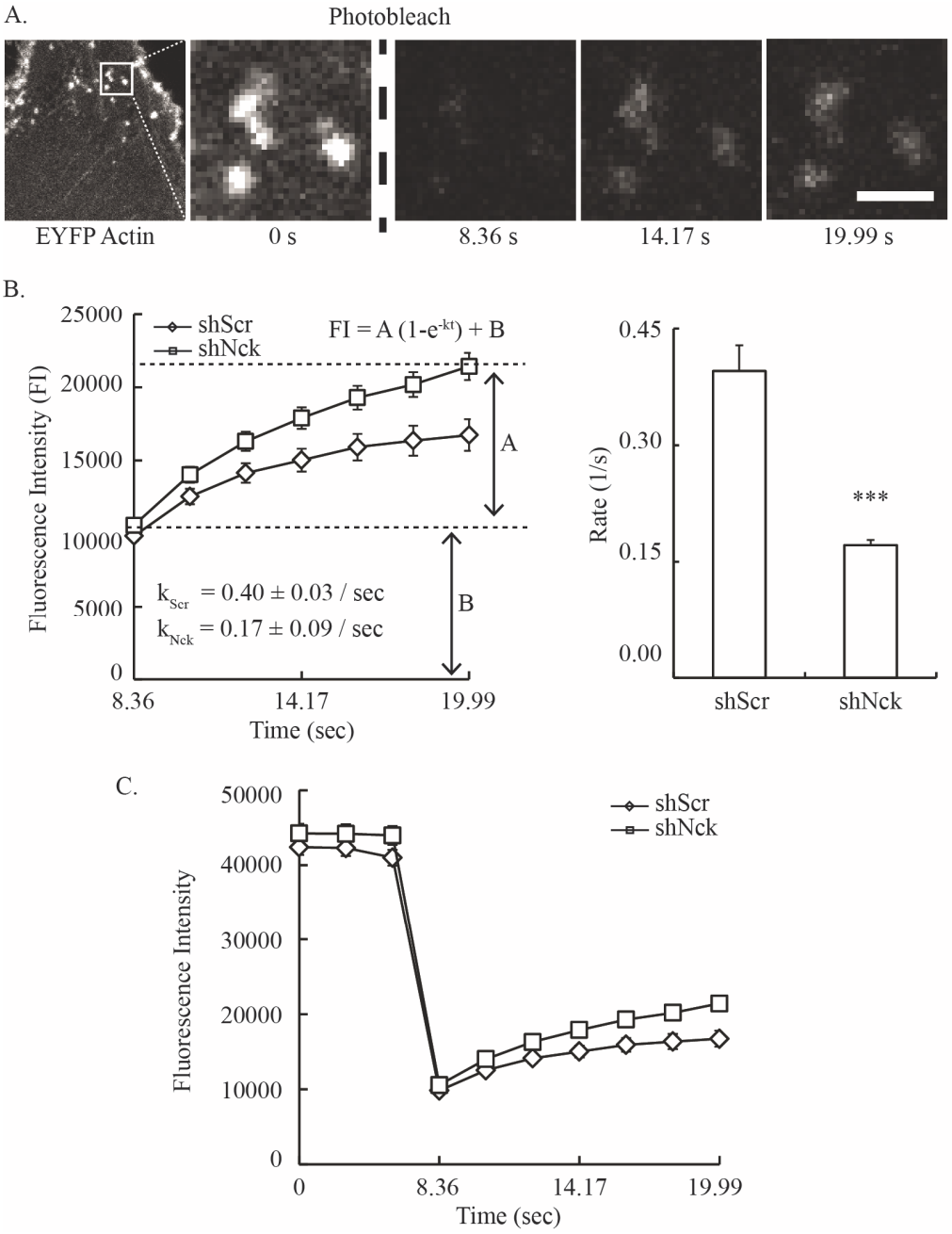

Figure 3.9. Loss of Nck reduces rate of actin polymerization at invadopodia. MDA-MB-231 cells were transiently transfected with small interference (si) RNA oligonucleotides encoding non-targeting sequences (siScr) or sequences targeting Nck (siNck). Subsequently, cells were seeded on fibronectin coated coverslips and incubated for 20 hours before FRAP microscopy. **A)** Representative confocal images depicting fluorescence recovery after photobleaching at invadopodia. Scale bar represents 2 microns. **B)** Rate (mean ± s.e.m.) of fluorescence recovery. * $p<0.05$. **C)** Representative plot of initial fluorescence intensity and recovery after photobleaching. Results shown are from a single experiment representative of data from three independent experiments. Data collected from a minimum of 30 images (3-15 puncta per image) from two culture dishes per experimental group.

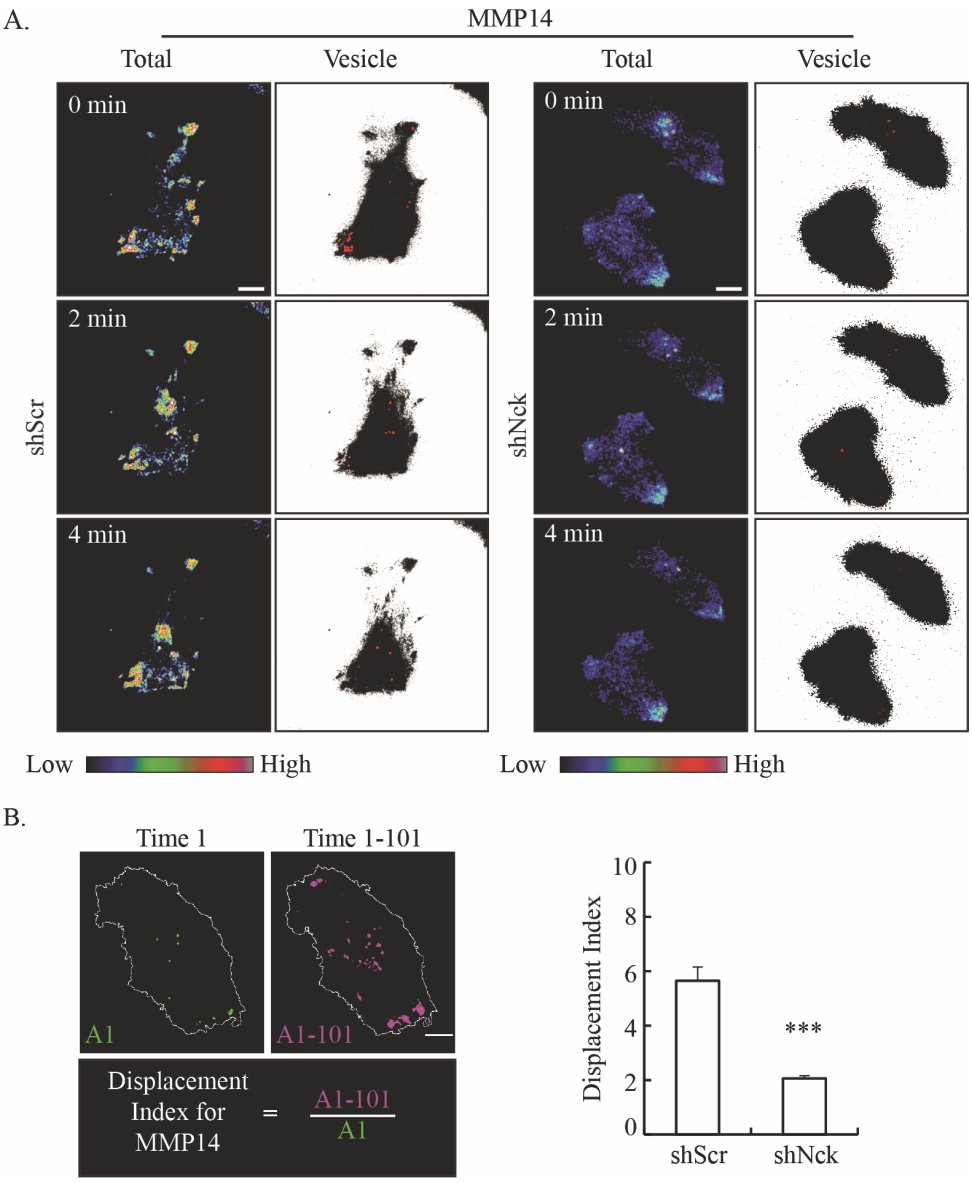

Figure 3.10. Loss of Nck decreases ventral surface mobility and polarized activity of MMP14 in breast carcinoma cells. MDA-MB-231 cells expressing MMP14-mCherry, LifeAct EYFP and short hairpin (sh) RNAs encoding non-targeting sequences (shScr) or sequences targeting Nck (shNck) and were cultured on fibronectin in the presence of complete medium and imaged every 3 seconds for 5 minutes. **A)** Representative TIRF images taken from time-lapse series. Images are presented using an intensity modulated display to associate intensity (activity) with color and hue (red = high activity; blue = low activity) or with vesicles highlighted red on black cell area background. Scale bar represents 10 microns. **B)** Displacement index (DI) was calculated by dividing the total area of MMP14 mCherry present during the 5 minute time-lapse (as a result of a maximum projection, magenta, right panel) by the area of MMP14 mCherry in the first image (green, left panel). Bar graph depicting displacement index (mean ± s.e.m., left). A total of 20 cells (time-lapse series) from three independent experiments were analyzed. *** indicates $p<0.001$. (adapted from 175)

endogenous MMP14 detected by immunolabeling (Figure 3.11). Confocal sections of the ventral cell surface were captured and MMP14 intensity per cell was normalized to the cell area. Based on this analysis we observed a significant reduction in MMP14 signal in the most ventral focal planes encompassing the cell membrane and membrane proximal areas, even though total MMP14 protein was unchanged as confirmed by western blot (Figure 3.11A).

Loss of Nck Increases Total Cdc42 Activity at the Ventral Cell Surface

Breast carcinoma invasion, migration and metastasis have been linked to Cdc42 activity levels and total abundance in highly metastatic breast cancer cells (180, 181). In addition, Cdc42 is critical for invadopodia formation through activation of N-WASp for actin polymerization and for polarized accumulation of MMP14 at invadopodia through interactions with IQGAP (167). To determine if Nck modulates the spatiotemporal patterns of Cdc42 activation, we performed time-lapse confocal imaging of the ventral surface of MDA-MB-231 cells expressing the Raichu Cdc42-FRET biosensor (182). The results show that silencing of Nck results in a greater than 20% increase over scrambled control in levels of active Cdc42 at the ventral surface (Figure 3.12).

Discussion

Our findings that the loss of Nck reduced invasion and metastasis prompted us to elucidate the underlying cellular and molecular mechanisms. Previous studies established that invadopodia formation and matrix remodeling capacity of mammary carcinoma cells directly correlate with their invasive and metastatic potential (56). To investigate the mechanism of Nck-dependent invasion we focused on regulation of actin

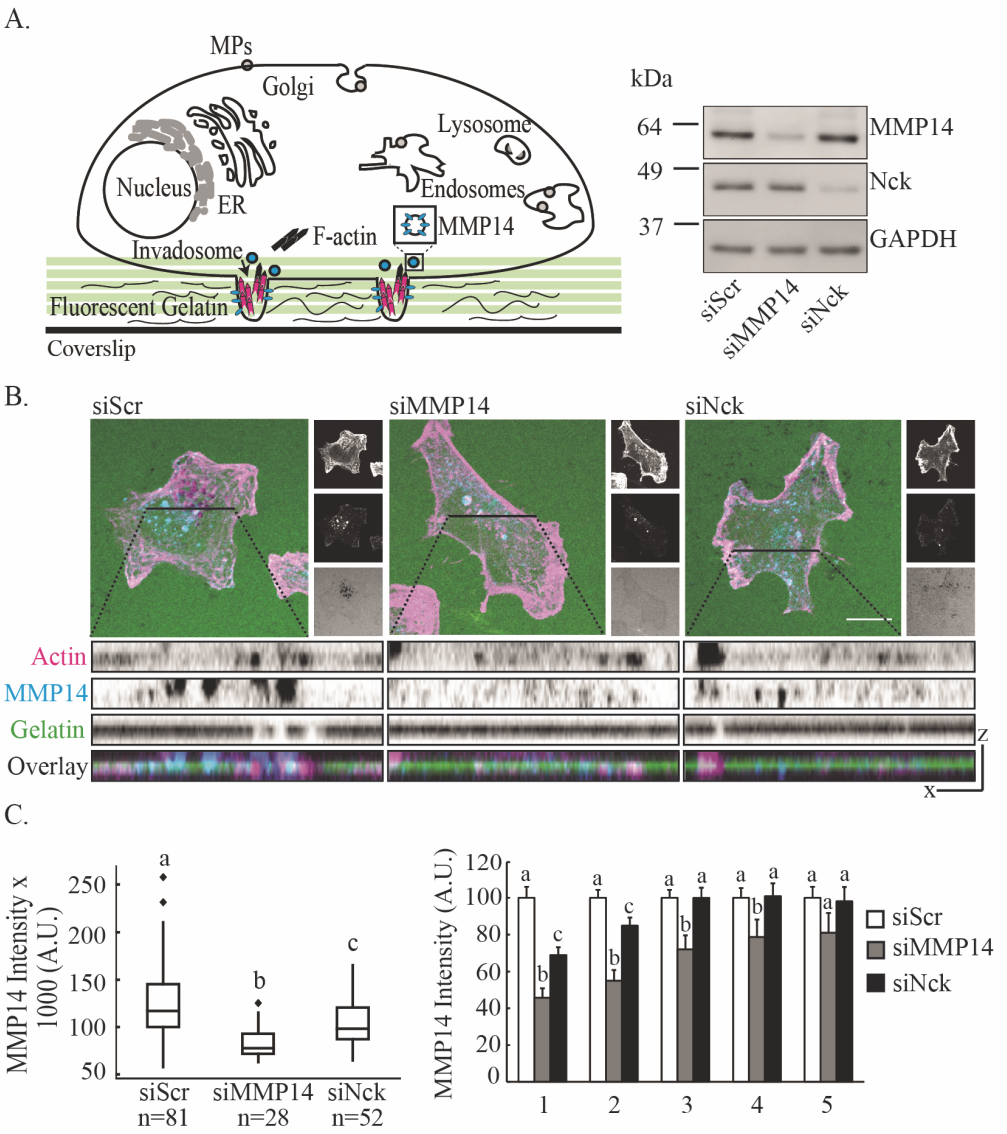

Figure 3.11. Loss of Nck decreases ventral surface accumulation of MMP14 in active breast carcinoma cells. MDA-MB-231 cells were transiently transfected with small interference (si) RNA oligonucleotides encoding non-targeting sequences (siScr) or sequences targeting MMP14 (siMMP14) or Nck (siNck). Cells were seeded on coverslips coated with fluorescent gelatin, incubated for 6 hours, and subsequently stained with anti-MMP14 (MMP14) and fluorescent phalloidin (F-actin). Samples were imaged from top to bottom of gelatin in five 0.5 micron z-slices. **A)** Graphical representation of actin and MMP14 localization at invadopodia. Green area indicates planes imaged by confocal microscope to measure MMP14 intensity at ventral surface of cell. **B)** Representative immunofluorescence images depicting single cells and X-Z planes of actin, MMP14, and fluorescent gelatin. Scale bar represents 10 microns. Representative western blot showing similar MMP14 protein levels in siScr and siNck and the efficacy of protein silencing using siRNA oligonucleotides. **C)** Boxplot of MMP14 intensity in arbitrary units at the most ventral plane in each condition (left). Bar graph depicting relative intensities (mean ± s.e.m., arbitrary units) of MMP14 normalized to the control of each plane imaged (right). Different letters within each group are different ($p<0.05$).

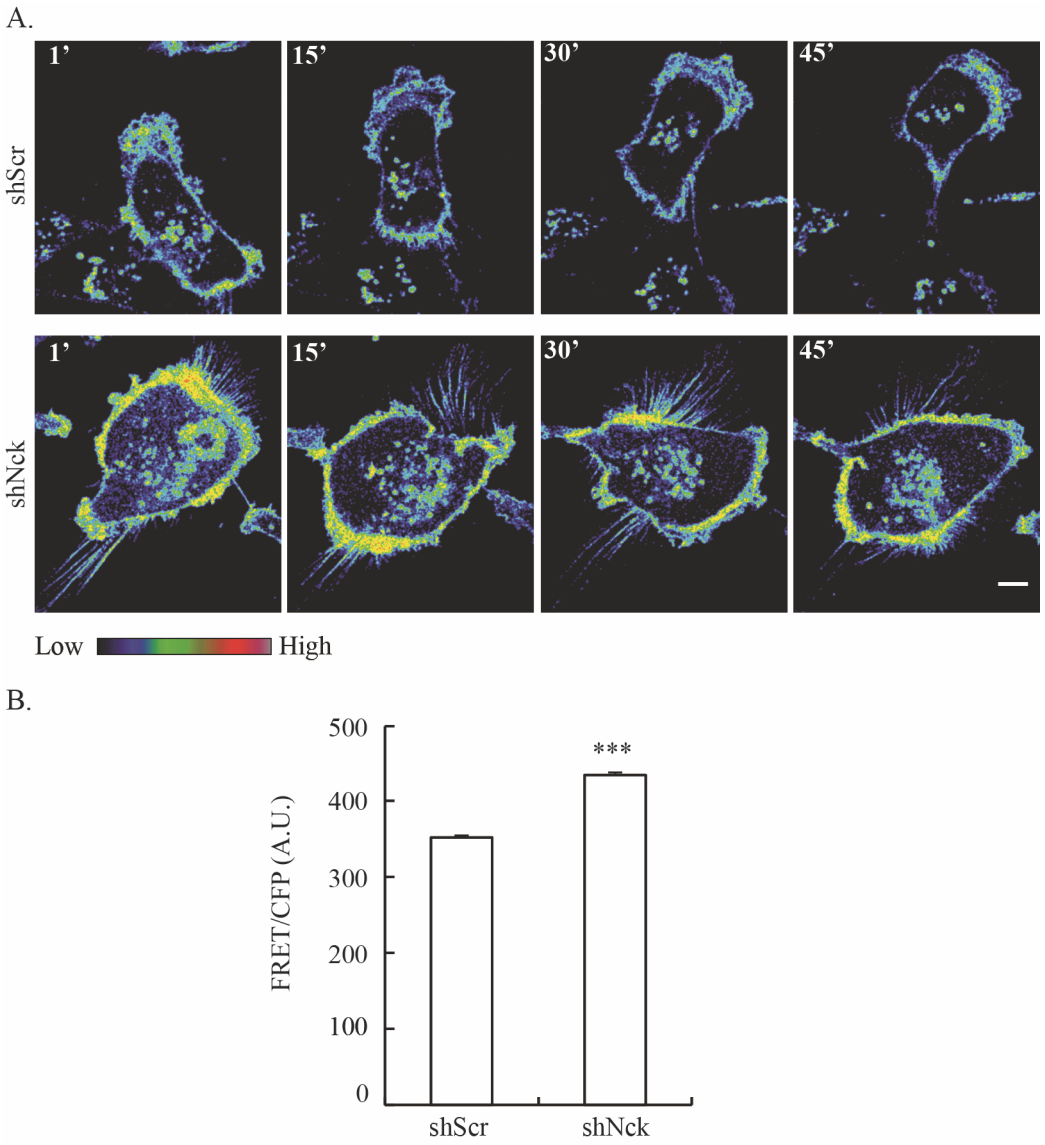

Figure 3.12. Loss of Nck increases Cdc42 activity at the ventral surface of invasive mammary carcinoma cells. MDA-MB-231 cells expressing the Raichu Cdc42 FRET biosensor and either short hairpin (sh) RNAs encoding non-targeting sequences (shScr) or sequences targeting Nck (shNck) were plated on fibronectin in the presence of complete medium. Confocal, time-lapse images of the ventral surface of the cells were acquired every minute for 30-60 minutes. **A)** Representative FRET/CFP ratio images taken from time-lapse series. Images are presented using an intensity modulated display to associate intensity (activity) with color and hue (red = high activity; blue = low activity). **B)** Quantitative analysis of FRET activity (mean +/- s.e.m., *** p-value <0.001) in arbitrary units (A.U.). FRET ratios were collected for each cell in 2-4 fields (2-4 cells per field) for every time point for analysis: n=642.

dynamics and cell surface exposure/activity of MMP14 in breast carcinoma cells. It has been shown that MMP14 is critical for tumor cell invasion (26), and evidence suggests that N-WASp is involved with anchoring MMP14 to invadopodial F-actin (65). Considering that Nck recruits and strongly activates N-WASp (121, 124), we hypothesized that Nck-modulation of actin dynamics regulates MMP14 accumulation/activity at invadopodia. To test this, we first ascertained that specific silencing of Nck does not alter the overall cellular levels of MMP14. Because recent evidence suggests that intracellular trafficking is an important mechanism regulating the activity/surface exposure of MMP14 (29, 164, 183-186), we speculated that altered function or localization of MMP14 at the cell surface contributes to the reduction in invasion and metastasis resulting from abrogation of Nck signaling.

The gelatin degradation assay (168) is an established, powerful method for the assessment of invadopodia dynamics and focalized, membrane-associated (MMP14-dependent) matrix degradation. In the course of our experiments, we identified that the matrix remodeling activity of mammary carcinoma cells is dependent on the history of the culture, i.e. cells cultured at high versus low densities display, respectively, decreased and increased indexes of matrix degradation. This unexpected yet important observation could be explained, presumably, by decreased expression levels of MMPs when cells reach high densities in 2D tissue culture conditions as previously suggested (187). The sensitivity to culture conditions highlights the need for careful interpretation when comparing findings generated by multiple groups, even when using the same materials and cell lines. This observation led us to perform subsequent experiments

using optimized cultures, namely cells cultured at low densities that express full invasive potential.

Results from our experiments using the fluorescent matrix degradation assay show that cells with Nck or MMP14 silenced display decreased indexes of matrix remodeling when compared to scrambled control cells. MMP14 silencing had a more pronounced effect on matrix remodeling than Nck silencing; however, both conditions altered actin dynamics to a similar extent. Thus, results from this study suggest that the Nck-dependent matrix remodeling is mediated, at least in part, by altered surface accumulation/activity of MMP14. Our findings that Nck silencing reduces endogenous MMP14 accumulation and mobility of MMP14 at the membrane/membrane proximal region of the cells provide strong support to the notion that loss of Nck disrupts MMP14 trafficking and/or membrane localization. Of interest, when cells were plated on non-permissive poly-L-lysine coated glass coverslips, we were unable to detect differences between the Nck silenced and scrambled control cells (Appendix E). Thus, a permissive stratum appears important for the efficient formation and full maturation of degrading invadopodia.

Altered actin dynamics in the Nck-deficient cells is likely a significant factor contributing to decreased invasiveness. Nck has been shown to associate with both cortactin and Tks5 to regulate N-WASp mediated actin polymerization at invadopodia (72, 100). Our results showing a decrease in the ratio of F-actin to cortactin in response to Nck silencing suggests structural defects in invadopodia formation that could potentially limit their transition to mature, fully invasive structures. The reduced rate of

recovery observed in our FRAP data also provides support that the loss of Nck alters the actin dynamics at invadopodia. Our results demonstrate that the loss of Nck reduces both the activity and number of invadopodia formed by invasive breast carcinoma cells. Clearly, further studies are necessary to fully dissect the contributions of Nck to tumor cell invasion through actin dynamics versus MMP-mediated proteolysis and matrix remodeling.

Cdc42 is a key GTPase that controls cell polarity/directional migration, cytoskeletal dynamics, polarized delivery of MMP14 at invadopodia, and invadopodia formation (56, 82-87, 167). In highly invasive cancer, overexpression of constitutively active Cdc42 or hyperactivation of endogenous Cdc42 impairs invasion (180, 188). We have shown that silencing Nck in endothelial cells increases Cdc42 activation in conjunction with increased formation of transient, multidirectional protrusions associated with the loss of directional cell migration in endothelial cells (137). Consistent with our previous findings, we show that silencing of Nck increases Cdc42 activity and decreases the invasive characteristics of invasive breast carcinoma. Our findings suggest that Nck silencing leads to dysregulated activation of Cdc42 at the ventral surface, and consequently, altered directional migration and polarized trafficking of MMP14.

In conclusion, this study provides new mechanistic insights suggesting that Nck modulates the spatiotemporal activation of Cdc42 to coordinate actin dynamics with the targeted delivery of MMP14 to invadopodia.

CHAPTER IV

SUMMARY AND CONCLUSIONS

Even with the ongoing development of new treatments, increased awareness, and improved screening methodologies, breast cancer remains a major health problem in the United States and worldwide. The lack of effective therapies for metastatic breast cancer, which accounts for greater than 90% of deaths due to this malignancy (11), represents a daunting challenge for scientists and clinicians. Thus, a better understanding of cancer biology, including the identification of new markers for early detection and new molecular targets for intervention, remains a critical need. We investigated the role of the SH2/SH3 domain containing Nck adaptor proteins, critical links between tyrosine phosphorylation and cytoskeletal remodeling, in breast cancer invasion and metastasis. Results from this study fill an important gap in our knowledge of how signaling integration by adaptors/scaffold proteins contributes to breast cancer progression by demonstrating that Nck promotes *i)* primary tumor growth, and *ii)* tumor invasion and metastasis.

For the first time, we show a requirement for Nck in breast carcinoma growth in 3D laminin-rich matrices and invasion in both 3D laminin-rich and collagen matrices. Loss of Nck also reduces both individual/single cell and collective cell invasion through laminin-rich matrices in response to EGF stimulation. We identified a requirement for MMP14 for individual/single cell invasion that was not required for collective invasion in laminin-rich matrices, a finding demonstrating important differences in mechanisms

driving distinct invasion modes. Using a nude mouse xenograft model, we also determined, though not required for tumor initiation, Nck signaling is a significant contributor in primary tumor growth and metastasis. These results validate Nck as an important target in aggressive breast cancer and lay the groundwork for future research to develop new and more efficacious therapeutics.

To better understand the mechanisms associated with reduced invasion and metastasis of breast carcinoma cells deficient in Nck signaling, we determined the dynamics of invadopodia formation and surface accumulation/activity of MMP14, a key matrix remodeling enzyme. We determined that, although the total cellular levels of MMP14 remained unaltered, the loss of Nck decreased invadopodia biogenesis and focalized matrix degradation. The attenuation of cellular mechanisms of invasion was a result of decreased accumulation of MMP14 at the ventral surface of invasive cells and altered actin dynamics at invadopodia. Importantly, Nck deletion led to increased, mislocalized activation of Cdc42, a key regulator of intracellular trafficking and directional cell migration. Our results support a model whereby Nck, by integrating extracellular signals that modulate cytoskeletal dynamics, specifies patterns of spatiotemporal activation of Cdc42 and the targeted delivery/membrane accumulation of MMP14 thus facilitating invadopodia formation and maturation.

Future Directions

We have demonstrated a role for Nck in invasion and metastasis of highly metastatic, triple negative breast cancer cells. The present findings provide a foundation for future studies to address:

- The role of Nck in other cell and tumor types
- Mechanisms of Nck-dependent modulation of tumor growth, including cell autonomous and non-autonomous regulation
- Contributions of Nck to tumor-associated disruption of the tissue architecture and angiogenesis
- Identification of the molecular mechanism underlying Nck-regulated Cdc42 activation
- Role of Nck in extracellular matrix remodeling and tumor cell-matrix adhesion in three dimensional cultures and tissues
- Efficacy of peptides/peptidomimetics to block specific Nck/effector interactions

REFERENCES

1. National Cancer Institute. What is cancer? [Internet]. 2012 [cited 2012 Oct 18]. Available from: http://www.cancer.gov/cancertopics/cancerlibrary/what-is-cancer.
2. Alberts B, Johnson A, Lewis J, Raff M, Roberts K, Walter P. Molecular biology of the cell. 5th ed. New York: Garland Science; 2007.
3. Nelson CM, Bissell MJ. Of extracellular matrix, scaffolds, and signaling: tissue architecture regulates development, homeostasis, and cancer. Annual Review of Cell and Developmental Biology. 2006;22:287-309.
4. Hanahan D, Weinberg RA. The hallmarks of cancer. Cell. 2000;100:57-70.
5. Hanahan D, Weinberg RA. Hallmarks of cancer: the next generation. Cell. 2011;144:646-74.
6. Knudson AG, Jr. Mutation and cancer: statistical study of retinoblastoma. Proceedings of the National Academy of Sciences of the United States of America. 1971;68(4):820-3.
7. Weinberg RA. The biology of cancer. New York: Garland Science; 2007.
8. Jaenisch R, Bird A. Epigenetic regulation of gene expression: how the genome integrates intrinsic and environmental signals. Nature Genetics. 2003;33 Suppl:245-54.
9. Ferlay J, Soerjomataram I, Dikshit R, Eser S, Mathers C, Rebelo M, et al. Cancer incidence and mortality worldwide: sources, methods and major patterns in GLOBOCAN 2012. International Journal of Cancer. 2015;136(5):E359-86.

10. American Cancer Society. Cancer facts & figures 2015 [Internet]. 2015 [cited 14 Apr 2015]. Available from: http://www.cancer.org/research/cancerfactsstatistics/cancerfactsfigures2015/index.

11. Weigelt B, Peterse JL, van 't Veer LJ. Breast cancer metastasis: markers and models. Nature Reviews Cancer. 2005;5(8):591-602.

12. National Cancer Institute. Breast cancer treatment (PDQ®) [Internet]. 2014 [cited 26 Mar 2015]. Available from: http://cancer.gov/cancertopics/pdq/treatment/breast/Patient.

13. Singh JC, Jhaveri K, Esteva FJ. HER2-positive advanced breast cancer: optimizing patient outcomes and opportunities for drug development. British Journal of Cancer. 2014;111(10):1888-98.

14. Langley RR, Fidler IJ. The seed and soil hypothesis revisited--the role of tumor-stroma interactions in metastasis to different organs. International Journal of Cancer. 2011;128(11):2527-35.

15. Kalluri R, Weinberg RA. The basics of epithelial-mesenchymal transition. The Journal of Clinical Investigation. 2009;119(6):1420-8.

16. Radisky DC. Epithelial-mesenchymal transition. Journal of Cell Science. 2005;118(19):4325-6.

17. Tomaskovic-Crook E, Thompson EW, Thiery JP. Epithelial to mesenchymal transition and breast cancer. Breast Cancer Research. 2009;11(6):213.

18. Nguyen DX, Bos PD, Massague J. Metastasis: from dissemination to organ-specific colonization. Nature Reviews Cancer. 2009;9(4):274-84.

19. Doyle AD, Petrie RJ, Kutys ML, Yamada KM. Dimensions in cell migration. Current Opinion in Cell Biology. 2013;25(5):642-9.

20. Lu P, Weaver VM, Werb Z. The extracellular matrix: a dynamic niche in cancer progression. The Journal of Cell Biology. 2012;196(4):395-406.

21. Linder S. The matrix corroded: podosomes and invadopodia in extracellular matrix degradation. Trends in Cell Biology. 2007;17(3):107-17.

22. Hynes RO, Naba A. Overview of the matrisome--an inventory of extracellular matrix constituents and functions. Cold Spring Harbor Perspectives in Biology. 2012;4(1):a004903.

23. Shiomi T, Lemaitre V, D'Armiento J, Okada Y. Matrix metalloproteinases, a disintegrin and metalloproteinases, and a disintegrin and metalloproteinases with thrombospondin motifs in non-neoplastic diseases. Pathology International. 2010;60(7):477-96.

24. Murphy G, Nagase H. Progress in matrix metalloproteinase research. Molecular Aspects of Medicine. 2008;29(5):290-308.

25. Kessenbrock K, Plaks V, Werb Z. Matrix metalloproteinases: regulators of the tumor microenvironment. Cell. 2010;141(1):52-67.

26. Sabeh F, Shimizu-Hirota R, Weiss SJ. Protease-dependent versus -independent cancer cell invasion programs: three-dimensional amoeboid movement revisited. The Journal of Cell Biology. 2009;185(1):11-9.

27. Lu C, Li XY, Hu Y, Rowe RG, Weiss SJ. MT1-MMP controls human mesenchymal stem cell trafficking and differentiation. Blood. 2010;115(2):221-9.

28. Murphy DA, Courtneidge SA. The 'ins' and 'outs' of podosomes and invadopodia: characteristics, formation and function. Nature Reviews Molecular Cell Biology. 2011;12(7):413-26.

29. Poincloux R, Lizarraga F, Chavrier P. Matrix invasion by tumour cells: a focus on MT1-MMP trafficking to invadopodia. Journal of Cell Science. 2009;122(17):3015-24.

30. Remacle AG, Rozanov DV, Fugere M, Day R, Strongin AY. Furin regulates the intracellular activation and the uptake rate of cell surface-associated MT1-MMP. Oncogene. 2006;25(41):5648-55.

31. Frittoli E, Palamidessi A, Disanza A, Scita G. Secretory and endo/exocytic trafficking in invadopodia formation: the MT1-MMP paradigm. European Journal of Cell Biology. 2011;90(2-3):108-14.

32. Friedl P, Alexander S. Cancer invasion and the microenvironment: plasticity and reciprocity. Cell. 2011;147(5):992-1009.

33. Friedl P, Borgmann S, Brocker EB. Amoeboid leukocyte crawling through extracellular matrix: lessons from the Dictyostelium paradigm of cell movement. Journal of Leukocyte Biology. 2001;70(4):491-509.

34. Wolf K, Muller R, Borgmann S, Brocker EB, Friedl P. Amoeboid shape change and contact guidance: T-lymphocyte crawling through fibrillar collagen is

independent of matrix remodeling by MMPs and other proteases. Blood. 2003;102(9):3262-9.

35. Petrie RJ, Gavara N, Chadwick RS, Yamada KM. Nonpolarized signaling reveals two distinct modes of 3D cell migration. The Journal of Cell Biology. 2012;197(3):439-55.

36. Firat-Karalar EN, Welch MD. New mechanisms and functions of actin nucleation. Current Opinion in Cell Biology. 2011;23(1):4-13.

37. dos Remedios CG, Chhabra D, Kekic M, Dedova IV, Tsubakihara M, Berry DA, et al. Actin binding proteins: regulation of cytoskeletal microfilaments. Physiological Reviews. 2003;83(2):433-73.

38. Goley ED, Welch MD. The ARP2/3 complex: an actin nucleator comes of age. Nature Reviews Molecular Cell Biology. 2006;7(10):713-26.

39. Pollard TD. Rate constants for the reactions of ATP- and ADP-actin with the ends of actin filaments. The Journal of Cell Biology. 1986;103(6):2747-54.

40. Pollard TD. Regulation of actin filament assembly by Arp2/3 complex and formins. Annual Review of Biophysics and Biomolecular Structure. 2007;36:451-77.

41. Machesky LM, Atkinson SJ, Ampe C, Vandekerckhove J, Pollard TD. Purification of a cortical complex containing two unconventional actins from Acanthamoeba by affinity chromatography on profilin-agarose. The Journal of Cell Biology. 1994;127(1):107-15.

42. Mullins RD, Heuser JA, Pollard TD. The interaction of Arp2/3 complex with actin: nucleation, high affinity pointed end capping, and formation of branching networks of filaments. Proceedings of the National Academy of Sciences of the United States of America. 1998;95(11):6181-6.

43. Higgs HN, Pollard TD. Regulation of actin filament network formation through ARP2/3 complex: activation by a diverse array of proteins. Annual Review of Biochemistry. 2001;70:649-76.

44. Krainer EC, Ouderkirk JL, Miller EW, Miller MR, Mersich AT, Blystone SD. The multiplicity of human formins: expression patterns in cells and tissues. Cytoskeleton (Hoboken). 2013;70(8):424-38.

45. Xu Y, Moseley JB, Sagot I, Poy F, Pellman D, Goode BL, et al. Crystal structures of a Formin Homology-2 domain reveal a tethered dimer architecture. Cell. 2004;116(5):711-23.

46. Zigmond SH, Evangelista M, Boone C, Yang C, Dar AC, Sicheri F, et al. Formin leaky cap allows elongation in the presence of tight capping proteins. Current Biology. 2003;13(20):1820-3.

47. Quinlan ME, Heuser JE, Kerkhoff E, Mullins RD. Drosophila Spire is an actin nucleation factor. Nature. 2005;433(7024):382-8.

48. Ahuja R, Pinyol R, Reichenbach N, Custer L, Klingensmith J, Kessels MM, et al. Cordon-bleu is an actin nucleation factor and controls neuronal morphology. Cell. 2007;131(2):337-50.

49. Lizarraga F, Poincloux R, Romao M, Montagnac G, Le Dez G, Bonne I, et al. Diaphanous-related formins are required for invadopodia formation and invasion of breast tumor cells. Cancer Research. 2009;69(7):2792-800.

50. Mersich AT, Miller MR, Chkourko H, Blystone SD. The formin FRL1 (FMNL1) is an essential component of macrophage podosomes. Cytoskeleton (Hoboken). 2010;67(9):573-85.

51. Lagal V, Abrivard M, Gonzalez V, Perazzi A, Popli S, Verzeroli E, et al. Spire-1 contributes to the invadosome and its associated invasive properties. Journal of Cell Science. 2014;127(2):328-40.

52. Campellone KG, Welch MD. A nucleator arms race: cellular control of actin assembly. Nature Reviews Molecular Cell Biology. 2010;11(4):237-51.

53. Fletcher DA, Mullins RD. Cell mechanics and the cytoskeleton. Nature. 2010;463(7280):485-92.

54. Svitkina TM, Borisy GG. Arp2/3 complex and actin depolymerizing factor/cofilin in dendritic organization and treadmilling of actin filament array in lamellipodia. The Journal of Cell Biology. 1999;145(5):1009-26.

55. Linder S, Aepfelbacher M. Podosomes: adhesion hot-spots of invasive cells. Trends in Cell Biology. 2003;13(7):376-85.

56. Yamaguchi H, Lorenz M, Kempiak S, Sarmiento C, Coniglio S, Symons M, et al. Molecular mechanisms of invadopodium formation: the role of the N-WASP-Arp2/3 complex pathway and cofilin. The Journal of Cell Biology. 2005;168(3):441-52.

57. Takenawa T, Suetsugu S. The WASP-WAVE protein network: connecting the membrane to the cytoskeleton. Nature Reviews Molecular Cell Biology. 2007;8(1):37-48.

58. Derry JM, Ochs HD, Francke U. Isolation of a novel gene mutated in Wiskott-Aldrich syndrome. Cell. 1994;78(4):635-44.

59. Miki H, Miura K, Takenawa T. N-WASP, a novel actin-depolymerizing protein, regulates the cortical cytoskeletal rearrangement in a PIP2-dependent manner downstream of tyrosine kinases. The EMBO Journal. 1996;15(19):5326-35.

60. Pollitt AY, Insall RH. WASP and SCAR/WAVE proteins: the drivers of actin assembly. Journal of Cell Science. 2009;122:2575-8.

61. Stradal TE, Rottner K, Disanza A, Confalonieri S, Innocenti M, Scita G. Regulation of actin dynamics by WASP and WAVE family proteins. Trends in Cell Biology. 2004;14(6):303-11.

62. Linder S, Wiesner C, Himmel M. Degrading devices: invadosomes in proteolytic cell invasion. Annual Review of Cell and Developmental Biology. 2011;27:185-211.

63. Oser M, Yamaguchi H, Mader CC, Bravo-Cordero JJ, Arias M, Chen X, et al. Cortactin regulates cofilin and N-WASp activities to control the stages of invadopodium assembly and maturation. The Journal of Cell Biology. 2009;186(4):571-87.

64. Gligorijevic B, Wyckoff J, Yamaguchi H, Wang Y, Roussos ET, Condeelis J. N-WASP-mediated invadopodium formation is involved in intravasation and lung metastasis of mammary tumors. Journal of Cell Science. 2012;125:724-34.

65. Yu X, Zech T, McDonald L, Gonzalez EG, Li A, Macpherson I, et al. N-WASP coordinates the delivery and F-actin-mediated capture of MT1-MMP at invasive pseudopods. The Journal of Cell Biology. 2012;199(3):527-44.

66. Linardopoulou EV, Parghi SS, Friedman C, Osborn GE, Parkhurst SM, Trask BJ. Human subtelomeric WASH genes encode a new subclass of the WASP family. PLoS Genetics. 2007;3(12):e237.

67. Gomez TS, Billadeau DD. A FAM21-containing WASH complex regulates retromer-dependent sorting. Developmental Cell. 2009;17(5):699-711.

68. Jia D, Gomez TS, Metlagel Z, Umetani J, Otwinowski Z, Rosen MK, et al. WASH and WAVE actin regulators of the Wiskott-Aldrich syndrome protein (WASP) family are controlled by analogous structurally related complexes. Proceedings of the National Academy of Sciences of the United States of America. 2010;107(23):10442-7.

69. Monteiro P, Rosse C, Castro-Castro A, Irondelle M, Lagoutte E, Paul-Gilloteaux P, et al. Endosomal WASH and exocyst complexes control exocytosis of MT1-MMP at invadopodia. The Journal of Cell Biology. 2013;203(6):1063-79.

70. Kirkbride KC, Sung BH, Sinha S, Weaver AM. Cortactin: a multifunctional regulator of cellular invasiveness. Cell Adhesion & Migration. 2011;5(2):187-98.

71. MacGrath SM, Koleske AJ. Cortactin in cell migration and cancer at a glance. Journal of Cell Science. 2012;125:1621-6.

72. Oser M, Mader CC, Gil-Henn H, Magalhaes M, Bravo-Cordero JJ, Koleske AJ, et al. Specific tyrosine phosphorylation sites on cortactin regulate Nck1-dependent actin polymerization in invadopodia. Journal of Cell Science. 2010;123:3662-73.

73. Clark ES, Whigham AS, Yarbrough WG, Weaver AM. Cortactin is an essential regulator of matrix metalloproteinase secretion and extracellular matrix degradation in invadopodia. Cancer Research. 2007;67(9):4227-35.

74. Magalhaes MA, Larson DR, Mader CC, Bravo-Cordero JJ, Gil-Henn H, Oser M, et al. Cortactin phosphorylation regulates cell invasion through a pH-dependent pathway. The Journal of Cell Biology. 2011;195(5):903-20.

75. Yamaguchi H, Condeelis J. Regulation of the actin cytoskeleton in cancer cell migration and invasion. Biochimica et Biophysica Acta. 2007;1773(5):642-52.

76. Gimona M, Buccione R, Courtneidge SA, Linder S. Assembly and biological role of podosomes and invadopodia. Current Opinion in Cell Biology. 2008;20(2):235-41.

77. Chen WT. Proteolytic activity of specialized surface protrusions formed at rosette contact sites of transformed cells. The Journal of Experimental Zoology. 1989;251(2):167-85.

78. David-Pfeuty T, Singer SJ. Altered distributions of the cytoskeletal proteins vinculin and alpha-actinin in cultured fibroblasts transformed by Rous sarcoma

virus. Proceedings of the National Academy of Sciences of the United States of America. 1980;77(11):6687-91.

79. Tarone G, Cirillo D, Giancotti FG, Comoglio PM, Marchisio PC. Rous sarcoma virus-transformed fibroblasts adhere primarily at discrete protrusions of the ventral membrane called podosomes. Experimental Cell Research. 1985;159(1):141-57.

80. Linder S. Invadosomes at a glance. Journal of Cell Science. 2009;122(17):3009-13.

81. Oser M, Dovas A, Cox D, Condeelis J. Nck1 and Grb2 localization patterns can distinguish invadopodia from podosomes. European Journal of Cell Biology. 2011;90(2-3):181-8.

82. Etienne-Manneville S, Hall A. Rho GTPases in cell biology. Nature. 2002;420(6916):629-35.

83. Jaffe AB, Hall A. Rho GTPases: biochemistry and biology. Annual Review of Cell and Developmental Biology. 2005;21:247-69.

84. Hall A. Rho GTPases and the control of cell behaviour. Biochemical Society Transactions. 2005;33(5):891-5.

85. Nakahara H, Otani T, Sasaki T, Miura Y, Takai Y, Kogo M. Involvement of Cdc42 and Rac small G proteins in invadopodia formation of RPMI7951 cells. Genes to Cells. 2003;8(12):1019-27.

86. Juin A, Di Martino J, Leitinger B, Henriet E, Gary AS, Paysan L, et al. Discoidin domain receptor 1 controls linear invadosome formation via a Cdc42-Tuba pathway. The Journal of Cell Biology. 2014;207(4):517-33.

87. Razidlo GL, Schroeder B, Chen J, Billadeau DD, McNiven MA. Vav1 as a central regulator of invadopodia assembly. Current Biology. 2014;24(1):86-93.

88. Di Paolo G, De Camilli P. Phosphoinositides in cell regulation and membrane dynamics. Nature. 2006;443(7112):651-7.

89. Saarikangas J, Zhao H, Lappalainen P. Regulation of the actin cytoskeleton-plasma membrane interplay by phosphoinositides. Physiological Reviews. 2010;90(1):259-89.

90. Yamaguchi H, Yoshida S, Muroi E, Kawamura M, Kouchi Z, Nakamura Y, et al. Phosphatidylinositol 4,5-bisphosphate and PIP5-kinase Ialpha are required for invadopodia formation in human breast cancer cells. Cancer Science. 2010;101(7):1632-8.

91. Chellaiah MA. Regulation of podosomes by integrin alphavbeta3 and Rho GTPase-facilitated phosphoinositide signaling. European Journal of Cell Biology. 2006;85(3-4):311-7.

92. Oikawa T, Itoh T, Takenawa T. Sequential signals toward podosome formation in NIH-src cells. The Journal of Cell Biology. 2008;182(1):157-69.

93. Sharma VP, Eddy R, Entenberg D, Kai M, Gertler FB, Condeelis J. Tks5 and SHIP2 regulate invadopodium maturation, but not initiation, in breast carcinoma cells. Current Biology. 2013;23(21):2079-89.

94. Hunter T. Tyrosine phosphorylation: thirty years and counting. Current Opinion in Cell Biology. 2009;21(2):140-6.

95. Lim WA, Pawson T. Phosphotyrosine signaling: evolving a new cellular communication system. Cell. 2010;142(5):661-7.

96. King CR, Kraus MH, Aaronson SA. Amplification of a novel v-erbB-related gene in a human mammary carcinoma. Science. 1985;229(4717):974-6.

97. Gherardi E, Birchmeier W, Birchmeier C, Vande Woude G. Targeting MET in cancer: rationale and progress. Nature Reviews Cancer. 2012;12(2):89-103.

98. Zhang S, Huang WC, Li P, Guo H, Poh SB, Brady SW, et al. Combating trastuzumab resistance by targeting SRC, a common node downstream of multiple resistance pathways. Nature Medicine. 2011;17(4):461-9.

99. Courtneidge SA, Azucena EF, Pass I, Seals DF, Tesfay L. The SRC substrate Tks5, podosomes (invadopodia), and cancer cell invasion. Cold Spring Harbor Symposia on Quantitative Biology. 2005;70:167-71.

100. Stylli SS, Stacey TT, Verhagen AM, Xu SS, Pass I, Courtneidge SA, et al. Nck adaptor proteins link Tks5 to invadopodia actin regulation and ECM degradation. Journal of Cell Science. 2009;122(15):2727-40.

101. Valiathan RR, Marco M, Leitinger B, Kleer CG, Fridman R. Discoidin domain receptor tyrosine kinases: new players in cancer progression. Cancer Metastasis Reviews. 2012;31(1-2):295-321.

102. Park HS, Kim KR, Lee HJ, Choi HN, Kim DK, Kim BT, et al. Overexpression of discoidin domain receptor 1 increases the migration and invasion of

hepatocellular carcinoma cells in association with matrix metalloproteinase. Oncology Reports. 2007;18(6):1435-41.

103. Fu HL, Sohail A, Valiathan RR, Wasinski BD, Kumarasiri M, Mahasenan KV, et al. Shedding of discoidin domain receptor 1 by membrane-type matrix metalloproteinases. The Journal of Biological Chemistry. 2013;288(17):12114-29.

104. Zhang K, Corsa CA, Ponik SM, Prior JL, Piwnica-Worms D, Eliceiri KW, et al. The collagen receptor discoidin domain receptor 2 stabilizes SNAIL1 to facilitate breast cancer metastasis. Nature Cell Biology. 2013;15(6):677-87.

105. Li W, Fan JH, Woodley DT. Nck/Dock: an adapter between cell surface receptors and the actin cytoskeleton. Oncogene. 2001;20(44):6403-17.

106. Buday L, Wunderlich L, Tamas P. The Nck family of adapter proteins: regulators of actin cytoskeleton. Cellular Signalling. 2002;14(9):723-31.

107. McCarty JH. The Nck SH2/SH3 adaptor protein: a regulator of multiple intracellular signal transduction events. BioEssays : News and Reviews in Molecular, Cellular and Developmental Biology. 1998;20(11):913-21.

108. Mayer BJ. SH3 domains: complexity in moderation. Journal of Cell Science. 2001;114:1253-63.

109. Bladt F, Aippersbach E, Gelkop S, Strasser GA, Nash P, Tafuri A, et al. The murine Nck SH2/SH3 adaptors are important for the development of mesoderm-derived embryonic structures and for regulating the cellular actin network. Molecular and Cellular Biology. 2003;23(13):4586-97.

110. Guan S, Fan J, Han A, Chen M, Woodley DT, Li W. Non-compensating roles between Nckalpha and Nckbeta in PDGF-BB signaling to promote human dermal fibroblast migration. The Journal of Investigative Dermatology. 2009;129(8):1909-20.

111. West NW, Garcia-Vargas A, Chalfant CE, Park MA. OSU-03012 sensitizes breast cancers to lapatinib-induced cell killing: a role for Nck1 but not Nck2. BMC Cancer. 2013;13:256.

112. Jones N, Blasutig IM, Eremina V, Ruston JM, Bladt F, Li H, et al. Nck adaptor proteins link nephrin to the actin cytoskeleton of kidney podocytes. Nature. 2006;440(7085):818-23.

113. Vogel WF, Aszodi A, Alves F, Pawson T. Discoidin domain receptor 1 tyrosine kinase has an essential role in mammary gland development. Molecular and Cellular Biology. 2001;21(8):2906-17.

114. Koo DH, McFadden C, Huang Y, Abdulhussein R, Friese-Hamim M, Vogel WF. Pinpointing phosphotyrosine-dependent interactions downstream of the collagen receptor DDR1. FEBS Letters. 2006;580(1):15-22.

115. Clouthier DL, Harris CN, Harris RA, Martin CE, Puri MC, Jones N. Requisite role for Nck adaptors in cardiovascular development, endothelial-to-mesenchymal transition and directed cell migration. Molecular and Cellular Biology. 2015;35(9):1573-87.

116. Frischknecht F, Moreau V, Rottger S, Gonfloni S, Reckmann I, Superti-Furga G, et al. Actin-based motility of vaccinia virus mimics receptor tyrosine kinase signalling. Nature. 1999;401(6756):926-9.

117. Scaplehorn N, Holmstrom A, Moreau V, Frischknecht F, Reckmann I, Way M. Grb2 and Nck act cooperatively to promote actin-based motility of vaccinia virus. Current Biology. 2002;12(9):740-5.

118. Gruenheid S, DeVinney R, Bladt F, Goosney D, Gelkop S, Gish GD, et al. Enteropathogenic E. coli Tir binds Nck to initiate actin pedestal formation in host cells. Nature Cell Biology. 2001;3(9):856-9.

119. Rohatgi R, Ma L, Miki H, Lopez M, Kirchhausen T, Takenawa T, et al. The interaction between N-WASP and the Arp2/3 complex links Cdc42-dependent signals to actin assembly. Cell. 1999;97(2):221-31.

120. Rohatgi R, Nollau P, Ho HY, Kirschner MW, Mayer BJ. Nck and phosphatidylinositol 4,5-bisphosphate synergistically activate actin polymerization through the N-WASP-Arp2/3 pathway. The Journal of Biological Chemistry. 2001;276(28):26448-52.

121. Rivera GM, Briceno CA, Takeshima F, Snapper SB, Mayer BJ. Inducible clustering of membrane-targeted SH3 domains of the adaptor protein Nck triggers localized actin polymerization. Current Biology. 2004;14(1):11-22.

122. Campellone KG, Rankin S, Pawson T, Kirschner MW, Tipper DJ, Leong JM. Clustering of Nck by a 12-residue Tir phosphopeptide is sufficient to trigger localized actin assembly. The Journal of Cell Biology. 2004;164(3):407-16.

123. Rivera GM, Vasilescu D, Papayannopoulos V, Lim WA, Mayer BJ. A reciprocal interdependence between Nck and PI(4,5)P(2) promotes localized N-WASp-mediated actin polymerization in living cells. Molecular Cell. 2009;36(3):525-35.

124. Ditlev JA, Michalski PJ, Huber G, Rivera GM, Mohler WA, Loew LM, et al. Stoichiometry of Nck-dependent actin polymerization in living cells. The Journal of Cell Biology. 2012;197(5):643-58.

125. Donnelly SK, Weisswange I, Zettl M, Way M. WIP provides an essential link between Nck and N-WASP during Arp2/3-dependent actin polymerization. Current Biology. 2013;23(11):999-1006.

126. Seals DF, Azucena EF, Jr., Pass I, Tesfay L, Gordon R, Woodrow M, et al. The adaptor protein Tks5/Fish is required for podosome formation and function, and for the protease-driven invasion of cancer cells. Cancer Cell. 2005;7(2):155-65.

127. Lock P, Abram CL, Gibson T, Courtneidge SA. A new method for isolating tyrosine kinase substrates used to identify fish, an SH3 and PX domain-containing protein, and Src substrate. The EMBO Journal. 1998;17(15):4346-57.

128. Huang M, Anand S, Murphy EA, Desgrosellier JS, Stupack DG, Shattil SJ, et al. EGFR-dependent pancreatic carcinoma cell metastasis through Rap1 activation. Oncogene. 2012;31(22):2783-93.

129. Labelle-Cote M, Dusseault J, Ismail S, Picard-Cloutier A, Siegel PM, Larose L. Nck2 promotes human melanoma cell proliferation, migration and invasion in vitro and primary melanoma-derived tumor growth in vivo. BMC Cancer. 2011;11:443.

130. Caldieri G, Ayala I, Attanasio F, Buccione R. Cell and molecular biology of invadopodia. International Review of Cell and Molecular Biology. 2009;275:1-34.

131. Egeblad M, Werb Z. New functions for the matrix metalloproteinases in cancer progression. Nature Reviews Cancer. 2002;2(3):161-74.

132. Burdall SE, Hanby AM, Lansdown MR, Speirs V. Breast cancer cell lines: friend or foe? Breast Cancer Research. 2003;5(2):89-95.

133. Cailleau R, Olive M, Cruciger QV. Long-term human breast carcinoma cell lines of metastatic origin: preliminary characterization. In Vitro. 1978;14(11):911-5.

134. Brunner N, Boysen B, Romer J, Spang-Thomsen M. The nude mouse as an in vivo model for human breast cancer invasion and metastasis. Breast Cancer Research and Treatment. 1993;24(3):257-64.

135. Swift S, Lorens J, Achacoso P, Nolan GP. Rapid production of retroviruses for efficient gene delivery to mammalian cells using 293T cell-based systems. Current Protocols in Immunology. 2001;31:10.17.14-29.

136. Antoku S, Saksela K, Rivera GM, Mayer BJ. A crucial role in cell spreading for the interaction of Abl PxxP motifs with Crk and Nck adaptors. Journal of Cell Science. 2008;121(18):3071-82.

137. Chaki SP, Barhoumi R, Berginski ME, Sreenivasappa H, Trache A, Gomez SM, et al. Nck enables directional cell migration through the coordination of polarized membrane protrusion with adhesion dynamics. Journal of Cell Science. 2013;126(7):1637-49.

138. Albini A, Benelli R. The chemoinvasion assay: a method to assess tumor and endothelial cell invasion and its modulation. Nature Protocols. 2007;2(3):504-11.

139. Artym VV, Matsumoto K. Imaging cells in three-dimensional collagen matrix. Current Protocols in Cell Biology. 2010;48:10.18.1-20.

140. Guzman A, Ziperstein MJ, Kaufman LJ. The effect of fibrillar matrix architecture on tumor cell invasion of physically challenging environments. Biomaterials. 2014;35(25):6954-63.

141. Dudley A, Sater M, Le PU, Trinh G, Sadr MS, Bergeron J, et al. DRR regulates AKT activation to drive brain cancer invasion. Oncogene. 2014;33(41):4952-60.

142. Scribner KC, Behbod F, Porter WW. Regulation of DCIS to invasive breast cancer progression by Singleminded-2s (SIM2s). Oncogene. 2013;32(21):2631-9.

143. Blouw B, Patel M, Iizuka S, Abdullah C, You WK, Huang X, et al. The Invadopodia scaffold protein Tks5 is required for the growth of human breast cancer cells in vitro and in vivo. PLoS One. 2015;10(3):e0121003.

144. Kwak HI, Gustafson T, Metz RP, Laffin B, Schedin P, Porter WW. Inhibition of breast cancer growth and invasion by single-minded 2s. Carcinogenesis. 2007;28(2):259-66.

145. Hettinger AM, Allen MR, Zhang BR, Goad DW, Malayer JR, Geisert RD. Presence of the acute phase protein, bikunin, in the endometrium of gilts during estrous cycle and early pregnancy. Biology of Reproduction. 2001;65(2):507-13.

146. Menon DB, Gopalakrishnan VK. Terpenoids isolated from the shoot of plectranthus hadiensis induces apoptosis in human colon cancer cells via the mitochondria-dependent pathway. Nutrition and Cancer. 2015;67(4):697-705.

147. Maller O, Martinson H, Schedin P. Extracellular matrix composition reveals complex and dynamic stromal-epithelial interactions in the mammary gland. Journal of Mammary Gland Biology and Neoplasia. 2010;15(3):301-18.

148. Schedin P, Keely PJ. Mammary gland ECM remodeling, stiffness, and mechanosignaling in normal development and tumor progression. Cold Spring Harbor Perspectives in Biology. 2011;3(1):a003228.

149. Yang YL, Leone LM, Kaufman LJ. Elastic moduli of collagen gels can be predicted from two-dimensional confocal microscopy. Biophysical Journal. 2009;97(7):2051-60.

150. Yin LL, Chung CM, Chen J, Fok KL, Ng CP, Jia RR, et al. A suppressor of multiple extracellular matrix-degrading proteases and cancer metastasis. Journal of Cellular and Molecular Medicine. 2009;13(9B):4034-41.

151. Kozera B, Rapacz M. Reference genes in real-time PCR. Journal of Applied Genetics. 2013;54(4):391-406.

152. Masuda H, Zhang D, Bartholomeusz C, Doihara H, Hortobagyi GN, Ueno NT. Role of epidermal growth factor receptor in breast cancer. Breast Cancer Research and Treatment. 2012;136(2):331-45.

153. Wu C, Haynes EM, Asokan SB, Simon JM, Sharpless NE, Baldwin AS, et al. Loss of Arp2/3 induces an NF-kappaB-dependent, nonautonomous effect on chemotactic signaling. The Journal of Cell Biology. 2013;203(6):907-16.

154. Yamada KM, Cukierman E. Modeling tissue morphogenesis and cancer in 3D. Cell. 2007;130(4):601-10.

155. Kim JB, Stein R, O'Hare MJ. Three-dimensional in vitro tissue culture models of breast cancer – a review. Breast Cancer Research and Treatment. 2004;85(3):281-91.

156. Levental KR, Yu H, Kass L, Lakins JN, Egeblad M, Erler JT, et al. Matrix crosslinking forces tumor progression by enhancing integrin signaling. Cell. 2009;139(5):891-906.

157. Mukherjee C, Bakthavachalu B, Schoenberg DR. The cytoplasmic capping complex assembles on adapter protein nck1 bound to the proline-rich C-terminus of mammalian capping enzyme. PLoS Biology. 2014;12(8):e1001933.

158. Seiler C, Davuluri G, Abrams J, Byfield FJ, Janmey PA, Pack M. Smooth muscle tension induces invasive remodeling of the zebrafish intestine. PLoS Biology. 2012;10(9):e1001386.

159. Leong HS, Robertson AE, Stoletov K, Leith SJ, Chin CA, Chien AE, et al. Invadopodia are required for cancer cell extravasation and are a therapeutic target for metastasis. Cell Reports. 2014;8(5):1558-70.

160. Hagedorn EJ, Kelley LC, Naegeli KM, Wang Z, Chi Q, Sherwood DR. ADF/cofilin promotes invadopodial membrane recycling during cell invasion in vivo. The Journal of Cell Biology. 2014;204(7):1209-18.

161. Hagedorn EJ, Ziel JW, Morrissey MA, Linden LM, Wang Z, Chi Q, et al. The netrin receptor DCC focuses invadopodia-driven basement membrane transmigration in vivo. The Journal of Cell Biology. 2013;201(6):903-13.

162. Rohatgi R, Ho HY, Kirschner MW. Mechanism of N-WASP activation by CDC42 and phosphatidylinositol 4, 5-bisphosphate. The Journal of Cell Biology. 2000;150(6):1299-310.

163. Padrick SB, Rosen MK. Physical mechanisms of signal integration by WASP family proteins. Annual Review of Biochemistry. 2010;79:707-35.

164. Goldenring JR. A central role for vesicle trafficking in epithelial neoplasia: intracellular highways to carcinogenesis. Nature Reviews Cancer. 2013;13(11):813-20.

165. Dimri M, Naramura M, Duan L, Chen J, Ortega-Cava C, Chen G, et al. Modeling breast cancer-associated c-Src and EGFR overexpression in human MECs: c-Src and EGFR cooperatively promote aberrant three-dimensional acinar structure and invasive behavior. Cancer Research. 2007;67(9):4164-72.

166. Hirata E, Yukinaga H, Kamioka Y, Arakawa Y, Miyamoto S, Okada T, et al. In vivo fluorescence resonance energy transfer imaging reveals differential activation of Rho-family GTPases in glioblastoma cell invasion. Journal of Cell Science. 2012;125(4):858-68.

167. Sakurai-Yageta M, Recchi C, Le Dez G, Sibarita JB, Daviet L, Camonis J, et al. The interaction of IQGAP1 with the exocyst complex is required for tumor cell invasion downstream of Cdc42 and RhoA. The Journal of Cell Biology. 2008;181(6):985-98.

168. Artym VV, Yamada KM, Mueller SC. ECM degradation assays for analyzing local cell invasion. Methods in Molecular Biology. 2009;522:211-9.

169. Cervero P, Panzer L, Linder S. Podosome reformation in macrophages: assays and analysis. Methods in Molecular Biology. 2013;1046:97-121.

170. Starnes TW, Cortesio CL, Huttenlocher A. Imaging podosome dynamics and matrix degradation. Methods in Molecular Biology. 2011;769:111-36.

171. Barhoumi R, Bowen JA, Stein LS, Echols J, Burghardt RC. Concurrent analysis of intracellular glutathione content and gap junctional intercellular communication. Cytometry. 1993;14(7):747-56.

172. Li A, Dawson JC, Forero-Vargas M, Spence HJ, Yu X, Konig I, et al. The actin-bundling protein fascin stabilizes actin in invadopodia and potentiates protrusive invasion. Current Biology. 2010;20(4):339-45.

173. Hodgson L, Shen F, Hahn K. Biosensors for characterizing the dynamics of rho family GTPases in living cells. Current Protocols in Cell Biology. 2010;46: 14.11.1-26.

174. Quintero OA, DiVito MM, Adikes RC, Kortan MB, Case LB, Lier AJ, et al. Human Myo19 is a novel myosin that associates with mitochondria. Current Biology. 2009;19(23):2008-13.

175. Castro-Castro A, Janke C, Montagnac G, Paul-Gilloteaux P, Chavrier P. ATAT1/MEC-17 acetyltransferase and HDAC6 deacetylase control a balance of acetylation of alpha-tubulin and cortactin and regulate MT1-MMP trafficking and breast tumor cell invasion. European Journal of Cell Biology. 2012;91(11-12):950-60.

176. Beaty BT, Condeelis J. Digging a little deeper: The stages of invadopodium formation and maturation. European Journal of Cell Biology. 2014;93(10-12):438-44.

177. Artym VV, Zhang Y, Seillier-Moiseiwitsch F, Yamada KM, Mueller SC. Dynamic interactions of cortactin and membrane type 1 matrix metalloproteinase at invadopodia: defining the stages of invadopodia formation and function. Cancer Research. 2006;66(6):3034-43.

178. Tehrani S, Tomasevic N, Weed S, Sakowicz R, Cooper JA. Src phosphorylation of cortactin enhances actin assembly. Proceedings of the National Academy of Sciences of the United States of America. 2007;104(29):11933-8.

179. Riedl J, Crevenna AH, Kessenbrock K, Yu JH, Neukirchen D, Bista M, et al. Lifeact: a versatile marker to visualize F-actin. Nature Methods. 2008;5(7):605-7.

180. Zuo Y, Wu Y, Chakraborty C. Cdc42 negatively regulates intrinsic migration of highly aggressive breast cancer cells. Journal of Cellular Physiology. 2012;227(4):1399-407.

181. Reymond N, Im JH, Garg R, Vega FM, Borda d'Agua B, Riou P, et al. Cdc42 promotes transendothelial migration of cancer cells through beta1 integrin. The Journal of Cell Biology. 2012;199(4):653-68.

182. Aoki K, Matsuda M. Visualization of small GTPase activity with fluorescence resonance energy transfer-based biosensors. Nature Protocols. 2009;4(11):1623-31.

183. Loskutov YV, Kozyulina PY, Kozyreva VK, Ice RJ, Jones BC, Roston TJ, et al. NEDD9/Arf6-dependent endocytic trafficking of matrix metalloproteinase 14: a novel mechanism for blocking mesenchymal cell invasion and metastasis of breast cancer [published online ahead of print Sept 22 2014]. Oncogene. 2014. http://www.nature.com/onc/journal/vaop/ncurrent/full/onc2014297a.html. Accessed Sept 23 2014.

184. Macpherson IR, Rainero E, Mitchell LE, van den Berghe PV, Speirs C, Dozynkiewicz MA, et al. CLIC3 controls recycling of late endosomal MT1-MMP and dictates invasion and metastasis in breast cancer. Journal of Cell Science. 2014;127(18):3893-901.

185. Williams KC, McNeilly RE, Coppolino MG. SNAP23, Syntaxin4, and vesicle-associated membrane protein 7 (VAMP7) mediate trafficking of membrane type 1-matrix metalloproteinase (MT1-MMP) during invadopodium formation and tumor cell invasion. Molecular Biology of the Cell. 2014;25(13):2061-70.

186. Williams KC, Coppolino MG. Phosphorylation of membrane type 1-matrix metalloproteinase (MT1-MMP) and its vesicle-associated membrane protein 7

(VAMP7)-dependent trafficking facilitate cell invasion and migration. The Journal of Biological Chemistry. 2011;286(50):43405-16.

187. Bachmeier BE, Albini A, Vene R, Benelli R, Noonan D, Weigert C, et al. Cell density-dependent regulation of matrix metalloproteinase and TIMP expression in differently tumorigenic breast cancer cell lines. Experimental Cell Research. 2005;305(1):83-98.

188. Reyes SB, Narayanan AS, Lee HS, Tchaicha JH, Aldape KD, Lang FF, et al. alphavbeta8 integrin interacts with RhoGDI1 to regulate Rac1 and Cdc42 activation and drive glioblastoma cell invasion. Molecular Biology of the Cell. 2013;24(4):474-82.

APPENDIX A

SHRNA TRANSWELL INVASION ASSAY

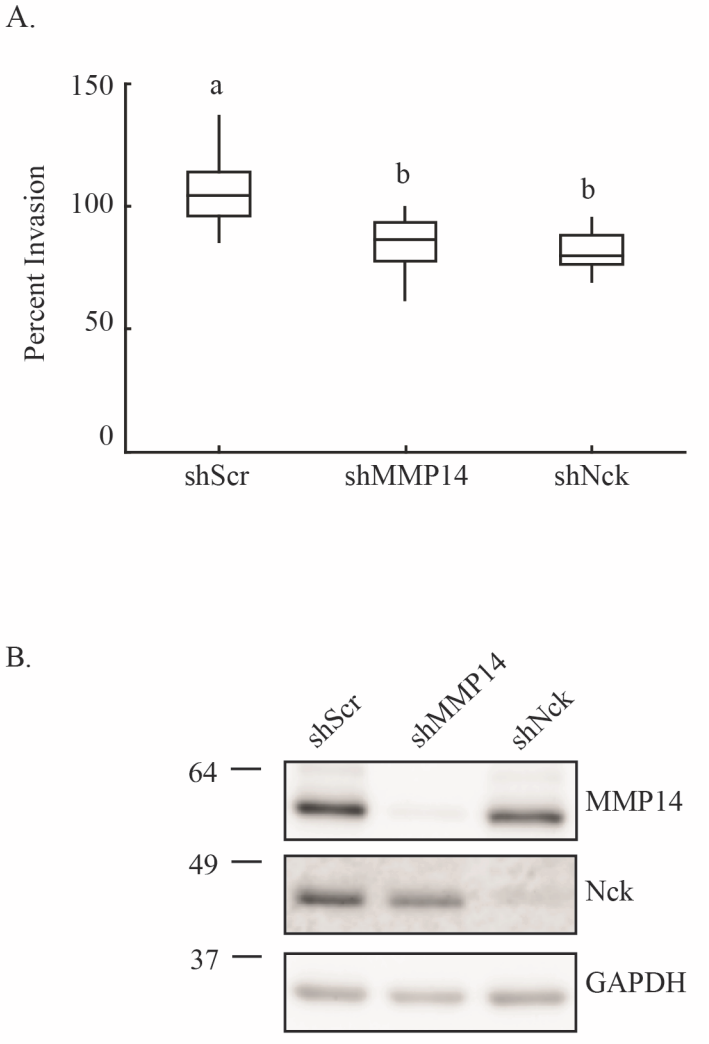

Loss of Nck decreases individual mammary carcinoma cell invasion. MDA-MB-231 cells stably expressing short hairpin (sh) RNAs encoding a non-targeting sequence (shScr) or sequences targeting MMP14 (shMMP14) or Nck (shNck). Cells were subjected to migration or invasion assays using BD BioCoatTM invasion chambers supplied with 8 micron PET filters uncoated or coated with a laminin-rich matrix (Matrigel) in the presence of EGF (10 ng/ml) used as a chemoattractant. A total of $5x10^4$ cells were seeded and incubated for 5 (migration) or 18 (invasion) hours. **A)** Box and whisker plot showing cell invasiveness calculated as percent invasion (invaded cells / migrated cells * 100). Results shown summarize data from one experiment performed in triplicate. **B)** Representative western blot showing the efficacy of protein silencing using shRNA oligonucleotides. a, b indicate statistical differences ($p<0.05$).

APPENDIX B

3D SPHEROID INVASION EGF STIMULATION STANDARDIZATION

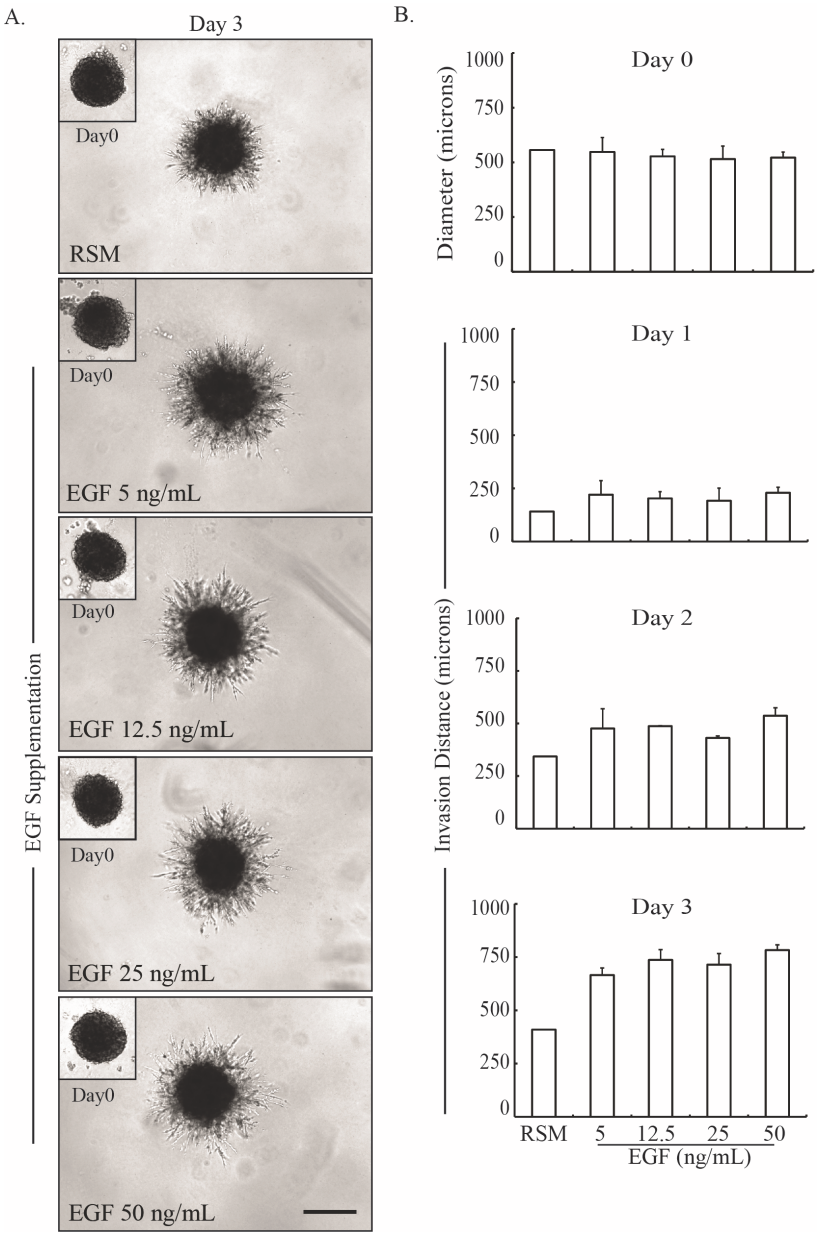

Epidermal growth factor (EGF) stimulates invasion of mammary carcinoma cells in 3D laminin-rich matrices. Spheroids of MDA-MB-231 cells were allowed to invade in the presence of reduced serum medium (RSM) or RSM supplemented with various concentrations of EGF. **A)** Representative images of MDA-MB-231 spheroids at day 0 (insets) and day 3 of invasion. Scale bar equals 500 microns. **B**) Bar graphs showing average spheroid diameter at day 0 and EGF-stimulated invasion distance following various intervals of incubation. Error bars on bar graphs indicate standard deviation. Spheroids (n) per condition: RSM n=1, 5-50ng/mL EGF n=2.

APPENDIX C

3D SPHEROID INVASION IN LAMININ-RICH MATRICES: DAY 1 AND DAY 2

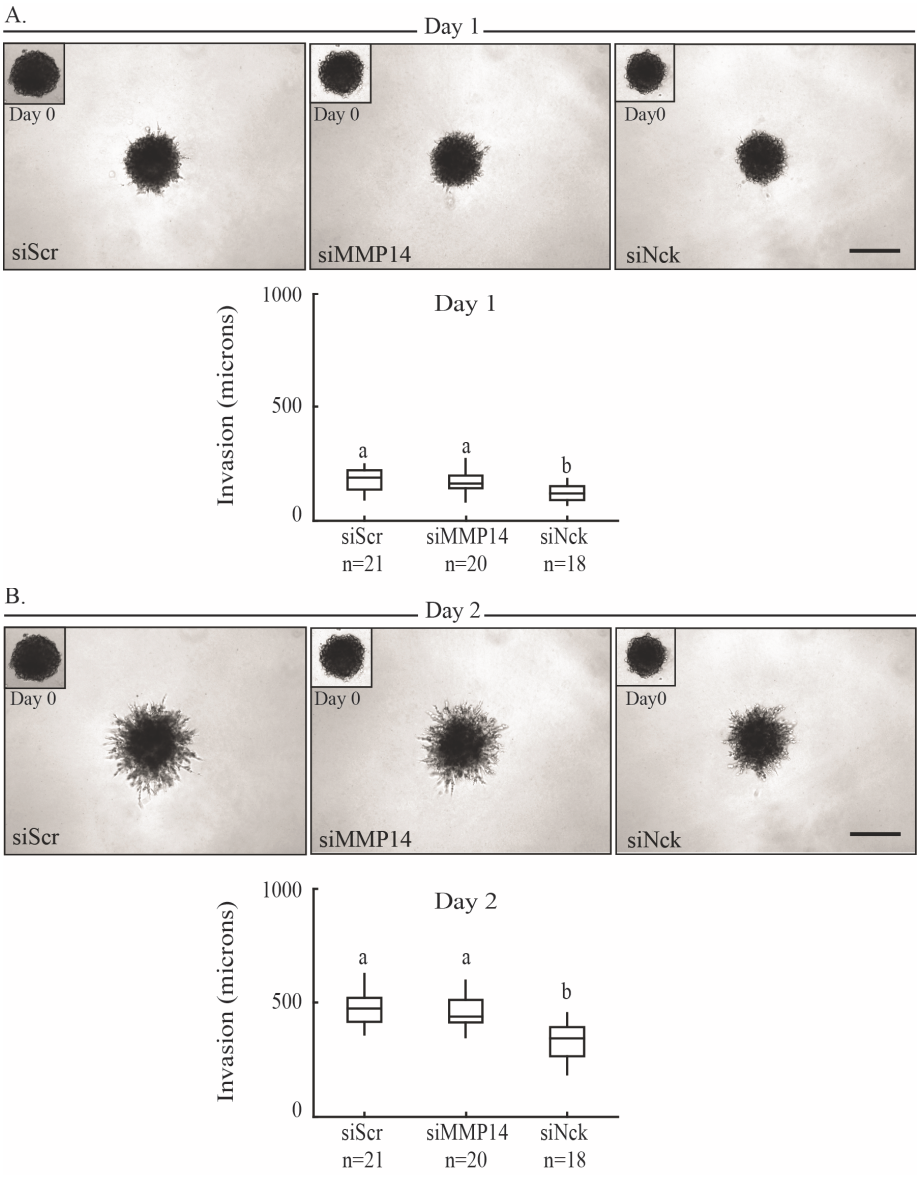

Loss of Nck reduces invasion of mammary carcinoma cells in 3D laminin-rich matrices. MDA-MB-231 cells were transiently transfected with small interference (si) RNA oligonucleotides encoding non-targeting sequences (siScr) or sequences targeting MMP14 (siMMP14) or Nck (siNck). **A-B)** Representative photomicrographs of spheroids (upper) after 1 (A) or 2 (B) days of invasion and box and whisker plots showing invasion distance (lower). Different letters represent statistically different values ($p<0.05$). Results shown summarize data from four independent experiments (n=3-6 spheroids/condition).

APPENDIX D

3D SPHEROID INVASION GM6001 CONTROL

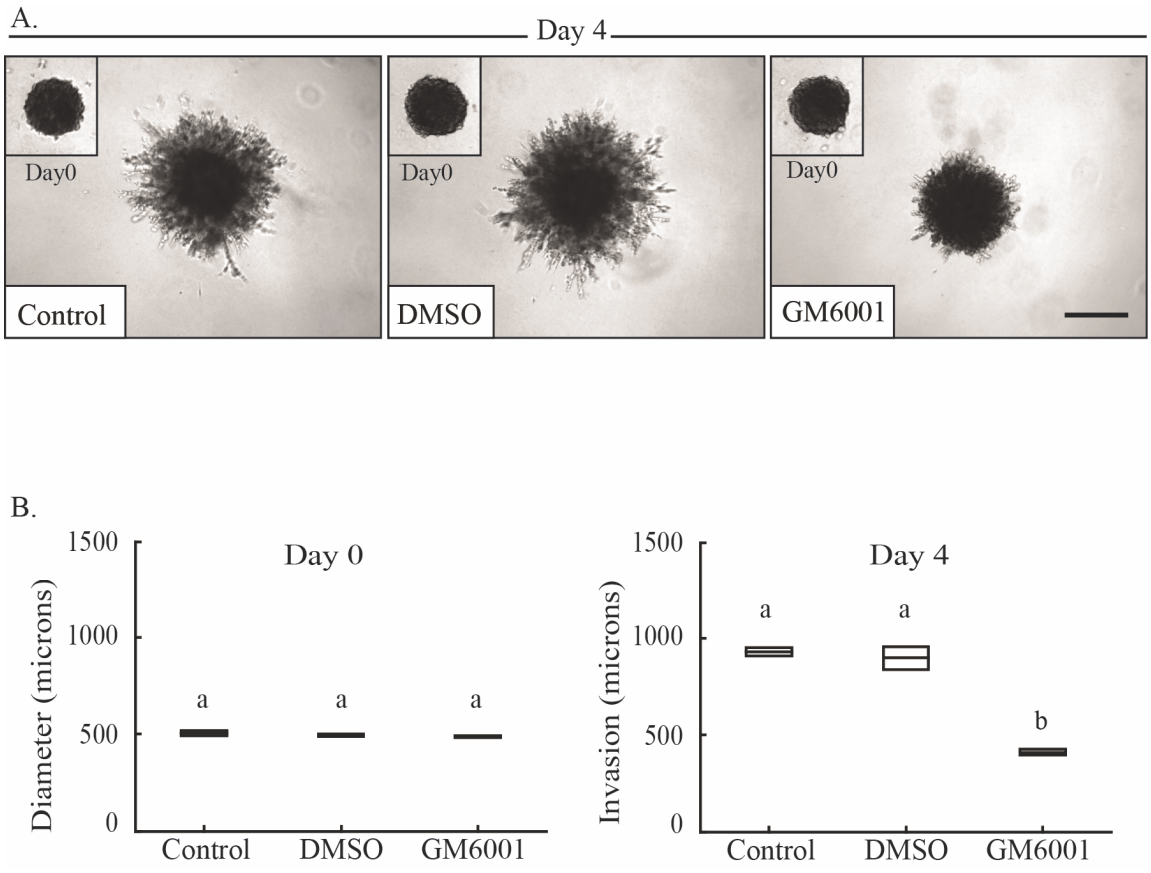

The general MMP inhibitor GM6001, but not the vehicle DMSO, inhibits mammary carcinoma cell invasion in 3D laminin-rich matrices. Spheroids of MDA-MB-231 cells were allowed to invade in complete medium supplemented with 50 ng/mL of EGF in the absence or presence of DMSO (%vol/vol) or DMSO plus 25 mM GM6001. **A)** Representative images of spheroids at day 0 (insets) or day 4 of invasion. Scale bar equals 500 microns. **B)** Box and whisker plot (right) showing spheroid diameter at day 0 (left) and invasion distance at day 4 (right). Different letters represent statistically different values ($p<0.05$). Data from one experiment performed in duplicate.

APPENDIX E

IMMUNOFLUORESCENCE OF MEMBRANE MMP14

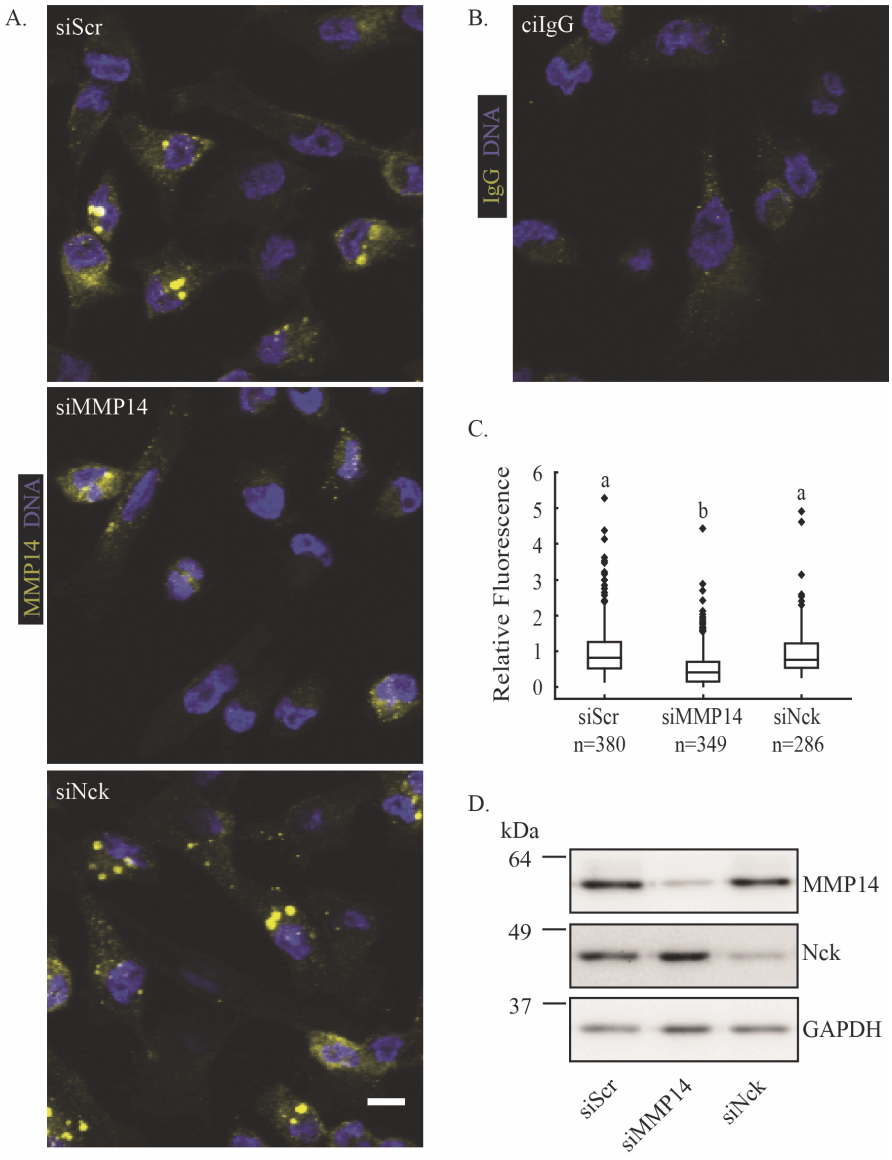

Steady-state membrane MMP14 levels are independent of Nck expression on poly-L-lysine coated glass. MDA-MB-231 cells were plated on poly-L-lysine and fixed but not permeabilized. Subsequently, cells were stained with control isotype IgG (ciIgG) or an antibody that recognizes the extracellular, catalytic domain of MMP14. Pseudocolor Z-projections of confocal stacks were generated after background subtraction. Pseudocolored images show nuclei (blue) and MMP14 **A)** or non-specific binding of ciIgG **B)** at the cell surface. White scale bar represents 10 microns. **C)** Fluorescence intensity was normalized to siScr for each experiment then replicates combined to generate relative fluorescence. Different letters represent statistically different values ($p<0.05$). **D)** Representative western blot showing efficacy of protein silencing.

APPENDIX F

FLUORESCENT GELATIN DEGRADATION

Part 1: Gelatin Labeling

Materials:

- 0.2% Gelatin
    a. 20 mg Gelatin from porcine skin, type A (Sigma Cat. No. G2500)
    b. 10 mL DPBS
    c. Incubate in a 37C water bath for 30 minutes vortex ever 5-10 minutes to help dissolve
    d. Filter sterilize dissolved gelatin with 0.2 μm syringe filter
- Alexa Fluor 488 protein labeling kit (Invitrogen Cat. No. A10235)
- 1 M sodium bicarbonate (prepare fresh, filter sterilize)
- Ring stand and clamp
- Amber-colored microcentrifuge tubes

Procedure:

Perform in biosafety cabinet with the lights turned off to protect gelatin from contamination and photo degradation of the Alexa dye.

1. Prepare 0.2% gelatin in DPBS and filter sterilize
2. Combine 50 μL 1 M sodium bicarbonate and 500 μl 0.2% gelatin in a tube containing the reactive dye and stir bar
3. Mix at room temperature protected from light, on a stir plate for 1 hour
4. Load resin from Alexa Fluor Protein Labeling kit into provided column up to 3 centimeters from the top
    a. Allow excess buffer (provided with kit, DPBS + 2 mM sodium azide, pH 7.2) to flow out of column
5. Load labeled gelatin into column
    a. Collect excess buffer in 500 μL aliquots and keep loading clean buffer (also in 500 aliquots) until 1st fraction flows out
6. Collect 1st fraction containing the Alexa 488-labeled gelatin
    a. Excess unlabeled gelatin will be in the 2nd fraction
7. Prepare 100 μL aliquots in amber-colored microcentrifuge tubes
    a. Store at -20°C.

Part 2: Fluorescent gelatin coating coverslips Perform in biosafety cabinet with the lights turned off to protect gelatin from contamination and photo degradation of the Alexa dye.

Materials:

- 0.2% Gelatin (see protocol in Part 1)
- Labeled gelatin from Part 1

- Acid-washed 18-millimeter coverslips
- DPBS, at room temperature
- 0.5% gluteraldehyde (need 1 mL per coverslip)
    - Dilute from 50% (Electron Microscopy Sciences, Cat. No. 16320) stored at 4^{o}C) in DPBS and filter sterilize. Must be prepared directly before use.
- 5 mg/mL sodium borohydride (need 1 mL per coverslip) dissolved in DPBS
    - Filter sterilize
    - Must be prepared directly before use
- Sterile forceps

Procedure:

1. Place acid-washed, sterile 18-millimeter coverslips in individual wells of 12-well plate
2. Add 1 mL of 0.005% poly-L-lysine solution per coverslip (0.01% poly-L-lysine, Cultrex 3438-100-01)
    a. Make a 1:1 dilution of stock poly-L-lysine in DPBS in a tube chilled on ice
3. Incubate 20 minutes at RT, then aspirate solution
4. Wash three times with DPBS (1 mL each wash)
5. Incubate coverslip in 1 mL of 0.5% gluteraldehyde for 15 minutes
6. Mix 0.2% gelatin and Alexa labeled gelatin (from Part 1 above) at an 8:1 ratio and incubate in a 37^{o}C water bath to warm the mixture
    a. You will need 80 µL of the fluorescent gelatin matrix for each coverslip (make enough of this solution for n+1 coverslips)
7. Aspirate gluteraldehyde and wash coverslips three times with 1 mL of DPBS
    a. Do not aspirate DPBS after the 3rd wash
8. Cut a sheet of parafilm and place it in a humidified chamber
    a. Humidified chamber is a 150-millimeter tissue culture plate covered with aluminum foil and a piece of Whatman paper wetted with ddH_2O placed in the bottom
9. Place 80 µL droplets of the preheated fluorescent gelatin on the Parafilm far enough apart to allow placement of coverslips without overlap
10. Using forceps, lift coverslips out of 12-well plate and place them directly on fluorescent gelatin
11. Incubate 45 minutes at RT
12. Carefully lift each coverslip and transfer to individual 12-well plates
    a. IMPORTANT: make sure to place them with the fluorescent gelatin facing up
13. Wash three times with DPBS (1 mL each wash)
14. Quench residual reactive groups in the gelatin matrix with 5 mg/mL sodium borohydride
    a. Add 1 mL of the solution to each well as soon as it starts bubbling
15. Incubate 15 minutes at RT with gentle rocking

a. Ensure bubbles are released from beneath the coverslips
b. Do not allow bubbles to settle on the side of the coverslip coated with the gelatin matrix to prevent damaging the gelatin

16. Wash three times with DPBS (2 mL each wash)
    a. If bubbles persist continue to wash until they have been eliminated
17. Incubate 30 minutes with 70% EtOH protected from light
18. Wash three times with DPBS (1 mL each wash)
    a. Do not aspirate DPBS after last wash and wrap each plate with parafilm and aluminum foil to prevent contamination and exposure to light
19. Store coated coverslips at 4^{o}C for up to 6 days or use immediately
    a. It is best coat coverslips the day before use

Part 3: Cell Preparation and Immunofluorescence Staining

**Protect your samples from light by wrapping your plates in aluminum foil when not handling them.

Materials:

- 3.7% Paraformaldehyde
- 5% Sucrose
- 0.2% Triton X-100
- 2% BSA
- Human serum (Jackson ImmunoResearch, 009-000-121)
- Goat serum (Sigma G9023-10 mL)
- NucBlue® Live ReadyProbes® Reagent (Life Technologies R37605)
- DPBS, at room temperature (RT)
- Texas Red®-X Phalloidin (Life Technologies T7471)
- Anti-Cortactin (p80/85), clone 4F11 (Millipore #05-180)
- Anti-MMP14 (Millipore, MAB3328)
- Alexa Fluor® 647 Goat Anti-Mouse IgG (H+L) (Life Technologies A-21235)
- TBS-T
- Prolong® Gold Antifade Mountant (Life Technologies P36934)

Procedure for actin and cortactin staining:

1. Count cells: for MDA-MB-231 cells in a 12 well plate, use 7.5x10^{4} cells in 1 mL media
2. Incubate coverslips in complete media for 30 minutes to 1 hour prior to addition of cells on gelatin matrix coated coverslip
3. Place 1 mL of the cell suspension on top of the gelatin-matrix coated coverslips
4. Incubate at 37^{o}C for 6 hours
5. 20 minutes prior to fixation add 2 drops NucBlue to each well
6. Warm a 3.7% paraformaldehyde/5% sucrose (in DPBS) solution to 37^{o}C
7. Aspirate cell-culture medium from each well, rinse with 1 mL DPBS and add 1 mL of warmed 3.7% paraformaldehyde with 5% sucrose
8. Incubate 20 minutes at RT

9. Wash three times with DPBS (1 mL each wash)
10. Permeabilize with 0.2% Triton X-100 in DPBS for 10 minutes at RT
11. Wash three times with DPBS (1 mL each wash)
12. Block in 2% BSA in DPBS for 30 minutes at RT
13. Incubate with 1:200 anti-cortactin diluted in 2% BSA for 1 hour at RT
14. Wash three times for 10 minutes with TBS-T
15. Incubate with 1:200 Texas Red®-X Phalloidin and 1:500 Alexa Fluor® 647 goat anti-mouse IgG diluted in 2% BSA for 1 hour at RT
16. Wash three times for 10 minutes with TBS-T
17. Rinse once with 1 mL DPBS
18. Dip in small flask of ddH_2O and allow excess ddH_2O to wick onto a folded KimWipe
19. Mount with 1-drop Prolong Gold
20. Protect from light and allow to cure for 24 hours at RT prior to imaging
21. Store at 4^oC protected from light until imaging

Procedure for actin and MMP14 staining:

1. Count cells: for MDA-MB-231 cells in a 12 well plate, use $7.5x10^4$ cells in 1 mL media
2. Incubate coverslips in complete media for 30 minutes to 1 hour prior to addition of cells on gelatin matrix coated coverslip
3. Place 1 mL of the cell suspension on top of the gelatin-matrix coated coverslips
4. Incubate at 37^oC for 6 hours
5. 20 minutes prior to fixation add 2 drops NucBlue to each well
6. Warm a 3.7% paraformaldehyde/5% sucrose (in DPBS) solution to 37^oC
7. Aspirate cell-culture medium from each well, rinse with 1 mL DPBS and add 1 mL of warmed 3.7% paraformaldehyde with 5% sucrose
8. Incubate 20 minutes at RT
9. Wash three times with DPBS (1 mL each wash)
10. Block in 2.5% human serum/5% goat serum in DPBS for 1 hour at RT
11. Incubate 1:100 anti-MMP14 diluted in 2.5% human serum/5% goat serum for 1 hour at RT
12. Wash three times for 10 minutes with TBS-T
13. Block in 2% BSA in DPBS for 30 minutes at RT
14. Wash three times for 10 minutes with TBS-T
15. Incubate with 1:200 Texas Red®-X Phalloidin and 1:500 Alexa Fluor® 647 goat anti-mouse IgG diluted in 2% BSA for 1 hour at RT
16. Wash three times for 10 minutes with TBS-T
17. Rinse once with 1 mL DPBS
18. Dip in small flask of ddH_2O and allow excess ddH_2O to wick onto a folded KimWipe
19. Mount with 1-drop Prolong Gold
20. Protect from light and allow to cure for 24 hours at RT prior to imaging
21. Store at 4^oC protected from light until imaging

Part 4: Image Acquisition

All samples were blinded during image acquisition and analysis. Images were acquired on two different imaging platforms for analysis:

- Olympus IX70 inverted microscope equipped with an Olympus Plan-Apo 60X/1.40 numerical aperture oil objective, a Spot RT3 Camera (7.4 μm x 7.4 μm pixel size) and Spot software
- Zeiss Laser Scanning Microscope 780 equipped with a Plan-Apo 40X/1.4 numerical aperture oil objective

Part 5: IX70 Image Processing and Analysis Using FIJI Software

Images acquired using the IX70 inverted microscope were used to quantify the percent of degrading cells in the population, the area of degradation and the cell area. The following methodology describes how the images were processed.

Processing Gelatin Channel

1. Select Analyze→Set Scale
    a. Image Pixel Size = (Camera pixel size x binning)/(Objective Lens Magnification x Lens Magnification)
        i. For IX70 60X/1.4 numerical aperture objective 0.123 μm/pixel
2. Take histogram of sample and determine the mode intensity of the image
3. Open the color picker menu (Ctrl+Shift+K) and change the value to match the mode
4. Select Image→Adjust→Threshold→Auto MaxEntropy (adjust to fit the bright artifacts) but do not apply
5. Select Analyze→Analyze Particles→OK (this should outline all bright artifacts in gelatin)
    a. Size 0-infinity
    b. Circularity 0.00-1.00
    c. Show Nothing
    d. Display results
    e. Include Holes
    f. Add to Manager

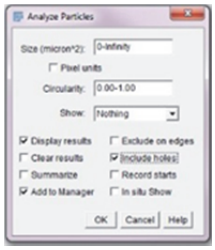

6. Go to the ROI manager and select More→Fill
    a. This is necessary to remove the bright artifacts present in the gelatin
7. Delete all ROI from the ROI manager
8. Select Process→Subtract Background→ OK
    a. Rolling ball radius: 50.0 pixels
    b. Check light background
9. Take histogram of image (Ctrl+H), record minimum intensity (Int_{low})
10. Determine the mean pixel values associated with undegraded gelatin
    a. Use the rectangle tool and select regions from the background subtracted image in areas without degradation or artifacts and measure the pixel values (Ctrl+M)

b. Summarize the mean pixel intensity and record ($Int_{undeg)}$ and delete all measurements after recording

11. Insert values into the equation described by Starnes et al. 2013
    a. Record minimum intensity (Int_{low}) and mean intensity (Int_{undeg})
    b. $thresh_{hi} = Int_{low} + [(Int_{undeg} - Int_{low}) - x]$
        i. $0.3 < x < 0.6$
            1. Starnes et al. recommends 0.3-0.6 for the degradation coefficient "x," but points out it may need to be optimized based on individual researchers application and conditions
            2. Set value to 0.6 for our conditions
12. Select Image→Adjust Threshold→Set
    a. Insert values for minimum (Int_{low})and maximum ($thresh_{hi}$)
    b. The thresholded areas should align with areas of degradation
    c. Leave this image open or save this work then proceed to process the actin channel

Processing Actin Channel

1. Open the actin channel image
2. Select Image→Adjust→Threshold→Auto Huang→Apply
3. Select Process→Binary→ Fill Holes
4. Select Analyze→Set Scale
    a. Image Pixel Size = (Camera pixel size x binning)/(Objective Lens Magnification x Lens Magnification)
        i. For IX70 60X/1.4 numerical aperture objective 0.123 μm/pixel
5. Select Analyze→Set Measurements
    a. Check: Area and Limit to Threshold
6. Select Analyze→Analyze Particles→OK (this should outline each cell)
    a. Size 50-infinity
    b. Circularity 0.01-1.00
    c. Show Outline
    d. Display results
    e. Include Holes
    f. Add to Manager
7. Record Area of Cell
8. Record Number of Cells

Measuring Degradation Using the Actin Channel Cell Outlines

1. Either select or open the background subtracted gelatin image from step 12 of Processing Gelatin Channel
2. Using the ROI(s) generated from step six of Processing Actin Channel select Measure on the ROI manager to get the area of degradation under each cell

Part 6: LSM780 Actin/Cortactin Image Processing and Analysis Using FIJI Software

Processing Actin Channel

1. Select Analyze→Set Scale
    a. Image pixel size = (Camera pixel size x binning)/(Objective Lens Magnification x Lens Magnification)
    b. For LSM 780 40X/1.4 numerical aperture objective 0.1 μM/pixel
2. Select an area with only one cell and Image→Duplicate hyperstack so only one cell is in the image
3. Separate the channels by selecting Image→Color→Split Channels
4. Select and duplicate the actin channel slices with invadopodia and change to Image→Type→8-bit
5. Smooth the image with Process→Smooth
6. Run Process→Subtract Background→OK
    a. Rolling Ball Radius=5
    b. Uncheck light background
    c. This reduces any actin stress fibers within the cell body
7. Select Process→Math→Gamma
    a. Value=1.3
8. Select Process→Filters→Convolve
    a. text1=[-1 -1 -1 -1 -1\n-1 -1 -1 -1 -1\n-1 -1 30 -1 -1\n-1 -1 -1 -1 -1\n-1 -1 -1 -1 -1\n]
    b. Select Normalize Kernel
9. Select Process→Binary→Make Binary
10. Select Analyze→Analyze Particles
    a. Size=0.05-0.5
    b. Circularity=0.05-1.0
    c. Check Add to Manager
11. Overlay particles on each slice of the actin channel and visually inspect to ensure all puncta were counted
12. Perform steps 4-11 with channels with actin puncta
13. Make final actin binary image by filling all puncta that were analyzed with Black (0,0,0)
14. Record the sizes of all puncta

Processing Cortactin Channel

1. Select and duplicate the actin channel slices with invadopodia and change to and 8-bit image (Image→Type→8-bit)
2. Select Process→Smooth
    a. This will smooth the image
3. Run Process→Subtract Background→OK
    a. Rolling Ball Radius=5
    b. Uncheck light background
    c. This reduces any actin stress fibers within the cell body

4. Select Process→Math→Gamma
    a. Value=1.3
5. Select Process→Filters→Convolve
    a. text1=[-1 -1 -1 -1 -1\n-1 -1 -1 -1 -1\n-1 -1 30 -1 -1\n-1 -1 -1 -1 -1\n-1 -1 -1 -1 -1\n]
6. Select Normalize Kernel
7. Select Process→Binary→Make Binary
8. Select Process→Image Calculator…→Select binary actin channel and binary cortactin channel as Image 1 and Image 2
    a. Operation: Multiply
    b. Check: Create new window
    c. This process will create a resulting image that only contains black pixels that corresponds with overlapping signal in both images (colocalization)

Processing Colocalized Image

1. Select Image→Adjust Threshold
    a. Upper threshold level = 255
    b. Lower threshold level = 255
    c. Puncta and cell artifacts should be red
2. Go to ROI Manager, Select All, and Select Measure
3. Record colocalized areas
    a. There should be the same number of measurements as in the actin puncta alone channel, although some values may be 0

<u>Part 7: LSM780 MMP14 Intensity Analysis Image Processing Using FIJI Software</u>

Processing Actin Channel

1. Select Analyze→Set Scale
    a. Image pixel size = (Camera pixel size x binning)/(Objective Lens Magnification x Lens Magnification)
    b. For LSM 780 40X/1.4 numerical aperture objective 0.1 μM/pixel
2. Image→Stack→Z-Project→Sum Slices
3. Image→Adjust→Threshold
    a. Adjust threshold to area of each cell
        i. Note-automatic does threshold most cells and their area, but some visual inspection may be necessary
4. Analyze→Analyze Particles
    a. Size=20-infinity
    b. Add to manager

Processing Gelatin Channel

1. Image→Stack→Z-Project→Sum Slices
2. Process→Filters→Gaussian Blur
    a. Sigma (Radius)=2.00
3. Process→Filters→Convolve

    a. “text1=[-1 -1 -1 -1 -1\n-1 -1 -1 -1 -1\n-1 -1 30 -1 -1\n-1 -1 -1 -1 -1\n-1 -1 -1 -1 -1\n] normalize”);
4. Take histogram
5. Record minimum intensity (Int_{low}) and mean intensity (Int_{undeg})
    a. $thresh_{hi} = Int_{low} + [(Int_{undeg} - Int_{low}) - x]$
    b. x = 0.6
6. Measure area of degradation in field
7. Measure area of degradation under cell area ROI

Processing MMP14 Channel

1. Analyze→Set Measurements
    a. Area, integrated density,
2. Record area
3. Record integrated density at all 5 slices of image stack

APPENDIX G

TRANSWELL INVASION/MIGRATION ASSAY

Materials:

- MDA-MB-231 complete media(10% FBS and 1% v/v penicillin streptomycin)
- MDA-MB-231 starvation media (0.2% FBS and 1% v/v penicillin streptomycin)
- DPBS
- Trypan Blue (Gibco Cat# 15250)
- EGF (BD recombinant hEGF Cat# 354052)
    a. Stock solution 100 ng/μL in 0.1% BSA stored at -80^{o}C
- Corning® BioCoat™ Matrigel® Invasion Chambers, Corning® Growth Factor Reduced (Ref: 354483)
- Corning® Control Inserts (Ref: 354578)
- 3.7% Paraformaldehyde (16% Solution Cat # 15710 Electron Microscopy Sciences)
- Olympus IX70 inverted microscope equipped with an Olympus Plan-Apo 10X/0.30 numerical aperture objective, a Spot RT3 Camera (7.4 μm x 7.4 μm pixel size) and Spot software

Procedure:

1 Day Prior to Experiment

1. Starve cells for ~24hours
    a. Starve siRNA treated cells 48 hours post transfection to begin assay at 72 hours post transfection

Day of Experiment

2. Remove BioCoat covered Boyden chambers from -20^{o}C and allow to come to room temperature
3. Rehydrate with 500 μl warm starvation media for 2 hours
4. While the gel is equilibrating – lift the cells and make single cell suspension of $5x10^4$ cells/ 500 μl ($10x10^4$ in 1 mL) starvation media (resuspend in 3 mL for counting with Trypan Blue then perform dilution)
5. Following 2 hours of gel equilibration, carefully remove media from invasion chamber and then add 500 μl of your cell suspensions ($5x10^4$ cells) very gently (Tip: Remove media by inverting invasion chamber over a 100 millimeter plate using forceps)
6. Fill the lower chamber with 750 μl of chemoattractant (starvation media plus EGF: 10 ng/mL)
7. Incubate at 37^{o}C, 5% CO_2 for 5 hours to assess migration
8. Incubate at 37^{o}C, 5% CO_2 for 18 hours to assess invasion

Important note: Always 1st place the insert in well and then add any solution very gently and slowly to the lower chamber through the insert gap

Fixation and staining:

1. Add 500 µl 3.7% paraformaldehyde in DPBS (made from 16% liquid stock) for 20 minutes at room temperature
    a. Fix cells 5 minutes then start removing Matrigel and non-invading cells
        i. Remove cells from inner side by Q-tip and place back in paraformaldehyde
2. Wash the inserts once in DPBS beaker gently and place in a clean well
3. Add 100 µL of NucBlue diluted in DPBS to 400 µL of DPBS in the well (2 drops NucBlue in 1 mL DPBS) and incubate for 20 minutes at RT (protect from light)
4. Observe under microscope under 10X dry objective
    a. They can be imaged in the 24 well plate with 10X objective
5. Analyze data using ImageJ software
    a. 10X Invasion Assay Script for ImageJ – can be performed manually or input as a new macro
        i. Run("Dilate");
        ii. run("Watershed");
        iii. roiManager("Show All with labels");
        iv. roiManager("Show All");
        v. run("Analyze Particles...", "size=0.002-Infinity circularity=0.00-0.99 show=[Overlay Outlines] display clear summarize add")
    b. Visually inspect that the nuclei have all been counted properly and adjust the count as required manually

Notes:

- Protocol was adapted from manufacturer's (Corning) product literature.

APPENDIX H

3D INVASION ASSAY – CULTREX® INVASION MATRIX

Materials:

- MDA-MB-231 complete media(10% FBS and 1% v/v penicillin streptomycin)
- MDA-MB-231 starvation media (0.2% FBS and 1% v/v penicillin streptomycin)
- DharmaFECT 4
- siRNA – Scrambled, MMP14, Nck1, Nck2
- 10X Spheroid Formation Matrix (Trevigen – This reagent should be thawed and 16.5 µL aliquots made then stored at -80°C)
- Cultrex® Invasion Matrix (Trevigen – This reagent should be thawed and 165 µL aliquots made and then stored at -80°C)
- DPBS
- Trypsin/EDTA Corning
- Trypan Blue (Gibco Cat# 15250)
- EGF (BD recombinant hEGF Cat# 354052)
    a. Stock solution 100 ng/µL in 0.1%BSA stored at -80°C
- Centrifuge with swing plate rotor (Eppendorf 5810 R centrifuge equipped with an A-4-81 rotor)
- Olympus IX70 inverted microscope equipped with an Olympus Plan-Apo 10X/0.30 numerical aperture objective, a Spot RT3 Camera (7.4 µm x 7.4 µm pixel size) Model 25.4 2 Mp Slider and Spot software

Procedure:

Alternate siRNA Treatment Methodology for 3D Invasion Assay

Day 1

1. Plate $5x10^4$ cells in a 35-millimeter plate
2. Thaw appropriate number of aliquots of 10X Spheroid Formation Matrix on ice at 4°C overnight

Day 2

1. Treat cells with 1 µL/mL DharmaFECT 4 and 25-50 nM siRNA for six hours
2. After six hours wash cell twice with DPBS
3. Add 120 µL of Trypsin/EDTA and keep at room temperature for 5 minutes
4. Use 1 mL complete media to neutralize trypsin and collect cells in 15 mL Falcon tube
5. Wash plate with 1 mL complete media to collect the remainder of the cells
6. Spin at 800 rpm for 3 minutes to pellet cells
7. Carefully aspirate media and resuspend cells in small volume complete media
8. Perform Trypan Blue exclusion assay to count the number of viable cells
9. From this make 0.3 x 10^4 cells/45 µL in ice cold complete media (enough for 1-2 more wells than you need)
    - 0.3 x 1000 / (cell count from hemocytometer) = X

- Take 45 – x = Y (Y is the amount of ice cold CM you should add)
- For triplicate spheroids make enough for 4-5 wells, so multiple both X and Y by 4 or 5

10. Mix the 148.5 µL cold cell suspension with the 16.5 µL of 10X spheroid mix
11. Plate 50 µL in chilled 3D culture qualified 96 well spheroid formation plate
12. Spin at 200 rcf for 3 minutes at room temperature
    - Important – set centrifuge acceleration to 9 and deceleration to 1 for a slow finish of the spin – this helps with spheroid formation
13. Place at 37^{o}C for 48 hours

Day 3

1. Thaw appropriate number of aliquots of Cultrex® Invasion Matrix on ice at 4^{o}C:

Day 4

1. Remove 3D culture qualified 96 well spheroid formation plate from 37^{o}C incubator and place on ice for at least 15 minutes
    - Place ice bucket in refrigerator
2. Cool centrifuge to 4^{o}C
3. Add 50 µL Invasion Matrix to each well and keep on ice
4. Transport on ice to centrifuge and spin at 300 rcf for 5 minutes
    - Important – set centrifuge acceleration to 9 and deceleration to 1 for a slow finish of the spin – this helps with spheroid formation
5. Place in 37^{o}C incubator
6. After 1 hour add 100 µL warm (37^{o}C) cell culture media (must be 37^{o}C not just room temp) with appropriate serum and chemoattractant
    - Stock to add is starvation media with 10 ng/mL EGF
7. Images should be acquired immediately after addition of media (time point 0) and then every 24 hours for 2-3 days
    - Can image spheroids up to 6 days

Notes:

- Protocol was adapted from Trevigen® Cultrex® 96-well 3D Spheroid BME Cell Invasion Assay product literature.

APPENDIX I

3D INVASION ASSAY – PURE COLLAGEN I

Materials:

- MDA-MB-231 complete media(10% FBS and 1% v/v penicillin streptomycin)
- MDA-MB-231 reduced serum media (2% FBS and 1% v/v penicillin streptomycin)
- 10X DMEM with phenol red – Low Glucose
- 1 M – HEPES
- 7.5% Sodium Bicarbonate
- DPBS
- 1 N NaOH – per Corning Protocol
- 1 N HCl – in the event you need to re-acidify to reach a pH of 7.4
- 9.06 mg/mL Corning® Collagen I High Concentration (HC), Rat Tail in 0.02 N Acetic Acid
- ColorpHast pH-indicator strips, range: 6.5-10 (Millipore)
- Microcentrifuge
- Starvation Media Recipe
    - DMEM High Glucose (HyClone)
    - 0.2% Fetal Bovine Serum
    - 1% Pen Strep
- CoolSink® XT 96U (Biocision)
- Olympus IX70 inverted microscope equipped with an Olympus Plan-Apo 10X/0.30 numerical aperture objective, a Spot RT3 Camera (7.4 μm x 7.4 μm pixel size) and Spot software

Procedure:

Alternate siRNA Treatment Methodology for 3D Invasion Assay

Day 1

1. Plate $5x10^4$ cells in a 35-millimeter plate
2. Thaw appropriate number of aliquots of 10X Spheroid Formation Matrix on ice at 4^oC overnight

Day 2

1. Treat cells with 1 μL/mL DharmaFECT 4 and 25-50 nM siRNA for six hours
2. After six hours wash cell twice with DPBS
3. Add 120 μL of Trypsin/EDTA and keep at room temperature for 5 minutes
4. Use 1 mL complete media to neutralize trypsin and collect cells in 15 mL Falcon tube
5. Wash plate with 1 mL complete media to collect the remainder of the cells
6. Spin at 800 rpm for 3 minutes to pellet cells
7. Carefully aspirate media and resuspend cells in small volume complete media
8. Perform Trypan Blue exclusion assay to count the number of viable cells

9. From this make 0.3 x 10^4 cells/45 µL in ice cold complete media (enough for 1-2 more wells than you need)
    - 0.3 x 1000 / (cell count from hemocytometer) = X
    - Take 45 – x = Y (Y is the amount of ice cold CM you should add)
    - For triplicate spheroids make enough for 4-5 wells, so multiple both X and Y by 4 or 5
10. Mix the 148.5 µL cold cell suspension with the 16.5 µL of 10X spheroid Mix
11. Plate 50 µL in chilled 3D culture qualified 96 well spheroid formation plate
12. Spin at 200 rcf for 3 minutes at room temperature
    - Important – set centrifuge acceleration to 9 and deceleration to 1 for a slow finish of the spin – this helps with spheroid formation
13. Place at 37°C for 48 hours

Day 4

Preparation of Collagen I

1. Turn on and fast cool microcentrifuge
2. Cool centrifuge to 0°C to embed spheroid in collagen
3. Place 3D culture qualified 96 well spheroid formation plate on cold sink and place on ice in the 4°C refrigerator to pre-chill the plate and the multicellular tumor spheroids (needs a minimum of 15 minutes to chill)
4. Components to place on ice
    - 10X DMEM
    - Rat Tail Collagen
    - DPBS
    - 1 N NaOH
    - Sterile tubes for mixing collagen
5. Determine final volume of diluted collagen (include a 20% excess for pipetting errors)
    - 3D Spheroid Assay requires 50 µL of collagen per well
6. 50 x Number of samples x 1.2 = total µL of diluted collagen to make
7. Calculate the volume of Corning Collagen I HC to be used
    - (Final volume x Final collagen concentration in mg/mL) / (Concentration of collagen in bottle (lot specific)) = volume of collagen to be added
8. Calculate the volume of sterile ice cold 1 N NaOH to be added:
    - Volume of collagen to be added x 0.023 mL = volume of 1 N NaOH
9. Calculate the volume of sodium bicarbonate (7.5%) and HEPES (1 M) to add
    - Add 2.5% v/v of both components
    - Total volume x 0.025 = amount to add
10. Calculate the volume of 10X DMEM to add
    - Add 10% v/v
    - Total volume x 0.1 = amount to add
11. Calculate the amount of DPBS to add to bring the final concentration of collagen (i.e. 2.2 mg/mL or 4.4 mg /mL)

- Final volume – volume collagen – volume 10X DMEM – volume sodium bicarbonate – volume HEPES = volume DPBS to add

12. Once all calculations are complete and double checked ensure all components that will come into contact with the collagen are chilled

Neutralization of Collagen I for Embedding

1. Take tube on ice and begin by adding calculated amount of 10X DMEM
2. Add calculated amount of 1 N NaOH to the 10X DMEM
3. Add sodium bicarbonate and HEPES
4. Add calculated volume DPBS and mix the solution well by pipetting up and down carefully avoiding the introduction of bubbles
5. The final step is the addition of the calculated amount of collagen to the mix
    - Once added gently pipet up and down to mix without causing bubbles or collagen precipitates to form
    - If bubbles appear the solution can be cold centrifuged for 3 minutes at 10,000 rpm
    - Be careful as any increases in temperature after the neutralization of the collagen will result in polymerization
6. Wait ~4 minutes after mixing all components to test pH
7. Test the pH of the collagen by pipetting a small amount onto a strip of pH paper and using the color scale to determine actual pH
    - pH must be between 7.1 and 7.4
    - If it is outside this range use ice cold 1 N NaOH or 1 N HCl to adjust final pH
    - Add small volume, mix gently and wait ~4 minutes before testing pH again
8. Can be kept on ice for a brief period of time – recommend using it immediately
9. Collagen will now be ready to be used for embedding multicellular tumor spheroids

3D Spheroid Embedding: Pure Collagen I Mixture

1. Once collagen is ready bring the chilled 96 well glass flat bottom plate still on ice into the tissue culture hood and disperse 20 μL of chilled collagen on bottom of each well, be careful not to introduce bubbles
    - One way to avoid introduction of bubbles is to plunge the pipet slightly beyond the first stop so that you pull slightly more collagen than 20 μL but only expel to the first stop
2. Once all needed wells are coated remove plate from ice and place in 37^{o}C incubator for 30 minutes to polymerize collagen I (Corning Product Technical Literature)
3. Do not keep at room temperature as this will alter the characteristics of collagen polymerization and may introduce experimental variability.
4. Once polymerization is completed place 96 well glass flat bottom plate on ice at 4^{o}C for at least 15 minutes to chill the plate then proceed with the next step
5. Make fresh collagen preparation

6. Once collagen is ready bring the chilled 96 well glass flat bottom plate still on ice into the tissue culture hood and add 100 μL of chilled collagen to each well, be careful not to introduce bubbles
    - One way to avoid introduction of bubbles is to plunge the pipet slightly beyond the first stop so that you pull slightly more collagen than 100 μL but only expel to the first stop
7. After all collagen has been added take chilled pre-formed spheroids and place them on ice
8. Use a P20 pipette set to 5 μL, plunge to just past the stop point and carefully aspirate the preformed spheroid
9. Next place the spheroid in the middle of the chilled 96 well plate containing the aliquoted collagen I
    - Care must be taken not to place the spheroid to high or too low in the aliquoted collagen I or this will prevent proper invasion and imaging
10. Once spheroids are placed remove plate from ice and place in 37^{o}C incubator for 1 hour to polymerize collagen I
    - Do not keep at room temperature as this will alter the characteristics of collagen polymerization and may introduce experimental variability
11. After 1 hour add appropriate media and growth factors for the experimental design warmed to 37-38^{o}C
    - Basic protocol is to add 100 μL of Reduced Serum Media + 10 ng/mL EGF
        i. Reduced serum media contains 2% FBS compared to Starvation Media that contains 0.2% FBS
        ii. EGF final concentration will be 5 ng/mL when added to the 100 μL of collagen I
12. Images should be acquired immediately after addition of media (time point 0) and then every 24 hours for 2-3 days
    - Can image spheroids up to 6 days

Notes:

- Spheroid formation for siRNA treated cells was limited to two days, while spheroid formation for shRNA expressing cells was allowed to proceed for 2 or 3 days based on assay performed
- The only change this makes to the protocol is the day the cells are embedded in invasion matrix
- Protocol adapted from Artym et al. 2010, Guzman et al. 2014, Corning Collagen I product literature and Trevigen® Cultrex® 96-well 3D Spheroid BME Cell Invasion Assay product literature

APPENDIX J

TRANSIENT TRANSFECTION WITH LIPOFECTAMINE 2000

Materials:

- MDA-MB-231 complete media (10% FBS and 1% v/v penicillin streptomycin)
- MDA-MB-231 complete media without antibiotic (10% FBS)
- Lipofectamine® 2000 Transfection Reagent (Life Technologies Catalog Number: 50470)
- Opti-MEM® Reduced Serum Medium (Life Technologies Catalog Number: 31985-062)
- Plasmid DNA
- 1.5 mL Eppendorf Tubes

Procedure:

Day 1

1. Plate $20x10^4$ MDA-MB-231 cells with complete media in a 35-millimeter dish and place in a 37°C incubator with 5% CO_2

Day 2

1. Label two Eppendorf tubes and add 250 μL of Opti-MEM media to each tube
   - Tube 1 - Plasmid DNA
   - Tube 2 - Lipofectamine 2000
2. Add 2 μg plasmid DNA to tube 1 and mix well by gently pipetting up and down
3. Add 5 μL of Lipofectamine 2000 reagent to tube 2 and mix well by gently pipetting up and down
4. Incubate at room temperature for 5 minutes
5. After 5 minutes take entire volume from Tube 2 and add it to Tube 1
6. Mix well by gently pipetting up and down then incubate at room temperature 20-30 minutes
7. Add 500 μL antibiotic free complete media to the transfection reagent plasmid mixture in Tube 1
8. Remove complete from cells and add entire contents of Tube 1 to the plate then place back in 37°C incubator
9. After one hour replace media with fresh antibiotic free complete media
10. After an additional four hours the media can be replaced with complete media containing antibiotic
11. Grow cells overnight then lift and re-plate with fresh complete media
12. The cells will be ready for use within 1-3 days based on the plasmids transfected

Notes:

- Adapted from manufacturer's protocol (Life Technologies) for Lipofectamine 2000

APPENDIX K

FLUORESCENCE RECOVERY AFTER PHOTOBLEACHING (FRAP)

Materials:

- MDA-MB-231 stably expressing pMSCV Actin-EYFP
- MDA-MB-231 complete media (10% FBS and 1% v/v penicillin streptomycin)
- DPBS (HyClone, ThermoScientific)
- Live Cell Imaging Media (Phenol-red free DMEM High Glucose supplemented with 10% FBS, 1% Pen/Strep and 25 mM HEPES)
- 35-millimeter glass bottom MatTek dishes (MatTek Corporation, Ashland, MA)
- Fibronectin (10 μg/mL in DPBS)
- Zeiss LSM780 Confocal Microscope Plan-Apo 40X/1.40NA oil objective

Procedure:

1. Three days prior to imaging perform siRNA mediated silencing using scrambled and Nck targeting sequences
2. Two days prior to imaging plate $10x10^4$ cells in a 60-millimeter tissue culture plate to synchronize growth at low density
3. One day prior to imaging:
    a. Coat MatTek dishes with 10 μg fibronectin (use 1 mL of 10 μg/mL fibronectin in DPBS for one hour at room temperature
    b. After 1 hour aspirate excess DPBS and add 200 μL live cell imaging media to the glass portion of the MatTek for 15 minutes and place in $37^oC/5\%$ CO_2 incubator
    c. Lift cells using 350 μL Trypsin/EDTA for 5 minutes at room temperature
    d. Collect cells in 15 mL Falcon tube and spin for 3 minutes at 800 rpm
    e. Re-suspend cells in 250 μL of Live Cell Imaging Media
    f. Count cells using hemocytometer
    g. Make dilutions of $4x10^4$ cells in 200 μL Live Cell Imaging Media
    h. Remove fibronectin coated plates from incubator and aspirate media
    i. Add $4x10^4$ cells in 200 μL to each fibronectin coated plate and place in $37^oC/5\%$ CO_2 incubator for one hour to allow cells to adhere
    j. After 1 hour add 2 mL imaging media to each plate and incubate for approximately 20 hours prior to imaging
4. Day of imaging
    a. Place plate on stage and allow 5 to 15 minutes for equilibration
    b. FRAP settings
        i. Acquisition
            1. Pixel dwell time: 0.79 μs/pixel
            2. Picture resolution: 512 x 512
            3. Laser power: 2.4% 514 nm
        ii. Photobleach

1. Pixel dwell time: 90 μs/pixel
2. Region of interest: 164 x 166
3. Laser power: 100% 514 nm

c. Collect 3 initial image scans prior to photobleaching
d. After initial image capture, region of interest was photobleached
e. Recovery of fluorescence was measured from 6 sequential scans beginning immediately postbleach, and then at 1.94 second intervals
f. Data were collected from at least 60 images from two culture dishes per treatment

5. Data analysis (adapted from Barhoumi et al. 1993 and Li et al. 2010)
   a. Rate constant estimation (k) was performed for fluorescence recovery by fitting the percent fluorescence intensity at a given time, FI to the equation below
      i. $FI = A\ (1\text{-}e^{-kt}) + B$
         1. A represents percent fluorescence recovery of the bleached structure at equilibrium
         2. B represents percent fluorescent intensity immediately after photobleaching
   b. Data from at least 80 actin-EYFP puncta from each group were pooled to obtain mean A and k values using a curve fitting regression analysis (GraphPad Software) to extrapolate fluorescence recovery as a function of time

APPENDIX L

WESTERN BLOT

Part 1: Harvesting Cells

Materials:

- Kinase Lysis Buffer (KLB) Stock
- DPBS
- 0.5 M phenylmethylsulfonyl fluoride in DMSO
- Aprotinin, from Bovine Lung
- 100 mM Sodium Pervanadate ($NaVO_4$)
- Microcentrifuge tubes (1.5 mL Eppendorph tubes)
- Refrigerated Table Top Centrifuge
- Cell scraper (BD Falcon 353085)

Procedure:

1. Turn on refrigerated centrifuge and cool to 4^{o}C
2. Label microcentrifuge tubes with appropriate sample names in duplicate and chill on ice
3. Prepare KLB by adding 1/500 phenylmethylsulfonyl fluoride, 1/100 $NaVO_4$, and 1/100 Aprotinin to KLB stock
4. Remove plate containing cells to be harvested from incubator and aspirate growth media
5. Wash cells gently with cold DPBS then aspirate the solution
6. Repeat step 5 one time
7. After second wash with DPBS place plate on ice
8. Add KLB to plate (amount varies by cell type, plate size and confluence)
    a. MDA-MB-231 confluent plates
        i. 35-millimeter – 50 μL
        ii. 60-millimeter – 100 μL
        iii. 100-millimeter – 200 μL
        iv. 150-millimeter – 300 μL
9. Scrape cells off the bottom of the plate using the cell scraper
    a. For multiple samples wash cell scraper in distilled water between samples
10. Transfer cells/solution to microcentrifuge tubes and vortex
11. Incubate on ice 15-30 minutes
12. Spin samples for 10 minutes at max speed in refrigerated centrifuge
13. Transfer supernatant to fresh tubes previously labeled in step 2
14. Keep on ice and proceed to measure protein concentration or store at -80^{o}C

Part 2: Determining Protein Concentration

Materials:

- Cell Lysate Samples
- 96-Well Tissue Culture Flat Bottom Plate (Falcon 353072)
- BSA Protein Standards in KLB (10 μg/μL, 5 μg/μL, 2.5 μg/μL, 1.25 μg/μL, 0.625 μg/μL, 0.3125 μg/μL)
- Bradford Reagent (Bio-Rad Protein Assay Dye Reagent Concentrate #500-0006)
- Microcentrifuge tubes (1.5 mL Eppendorph tubes)
- Plate Reader (FLOUstar Omega)

Procedure – Preparation and Loading of Samples:

1. Prepare Bradford reagent by making a 1:5 dilution in deionized distilled water (ddH_2O)
2. Prepare microcentrifuge tubes by labeling one for each sample being quantified
    a. Include 7 additional tubes for the blank and protein standard
3. Pipet 1 mL of diluted Bradford reagent into each microcentrifuge tube
4. Add 5 μL of KLB to tube labeled blank
5. Add 5 μL of each standard to the appropriately labeled tubes
6. Add 5 μL of each sample to the appropriately labeled tubes
7. Mix samples well by inverting tubes several times until the color is visibly homogenous
8. Start 10 minute timer
    a. Bradford reagent reaction should take place for a minimum of 10 minutes but should not exceed 1 hour
9. Aliquot 200 μL of each mixture in triplicate into 96-well plate
10. After 10 minutes, but before 1 hour absorbance should be measured on a plate reader
11. Measure absorbance on plate reader
12. Create a standard curve to determine protein concentrations
    a. If using all 6 standards a 4-parameter curve should be generated
    b. If using only the 4 lowest concentration standards a linear curve should be used

Part 3: Sample Preparation for Sodium Dodecyl Sulfate-Polyacrylamide Gel Electrophoresis (SDS-PAGE)

Materials:

- 5X Sample Buffer
- Samples with known protein concentration
- Microcentrifuge tubes (1.5 mL Eppendorph tubes)
- Microcentrifuge tube locks
- Heat block (set to 105^{o}C)
- Table top microcentrifuge

Procedure:

1. Combine 4 parts protein sample with 1 part 5X sample buffer in a microcentrifuge tube
2. Vortex sample and lock lid closed with a tube lock and place in 105^{o}C heat block for 5 minutes
3. Cool sample on ice and briefly spin down contents in microcentrifuge
4. Normalize all protein concentrations using 1X Sample Buffer (5X Sample Buffer diluted with distilled water)
    a. Example – all protein concentrations should be at 0.4 μg/μL so the same volume of each sample can be used for SDS-PAGE
5. Treated samples can be used immediately or stored at -20^{o}C

Part 4: SDS-PAGE Gel Casting

Materials:

- 30 % Acrylamide Solution (Protogel EC890)
- 1 M Tris, pH 8.8
- 1 M Tris, pH 6.8
- 10% Sodium dodecyl sulfate (SDS)
- 10% Ammonium persulfate (APS)
- TEMED
- n-Butanol (H_2O-Saturated)
- Mini-PROTEAN® Tetra Cell System
    - Spacer plate, desired thickness,
    - Short plate
    - Casting frame
    - Casting stand
    - Casting stand gaskets
    - Gel comb
- 15 mL Falcon tube

Procedure –Gel Casting System Assembly:

1. Place casting frame on a flat surface with pressure cams in the open position
2. Place short plate on top of spacer plate
3. Orient the plates so labels can be read normally
4. Slide the glass plates into the plastic casting frame with the shorter plate towards the front of the frame (side with handles for pressure clamps)
    a. Ensure that both plates are flush with the flat surface at the bottom to prevent leaking
5. Engage the pressure clamps
6. Place gray casting stand gaskets in appropriate location on casting stand
7. Place casting frame on casting stand while engaging spring-loaded lever on the top

a. Alternated pressure on the left and right side of the casting frame to properly seat the plates on the casting stand gasket to prevent leaks

Procedure – Gel Casting:

1. Prepare resolving gel in 15 mL Falcon tube
2. Mix gently by inversion without introducing bubbles into the solution
3. Pipet the resolving gel solution into the opening between the spacer plate and the short plate
4. Immediately overlay with n-Butanol
5. Allow 20-30 minutes to polymerize
    a. Excess resolving gel in 15 mL Falcon tube will indicate polymerization status of gel
6. Pour off n-Butanol and rinse gel surface thoroughly with ddH_2O
7. Prepare stacking gel in 15 mL Falcon tube
8. Pipet stacking gel solution to the top of the short plate
9. Insert comb with appropriate number of wells between the spacers
10. Allow the stacking gel to polymerize for 20-30 minutes
    a. Excess stacking gel in 15 mL Falcon tube will indicate polymerization status of gel
11. Leave the comb in the gel and rinse well with dH_2O
12. The gel can be used immediately
    a. Alternatively the gel can be wrapped in a damp paper towel (use ddH_2O) and plastic wrap and stored at 4^oC overnight

<u>Part 5: SDS-PAGE Protein Separation</u>

Materials:

- Hand-Cast Gels
- 10X Tank Buffer Stock
- ddH_2O
- Mini-PROTEAN® Tetra Cell System
- Gel Releaser
- Power Supply (BioRad PowerPac™ Basic)
- Running Buffer
- Sample Loading Tip (Pipet Tips with Microcapillary for Loading Gels, VWR 37001-150)

Procedure:

1. Place the clamping frame on a flat bench top surface in the open position
2. Set the electrophoresis module on a clean flat surface
3. Ensure the short plate is facing inward and place the first gel cassette on the molded supports of the electrophoresis module
    a. By placing the gel at a 30^o angle away from center of the clamping frame it will seat to the bottom of the supports

4. Repeat with a second gel on the opposite side or use a Mini Cell Buffer dam in its place if only running a single gel
5. Pull both gels towards vertical and firmly hold in place
    a. The short plate should sit just below the notch in at the top of the green gasket
6. Clamp the frame closed ensuring the gels do not shift during the process
7. Once assembled place the electrophoresis module in the Mini-PROTEAN Tank
    a. Ensure that the positive and negative electrodes are lined up properly
        i. These are color coded red and black on both the tank and the assembly
8. Use 10X Tank Buffer and dilute to 1X
    a. Make 700 mL for 1 or 2 gels – 70 mL 10X Tank Buffer and 630 mL of dH_2O
9. Fill the upper chamber between the gels with Tank Buffer
    a. Observe for leaking of Tank Buffer into the Mini-PROTEAN Tank
        i. If leaking is observed, disassemble and reassemble according to steps 1-7
10. Pour the remainder of the Tank Buffer into the bottom of the Mini-PROTEAN Tank
11. Optional Step – A sample loading guide can be placed between the gels at this time to aid in sample loading
12. Load samples into each assembly
    a. Use a pipet with sample loading tips
    b. Load sample slowly allowing it to settle in the bottom of the well evenly
    c. Use care not to puncture the bottom or the sides of the well
13. Place the lid on the Mini-PROTEAN Tank ensuring that the red and the black color coded regions are aligned properly
14. Insert the electrical leads into the power supply matching the red and black lead colors
15. Apply power and begin electrophoresis
    a. Recommended that voltage be set at 200V and remain constant for SDS-PAGE
    b. Run time is 40-70 minutes
        i. protein of interest size and acrylamide concentration can alter the time required
16. After electrophoresis is completed, turn off the power supply and disconnect the electrical leads
17. Remove the tank lid and lift out the assembly
18. Pour off and discard the running buffer
19. Open the arms of the electrophoresis assembly and remove the gel cassettes
20. Use the gel releaser to gently separate the short plate from the spacer plate
21. Use the gel separator to cut then remove the stacking gel from the resolving gel
22. Discard the stacking gel
23. The resolving gel is ready for transfer to nitrocellulose

Part 6: SDS-PAGE Protein Transfer to Nitrocellulose

Materials:

- SDS-PAGE, post protein separation
- Transfer Buffer (stored at 4^{o}C)
- Nitrocellulose Membrane (BioTrace™ NT 66485)
- Whatman™ Chromatography Paper (3030-6188)
- Mini Trans-Blot® Cell (BioRad)
- Power Supply (BioRad PowerPac™ Basic)
- Diagger Stirrer

Procedure:

*Nitrocellulose membrane should never be handled with bare hands, always used gloved hands and forceps to ensure best blots

1. Cut nitrocellulose membrane and filter paper to the gel dimensions
    a. For gels cast using the Mini-PROTEAN Tetra Cell System
        i. Nitrocellulose dimension: 6.5centimeters by 9 centimeters
        ii. Whatman paper can be folded in half twice then cut along the folds to create four rectangles
2. Equilibrate resolving gel and soak the nitrocellulose membrane, filter paper and fiber pads in transfer buffer (15 minutes to 1 hour based on gel thickness)
3. Place standard stir bar in bottom of buffer tank while components are equilibrating
4. Important: Prepare transfer stack in the gel holder cassette in the following order (all components should be pre-wetted before beginning this step)
    a. Black side of cassette
    b. Fiber pad
    c. Whatman paper
    d. Equilibrated gel
    e. Nitrocellulose membrane
    f. Whatman paper
    g. Fiber pad
    h. Clear side of cassette
5. Close the gel holder cassette firmly without moving the internal components
6. Lock the gel holder cassette and place it in the electrode module
7. Repeat for second gel holder cassette if necessary
8. Place frozen cooling unit in the buffer tank
9. Completely fill tank with transfer buffer
10. Place unit on stirrer and set speed as fast as possible to maintain even buffer temperature and ion distribution
11. Place lid on tank lining up the red and black guides
12. Plug cables from lid into the power supply and run the blot
    a. 2 to 3 hour transfer

b. 100 V
c. 350 mA

13. Once run is complete unplug cables and remove lid from buffer tank
14. Remove gel holder cassette and disassemble the transfer stack
    a. The gel can be stained with coomassie blue to confirm efficient protein transfer or it can be discarded
    b. Nitrocellulose membrane is ready for western blot
        i. Do not let the membrane dry out, it should be immediately placed in TBS-T

Part 7: Western Blot

Materials:

- Nitrocellulose Membrane –Post Protein Transfer
- TBS-T (Tris-Buffered Saline and Tween 20)
- Specific Antibodies
- Polyester Pouches
- Heat Sealer (Hualian FS-305)
- Chemiluminescent Horseradish Peroxidase (HRP) Substrate
- ImageQuant™ LAS 4000 Mini Documentation System
- The Belly Dancer
- Clear Sheet Protectors

Procedure – Blocking Non-specific Binding

*Perform each wash by placing the nitrocellulose membrane in a small dish with enough TBS-T to cover the membrane and then place it on the belly dancer shaking for 5 minutes

**Perform incubations in a polyester pouch - ensure bubbles are minimal prior to sealing the pouch

1. Wash nitrocellulose membrane in a small dish with TBS-T
2. Incubate in 10 mL of blocking solution for 1 hour at room temperature on The Belly Dancer
    a. Each antibody has an optimized blocking solution
3. After 1 hour remove nitrocellulose membrane from polyester pouch and place in TBS-T prior to proceeding to the next step

Procedure - Primary Antibody

1. Make dilution of primary antibody in 5 mL of blocking solution or antibody appropriate solution
2. Incubate nitrocellulose membrane in primary antibody overnight at $4^{o}C$ with shaking
3. Wash 5 times with TBS-T

Procedure – Secondary Antibody

1. Make dilution of secondary antibody in 5 mL of the same blocking solution used for the primary antibody

2. Incubate in secondary antibody for 1 hour at room temperature
3. Wash nitrocellulose membrane 5 times with TBS-T
    a. Leave the membrane in the last wash until ready to proceed

Procedure – Detection of Signal

1. Cut clear sheet protector into rectangles larger than your nitrocellulose membrane
2. Mix 500 μL of each component from the Western Lightening® kit in an microcentrifuge tub
3. Place a small stack of KimWipes on the bench
4. Using forceps remove the membrane from the TBS-T and allow excess solution to wick off the membrane into the stack of KimWipes
5. Transfer nitrocellulose membrane between the sides of the sheet protector
6. Add the Western Lightening® solution to the membrane and lay the upper portion of the sheet protector down to evenly distribute the solution across the entire membrane
7. Protect from light and allow to incubate for 1 minute
8. Remove the membrane with forceps and allow excess Western Lightening® solution to wick into the KimWipes
9. Place in a fresh sheet protector and protect from light
10. Transport to ImageQuant™ LAS 4000 mini documentation system
11. Place sheet protector with membrane in the documentation
12. Acquire images at multiple time settings
    a. An initial image at 20-30 seconds exposure will allow you to properly align your blot within the machine and determine an appropriate exposure time

Procedure – Stripping Membrane and Re-Probing for Alternate Target

1. Once imaging is complete place membrane in TBS-T
2. Prepare 20 mL of fresh stripping buffer per membrane to be stripped
3. Incubate in a 55^{o}C shaking water bath for 45 minutes
4. Wash 5 times with TBS-T
5. Once wash steps are complete proceed to the procedure for blocking non-specific binding and continue through the protocol again

Part 8: Western Blot Quantitation Using ImageJ or FIJI

1. Open gel image in ImageJ or FIJI
2. Outline region of gel containing all bands to be quantified with rectangle tool
3. Duplicate region – processing is performed on duplicated region
    1. Note: you can do all bands at once (GAPDH and MMP14 or Nck; however, this can make separating the MMP14 bands difficult due to scaling: recommend quantifying each probed protein separately even if probed on same blot)
4. Run background subtraction
    a. Rolling ball radius: 50 pixels

b. Check light background

5. Outline each lane or band using the Analyze→gels→select first lane tool, then label all consecutive bands using the Analyze→gels→select next lane tool
    a. Once all lanes have been selected use the Analyze→gels→select plot lanes tool
6. Once the plot is created ensure that you close any gaps to only collect the area where there is signal
7. Use the wand tool and click in each region to get the area
8. Cut and paste measurements into excel
9. In excel you can normalize each protein concentration to a loading control (GAPDH is a standard loading control) and then convert the output into a percent of control measurement for graphing and comparison purposes

Part 9: Western Blot Solutions

Resolving buffer -1 M Tris-Cl (pH 8.8)

- 60.6 g Tris (FW 121.1); Sigma cat# T1503-1KG
- 300 mL ddH_2O

Adjust to pH 8.8 using 2.5 N HCl

- Add ddH_2O to make a final volume of 500 mL

Store up to 3 months at 4°C in the dark

Stacking buffer - 1 M Tris-Cl (pH 6.8)

- 60.6 g Tris (FW 121.1) Sigma cat# T1503-1KG
- 300 mL ddH_2O

Adjust to pH 6.8 using 2.5 N HCl

- Add ddH_2O to make final volume to 500 mL

Store up to 3 months at 4°C in the dark

10% SDS

- 10 g SDS
- ddH_2O to 100 mL

Store up to 6 months at room temperature

10% APS

- 1.0 g ammonium persulfate
- ddH_2O to 10.0 mL

Store 0.5 mL aliquots at -20° C for up to 6 months

5X Sample Buffer

- 6.0 mL Stacking buffer (1 M Tris, pH 6.8)
- 2.0 g SDS
- 9.0 mL glycerol

- 6.0 mg bromophenol blue
- 5.0 mL β-Mercaptoethanol

Store 0.5 mL aliquots at -20° C for up to 6 months

n-Butanol (H_2O-Saturated)

- 50 mL n-butanol
- 5 mL ddH_2O

Combine and shake in a bottle
Store at room temperature

10X Tank Buffer Stock, pH 8.3

- 30.3 g Tris
- 144.0 g glycine
- 10.0 g SDS
- dH_2O to 1 L

Do not adjust with acid or base
Store at 4° C
Mix thoroughly before use

Transfer Buffer

- 24.24 g Tris
- 115.28 g glycine
- 8.0 g SDS
- dH_2O to 6.4 L
- Add methanol up to 8 L

Kinase Lysis Buffer (KLB)

- 12.5 mL 1 M Tris, pH 7.4
- 15 mL 5 M NaCl
- 5 mL 0.5 M EDTA
- 5 mL Triton X-100
- 5 mL 1 M β-GP(β-glycerophosphate)
- 50 mL 100 mM Na3VO4
- 50 mL Glycerol
- 347.5 mL H2O

Store at 4°C. Add fresh with each use:

- 1/500 0.5 M phenylmethylsulfonyl fluoride in DMSO
- 1/100 Aprotinin
- 1/500 50 mM Na3VO4

100 mM Sodium Orthovanadate (Na_3VO_4)

- 0.92 g Na3VO4
- 40 mL ddH_2O

Solution will be orange in color
When dissolved the pH should be approximately 12
Use HCl to adjust pH to 10
Use a boiling water bath to heat for about 5 minutes then cool on ice
Repeat 5-6 times
Color should now be light yellow
Measure to confirm pH is lower
Raise pH to 10 with NaOH
Repeat boiling and cooling until color is gone
Measure pH to confirm it is stable at 10

- dH_2O to 50 mL
- Aliquot and freeze at -20°C

Stripping Buffer

- 4 mL 10% SDS
- 1.25 mL 1 M Tris pH 6.8
- 143 µl β-Mercaptoethanol
- 14.6 mL ddH_2O

SDS-PAGE Resolving Gel – 10 mL/12%

- 2.1 mL H_2O
- 4.0 mL 30% Acrylamide mix
- 3.8 mL 1 M Tris (pH 8.8)
- 0.1 mL 10% SDS
- 0.1 mL 10% APS
- 0.004 mL TEMED

SDS-PAGE Stacking Gel –5 mL

- 3.44 mL H_2O
- 0.83 mL 30% Acrylamide mix
- 0.63 mL 1 M Tris (pH 8.8)
- 0.05 mL 10% SDS
- 0.05 mL 10% APS
- 0.005 mL TEMED

Notes:

- Adapted from BioRad Mini-PROTEAN® Tetra Cell Product Literature

APPENDIX M

3D GROWTH ASSAY

Materials:

- MDA-MB-231 complete media(10% FBS and 1% v/v penicillin streptomycin)
- MDA-MB-231 stable silenced cell lines (shScramble and shNck)
- 10X Spheroid Formation Matrix (Trevigen – This reagent should be thawed and 16.5 μL aliquots made then stored at -80^{o}C)
- DPBS
- Trypsin/EDTA (Corning)
- Trypan Blue
- Centrifuge with swing plate rotor (Eppendorf 5810 R centrifuge equipped with an A-4-81 rotor)
- Olympus IX70 inverted microscope equipped with an Olympus Plan-Apo 10X/0.30 numerical aperture objective, a Spot RT3 Camera (7.4 μm x 7.4 μm pixel size) Model 25.4 2 Mp Slider and Spot software

Procedure:

Day 1

1. Plate 10x10^{4} cells in a 60-millimeter plate
2. Thaw appropriate number of aliquots of 10X Spheroid Formation Matrix on ice at 4^{o}C overnight

Day 2

1. Lift cells with 350 μL of Trypsin/EDTA and keep at room temperature for 5 minutes
2. Use 1 mL complete media to neutralize trypsin and collect cells in 15 mL Falcon tube
3. Wash plate with 1 mL complete media to collect the remainder of the cells
4. Spin at 800 rpm for 3 minutes to pellet cells
5. Carefully aspirate media and resuspend cells in 250 μL volume complete media
6. Perform Trypan Blue exclusion assay to count the number of viable cells
7. From this make 0.3 x 10^{4} cells/45 μL in ice cold complete media (enough for 1-2 more wells than you need)
    a. 0.3 x 1000 / (cell count from hemocytometer) = X
    b. Take 45 – x = Y (Y is the amount of ice cold complete media required)
    c. For triplicate spheroids make enough for 4-5 wells
        i. Multiple both X and Y by 4 or 5
8. Mix the 148.5 μL cold cell suspension with the 16.5 μL of 10X spheroid mix
9. Plate 50 μL in chilled 3D culture qualified 96-well spheroid formation plate
10. Spin at 200 RCF for 3 minutes at room temperature
    a. Important – set centrifuge acceleration to 9 and deceleration to 1
11. Place at 37^{o}C for 72 hours

12. Add 50 μL warm complete media
13. Image every 24 hours for 4-6 days
    a. After 4 days add 25 μL warm complete media

Notes:

- Method described in Trevigen product literature

APPENDIX N

XENOGRAFT IN NUDE MOUSE

Part 1: Generation of Cell Population

Materials:

- Fresh short hairpin (sh) virus collected day of infection and filter sterilized
  - shNck1
  - shNck2
  - shScramble (shScr)
- CRM-HTB-26
- Puromycin (10 mg/mL stock)
- Hygromycin (100 mg/mL stock)
- Trypsin EDTA
- DPBS
- MDA-MB-231 complete media (10% FBS and 1% v/v penicillin streptomycin)
- MDA-MB-231 freezing media (10% DMSO + 90% FBS)
- Texas A&M Animal Care and Use Committee (AUP 2014-0194)

Procedure:

1. Cells should be infected with freshly prepared, filter sterilized retrovirus
2. The day following virus infection cells should be lifted with trypsin/EDTA and passaged to a 60-millimeter plate
3. Select the shScr population with 1 μg/mL puromycin for two days
4. Select the shNck population with 1 μg/mL puromycin for two days
5. After two days exchange media for fresh complete media
6. Observe growth of shScr until ready to passage to 100-millimeter plate
7. For shNck population allow cells to recover one day then select with 800 μg/mL hygromycin for two days
8. After two days exchange media for fresh complete media
9. Observe growth of shNck until ready to passage to 100-millimeter plate
10. Grow shScr population four days and expand to maximum number of 100-millimeter plates
11. Grow expanded shScr population four days then lift and freeze in MDA-MB-231 freezing media
12. Place in Mr. Frosty™ at -80^{o}C for 24 hours then store in liquid nitrogen until ready to use
13. Grow shNck population for five to seven days and expand to maximum number of 100-millimeter plates
    a. Note after double selection the shNck population grows at a much slower rate than shScr population
14. Grow expanded shNck population five to seven days then lift and freeze in MDA-MB-231 freezing media

15. Place in Mr. Frosty™ at -80^{o}C for 24 hours then store in liquid nitrogen until ready to use

Part 2: Expansion of Cell Population

Materials:

- 150-millimeter tissue culture plates
- MDA-MB-231 complete media (10% FBS and 1% v/v penicillin streptomycin)
- DPBS
- Trypsin EDTA

Procedure:

1. Approximately two weeks prior to experiment start date remove cell populations from liquid nitrogen
2. Thaw and resuspend in MDA-MB-231 complete media
3. Spin cells for 3 minutes at 800 rpm
4. Remove supernatant
5. Resuspend in complete media and plate $100x10^4$ cells in 150-millimeter tissue culture plate
6. Grow cells for five to seven days
    a. Cell population grows slower during first passage out of liquid nitrogen than during normal sub-culture
7. Cells should be passage twice before used for animal experiments
8. Plan to have enough cells for $5x10^6$ cells per mouse
    a. This is more than required but the excess is required due to the syringe used to inject the mice

Part 3: Lifting and Preparing Cell Population for Injection

Materials:

- MDA-MB-231 complete media (10% FBS and 1% v/v penicillin streptomycin)
- DMEM high glucose, plus L-glutamine and phenol red without sodium pyruvate
- DPBS
- Trypsin EDTA
- Growth Factor Reduced Matrigel (BD 9.9 mg/mL)
- 1.5 mL Eppendorf tubes

Procedure:

1. Approximately one hour before injection of MDA-MB-231 cell populations into mice wash 150-millimeter plates containing cell populations twice with 10 mL room temperature DPBS
    a. Aspirate DPBS between washes
2. Aspirate second DPBS wash and add 1.5 mL Trypsin EDTA to 150-millimeter plate
    a. Leave the plate at room temperature for 5 minutes
3. Use complete media to neutralize the trypsin and collect the cells

4. Resuspend the cells well and determine total volume of media
5. Use a small aliquot of cells and trypan blue to count the number of viable cells
6. Determine the total number of cells
7. Based on the total number of cells expressed as number of cells x 10^6 use a multiplication factor of 0.2 to determine the total volume required to resuspend the cells to achieve $2x10^6$ cells per 100 μL of solution
8. Multiple the total volume required by 0.25 to determine the amount of DMEM high glucose, plus L-glutamine and phenol red without sodium pyruvate required
9. Multiple the total volume required by 0.75 to determine the amount of Matrigel required
10. Spin cells 3-8 minutes at 800 rpm depending on the volume of media collected
    a. Small volumes of less than 5 mL can be spun 3 minutes
    b. Large volumes of 50 mL should be spun 8 minutes
11. Aspirate all media off of the cells
12. Place on ice to chill
13. Resuspend in ice cold DMEM high glucose, plus L-glutamine and phenol red without sodium pyruvate and Matrigel in the previously determined volumes
14. Aliquot ~250 μL or more of the cell solution in ice cold 1.5 mL Eppendorf tubes
15. Cells are now ready for transport on ice to animal housing facility

Part 4: Injection of MDA-MB-231 Cells into Mice

Materials:

- Cells prepared for injection in Part 3
- Mice (Jackson Laboratory, stock number 002019, NU/J, 6-9 weeks old, female)
- Chilled syringes (27 gauge)
- Sterile gloves
- Identification tags

Procedure:

1. Chill syringes on ice
2. Load approximately 250 μL of cells in syringe
3. Bilaterally inject 100 μL of cells subcutaneously into the flank
4. Apply identification tag to each mouse as they are injected with cells
5. Keep experimental groups housed in separate cages
    a. Do not exceed the recommended number of mice to be housed per cage

Part 5: Sample Collection and Processing

Materials:

- Calipers
- Dissection supplies – forceps, scalpel, scissors
- Direct-zol™ RNA MiniPrep with TRI-Reagent® kit (Zymo Research R2052)
- iScript™ cDNA Synthesis Kit (Bio-Rad 170-8990)
- Bio-Rad CFX384 Real-Time System

- FastStart Universal SYBR Green Master (Rox) mix (Roche)

Procedure:

1. Tumor volume was assessed weekly using calipers
    a. Volume was calculated as (LxS^2)x0.5 and expressed as mean volume ± SEM as described by Blouw et al. 2015
        i. L = longest measurement
        ii. S = shortest measurement
2. Mice were sacrificed at 9 weeks post injection in accordance with protocols approved by the Texas A&M Animal Care and Use Committee (AUP 2014-0194)
3. Xenograft tumors were removed and weighed prior to sectioning
    a. Sections were snap-frozen in liquid nitrogen and stored at -80^{o}C for DNA/RNA purification or fixed in 4% paraformaldehyde and paraffin embedded for immunohistochemistry
4. Lungs and liver were removed and sectioned
    a. Sections were snap-frozen in liquid nitrogen and stored at -80^{o}C for DNA/RNA purification or fixed in 4% paraformaldehyde and paraffin embedded for immunohistochemistry
5. RNA isolation was performed following the manufacturers protocol using the Direct-zol™ RNA MiniPrep with TRI-Reagent® kit
    a. A small portion of tissue was cut using forceps and a scalpel and placed in 500 µL Tri-Reagent
    b. The tissue was homogenized using an Omni International Tissue Master 125 electric tissue homogenizer
        i. Between each tissue homogenized the probe was washed in a series of 4 – 50 mL Falcon tubes filled with 40 mL ddH_2O
    c. Samples were centrifuged at 12,000 rpm for 1 minute
    d. 100% ethanol was added at a 1:1 ratio and mixed by vortexing
    e. Mixture was loaded on Zymo-Spin™ IIC Column in a collection tube and centrifuged at 12,000 rpm for 30 seconds
    f. Column was transferred to a new collection tube and 400 µL RNA wash buffer was added and centrifuged into the collection tube
    g. Contents of collection tube was poured out and 80 µL of DNase I in DNA digestion buffer was added to the column and incubated for 15 minutes at room temperature
    h. Column was washed twice with 400 µL Direct-zol™ RNA PreWash
    i. A final wash with 700 µL RNA Wash Buffer and centrifuged for 2 minutes
    j. Transfer column to an RNase free tube
    k. Add 40 µL DNase/RNase-Free Water and centrifuge for 30 seconds
    l. Place samples on ice and quantify RNA using NanoDrop 1000
6. Synthesis of cDNA was performed using iScript™ cDNA Synthesis Kit

a. Combine following components in RNase free PCR tube to a final volume of 20 μL
    i. 4 μL 5x iScript advanced reaction mix
    ii. 1 μL iScript advanced reverse transcriptase
    iii. 2 μg RNA template
    iv. Nuclease-free water to 20 μL
b. Use the following protocol in a thermal cycler
    i. 5 minutes at 25°C
    ii. 30 minutes at 42°C
    iii. 5 minutes at 85°C
    iv. ∞ at 4°C
c. Either store cDNA at -20°C or use immediately for real-time PCR

7. Real-time PCR reactions were performed using FastStart Universal SYBR Green Master (Rox) mix (Roche)
    a. Primers for determining lung metastasis
        i. Human GAPDH Forward
            1. 5'-CCA GGT GGT CTC CTC TGA CTT C-3'
        ii. Human GAPDH Reverse
            1. 5'-CCA GGT GGT GAG GGC AAT G-3'
    b. Primers for normalization
        i. β-actin Forward
            1. 5'-GTT TGA GAC CTT CAA CAC CCC-3'
        ii. β-actin Reverse
            1. 5'- GTG GCC ATC TCT TGC TCG AAG TC-3'
    c. Program used for RT-PCR on Bio-Rad CFX384 Real-Time System
        i. 95°C for 10 minutes
        ii. 95°C for 15 seconds
        iii. 60°C for 1 minute
        iv. Plate read
        v. Repeat ii. to iv. 39 times
        vi. 95°C for 10 seconds
        vii. Melt curve 65°C to 95°C – Increment 0.5°C for 5 seconds + Read
        viii. End
    d. Real-time PCR data were analyzed by the $\Delta\Delta C_T$ method

APPENDIX O

TOTAL INTERNAL REFLECTION FLUORESCENCE (TIRF) MICROSCOPY OF MMP14

Materials:

- MDA-MB-231 stably expressing:
  - Scrambled shRNA plus pMSCV LifeAct-EYFP
  - Nck1 and Nck2 shRNA plus pMSCV Life-Act EYFP
- Lipofectamine 2000
- pcDNA3.1 MT1-MMP mCherry
- MDA-MB-231 complete media (10% FBS and 1% v/v penicillin streptomycin)
- DPBS (HyClone, ThermoScientific)
- Live Cell Imaging Media (Phenol-red free DMEM High Glucose supplemented with 10% FBS, 1% Pen/Strep and 25 mM HEPES)
- 35-millimeter glass bottom MatTek dishes (MatTek Corporation, Ashland, MA)
- Fibronectin (10 μg/mL in DPBS)
- Zeiss Axio Observer Z1 TIRF 3 microscope, equipped with a plan-apochromat 100X/1.46NA oil objective and a Roper S/W PVCAM

Procedure:

1. Three days prior to imaging plate $20x10^4$ cells in a 35-millimeter tissue culture plate for Lipofectamine 2000 transfection
2. Two days prior to imaging transfect 2 μg pcDNA3.1 MT1-MMP mCherry using 5 μL Lipofectamine 2000 (see Appendix J)
3. One day prior to imaging:
   a. Coat MatTek dishes with 10 μg fibronectin (use 1 mL of 10 μg/mL fibronectin in DPBS for one hour at room temperature
   b. After one hour aspirate excess DPBS and add 200 μL live cell imaging media to the glass portion of the MatTek for 15 minutes and place in $37^oC/5\%$ CO_2 incubator
   c. Lift cells using 350 μL Trypsin/EDTA for 5 minutes at room temperature
   d. Collect cells in 15 mL Falcon tube and spin for 3 minutes at 800 rpm
   e. Re-suspend cells in 250 μL of Live Cell Imaging Media
   f. Count cells using hemocytometer
   g. Make dilutions of $4x10^4$ cells in 200 μL Live Cell Imaging Media
   h. Remove fibronectin coated plates from incubator and aspirate media
   i. Add $4x10^4$ cells in 200 μL to each fibronectin coated plate and place in $37^oC/5\%$ CO_2 incubator for one hour to allow cells to adhere
   j. After one hour add 2 mL imaging media to each plate and incubate for approximately 20 hours prior to imaging
4. Day of imaging

a. Exchange media with 2 mL fresh Live Cell Imaging Media 1 hour prior to imaging
b. Place plate on stage and allow >15 minutes for equilibration
c. Images of EYFP/mCherry were captured every 3 seconds for 5 minutes
    i. Laser power: 5% 488nm/exposure 100 ms; 1 % 561 nm/exposure 100 ms

APPENDIX P

RETROVIRUS PREPARATION

Materials:

- 293T (Human Embryonic Kidney Cells ATCC® CRL-3216™)
- 293T complete media (HyClone DMEM/High Glucose catalog number SH30243.01 plus 10% FBS and 1% v/v penicillin streptomycin)
- Retroviral DNA Plasmid (Store at -20°C)
    - pMSCV
    - pSuper
- pHCMV-G plasmid (Store at -20°C)
- pMD.Gag.pol plasmid (Store at -20°C)
- 2 M $CaCl_2$ (Store at -20°C)
- 2X Transfection Buffer (Store at -20°C)
- 50 mM Chloroquine (Store at -20°C)
- Syringe filter (PVDF 0.22 μm 30 mm diameter Denville F5508)
- 1.5 mL Eppendorf tubes

Procedure:

1. One day prior to virus production sub-culture 293T cells to achieve 80% confluence the following day
    a. 60-millimeter plate – approximately 300-350x10^4 cells
    b. 100-millimeter plate – approximately 900-950x10^4 cells
2. Day of virus production add Chloroquine to 293T cells with a final concentration of 25 μM just prior to transfection
    a. 60-millimeter plate – 2.5 μL in 5 mL 293T growth media
    b. 100-millimeter plate – 5 μL in 10 mL 293T growth media
3. In a sterile polypropylene tube combine
    a. Sterile water
        i. 60-millimeter plate – Adjust so final volume is 250 μL
        ii. 100-millimeter plate – Adjust so final volume is 500 μL
    b. Plasmid DNA
        i. Retroviral DNA Plasmid
            1. 60-millimeter plate – 12 μg
            2. 100-millimeter plate – 24 μg
        ii. pMD.Gag.pol plasmid
            1. 60-millimeter plate – 6 μg
            2. 100-millimeter plate – 12 μg
        iii. pHCMV-G plasmid
            1. 60-millimeter plate – 2 μg
            2. 100-millimeter plate – 4 μg

c. 2 M $CaCl_2$
    i. 60-millimeter plate – 62.5 μL
    ii. 100-millimeter plate – 125 μL
4. Once components from Step 3 have been combined in a polypropylene tube add 2X Transfection Buffer – MUST BE ADDED DROPWISE WHILE VORTEXING
    a. Pre-warm solution to 37°C
    b. 60-millimeter plate – 250 μL
    c. 100-millimeter plate – 500 μL
5. Add entire mixture dropwise over the entire plate of 293T cells with chloroquine
6. Gently swirl the plate and immediately place in 37°C/5% CO_2/humidified incubator
7. After 4-6 hours exchange media with fresh complete media and place back in 37°C/5% CO_2/humidified incubator for 20 hours
    a. 60-millimeter plate – 2 mL
    b. 100-millimeter plate – 5 mL
8. After 20 hours collect media with virus and replace media
    a. 60-millimeter plate – 2 mL
    b. 100-millimeter plate – 5 mL
9. After 8 hours collect media with virus
    a. 60-millimeter plate – 2 mL
    b. 100-millimeter plate – 5 mL
10. Virus can be used immediately after filter sterilization using a 0.22 μm syringe filter
    a. Immediate use provides highest viral titer
11. Virus can be stored at -80°C after centrifugation at 4000 rpm for 5 minutes
12. After centrifugation store 1 mL aliquots in 1.5 mL Eppendorf tubes
13. Place in -80°C and leave until ready to use
    a. Viral titer decreases with freeze/thaw cycle
    b. Once thawed the aliquot should be used or discarded

Notes:

- 2X transfection buffer: 6.5 g HEPES, 8.0 g NaCl, 0.105 g Na2HPO4 in 500 mL H2O; pH solution to 7.05

APPENDIX Q

RETROVIRUS INFECTION

Materials:

- Retrovirus
- MDA-MB-231 complete media (10% FBS and 1% v/v penicillin streptomycin)
- Polybrene (4 mg/mL stock, store at -20^{o}C)

Procedure:

1. Sub-culture MDA-MB-231 cells one day prior to retrovirus infection
    a. 35-millimeter plate –10x10^{4} cells in 2 mL complete media
2. Add 8 μg/mL polybrene to each tube of virus and vortex briefly
    a. Rapidly thaw frozen aliquots of retrovirus prior to addition of polybrene
    b. Polybrene should be added immediately to fresh virus
3. Aspirate media from cells and add retrovirus/polybrene mixture to begin infection
4. Incubate cells for 4 hours
    a. If a double infection is required repeat steps 2-4 after first retrovirus has been incubated for 4 hours
5. After infection aspirate media and replace with fresh complete media
6. Grow cells overnight then sub-culture
    a. Antibiotic selection can be performed with sub-culture of cells

APPENDIX R

IMMUNOFLUORESCENCE LABELING MEMBRANE MMP14

Part 1: Cell Preparation and Immunofluorescence Staining

Materials:

- MDA-MB-231 complete media (10% FBS and 1% v/v penicillin streptomycin)
- DPBS (HyClone, ThermoScientific)
- NucBlue® Live ReadyProbes™ Reagent (Molecular Probes)
- Human serum (Jackson ImmunoResearch, 009-000-121)
- Goat serum (Sigma G9023-10 mL)
- Syringe filter (MillexGV 0.22 μm Durapore PVDF – Millipore)
- Anti-MMP14 antibody (Millipore MAB3328)
- Goat anti-mouse IgG 488 (Invitrogen A11029)
- Parafilm
- Tween-20
- Prolong Gold (Invitrogen P36934)

Procedure:

1. 48 hours after time 0 siRNA Treatment – lift and re-plate cells on poly-L-lysine coated coverslips ($40x10^4$ cells per mL)
2. Add 1000 μL fresh complete media to coverslip, allow surface tension to hold in place
3. Add 1000 μL cells dropwise to distribute evenly over coverslip
4. 72 hours after time 0 siRNA treatment – add NucBlue® Live ReadyProbes™ Reagent to media 20 minutes prior to wash and fixation - check that cells are ~70-80% confluent – aspirate media and wash 2 times with room temperature DPBS
5. Fix for 15 minutes with 3.7% paraformaldehyde in DPBS (750 μL/coverslip)
6. Prepare humidified chamber–150-millimeter plate lined with Whatman paper soaked in ddH_2O –place parafilm on top of Whatman paper for incubations
7. Wash cells 2 times for 5 minutes each with 2 mL room temperature DPBS (DPBS washed coverslips dry out quickly, act accordingly)
8. Block for 1 hour at room temperature in 100 μL 2.5% human serum and 5% goat serum in DPBS
9. Incubate cells with primary antibody diluted in blocking solution (1:100) for 1 hour at room temperature (primary antibody: mouse anti- MMP14)
10. Spin antibody in blocking solution prior to use: 12,000 rpm for 5 minutes (http://www.cbi.pitt.edu/protocols/cellimuno.htm)
11. Drain excess fluid from coverslip without allowing it to dry
12. Place a 100 μl drop on parafilm and place the coverslip cell side down on top of the drop

13. In a new 12 well plate wash 3 times with 2 mL/well DPBS for 10 minutes at room temperature protected from light
14. Incubate cells for 1 hour at room temperature with fluorescent goat anti-mouse IgG 488 diluted in blocking solution (1:500)
15. Spin antibody in blocking solution prior to use: 12,000 rpm for 5 minutes
16. Drain excess fluid from coverslip without allowing it to dry
17. Place a 100 µl drop on parafilm and place the coverslip cell side down on top of the drop
18. Store in dark location for incubation
19. Wash 2 times with 2 mL/well 0.05% Tween-20 in DPBS in 12-well plate for 10 minutes at room temperature
20. Wash 1 time with 2 mL/well DPBS in 12-well plate for 10 minutes at room temperature
21. Just before mounting in Prolong Gold dip coverslip in sterile filtered ddH2O then drain excess fluid
22. Mount in small drop (5-10 µL) Prolong Gold (avoid bubbles-if they form leave them alone, attempting to remove will potentially ruin any usable portions of the slide) on a clean glass slide, then store in the dark at room temperature for 24 hours to allow solution to cure
23. Optional: Seal with finger nail polish around the edges of the coverslips
24. Image using LSM510 confocal microscope
    a. Ensure z-stack includes all signal from ventral to apical surface of the cells

Part 2: Image Processing and Analysis Using ImageJ Software

Images were collected with a Plan-Neofluor 40X/1.3NA oil objective using a Zeiss LSM510 confocal microscope. Stack depths were varied to collect the entire depth of the cell starting below the ventral surface of the cell through the top of the cell. There were instances when cells would stack and greater than 20 slices would be taken, in addition, there are some cells where the very top of the cell is not collected due to stacking. During image analysis these regions were excluded from the analysis

Procedure:

1. Open Image: Image→Color→Split Image
2. DIC Stack – Find membrane focal plane
    c. Duplicate focal plane only and close DIC Stack
    d. Save in data analysis working folder
    e. Auto adjust brightness and contrast
    f. Outline cell and add to ROI manager
        i. Save all ROI as an ROI set in working folder
3. MMP14 Labeled Channel – Image→Stacks→Z-project (Sum of Slices)
    b. Use rectangle tool to select a region with no cells or membrane and take a measurement

c. Use the mean from this measurement to subtract the background from the image
    i. Process→Math→Subtract
d. Save image in data analysis working folder after subtracting the background
e. Take measurement for each ROI generated from the DIC image above
    i. Save measurements in an excel file for analysis using excel or Minitab

Notes:

- Filter sterilize all solutions using MillexGV 0.22 μm Durapore PVDF filter to remove any particulates that may interfere with imaging or image analysis
- Protocol adapted from:
    - Wiesner C, Faix J, Himmel M, Bentzien F, Linder S. KIF5B and KIF3A/KIF3B kinesins drive MT1-MMP surface exposure, CD44 shedding, and extracellular matrix degradation in primary macrophages. Blood. 2010;116(9):1559-69
    - Hagedorn M, Neuhaus EM, Soldati T. Optimized fixation and immunofluorescence staining methods for Dictyostelium cells. Methods in Molecular Biology. 2006;346:327-38.

APPENDIX S

PSUPER SHRNA PLASMID CONSTRUCTION

Materials:

- Forward custom oligo (100 μM in nuclease free water)
- Reverse custom oligo (100 μM in nuclease free water)
- pSUPER.retro.puro (pSUPER RNAi System™ - original format)
- Autoclaved ddH_2O (H_2O)
- 10X Ligase Buffer (Promega T4 DNA Ligase Buffer 10X C126A 27464315)
- PCR machine
- Hind III restriction enzyme (NEB)
- Bgl II restriction enzyme (NEB)
- QIAquick Gel Extraction Kit (28704)
- QIAprep Spin Miniprep Kit (27104)
- NanoDrop 1000 spectrophotometer
- Competent DH5α
- LB Agar
- LB Broth

Procedure:

1. Anneal oligonucleotides

H_2O	41.1 μL
Forward oligo	1.5 μL (100 μM)
Reverse oligo	1.5 μL (100 μM)
10X Ligase Buffer	4.9 μL
Total	49 μL

   a. Use PCR machine: set-up reaction as follows – incubate at 94°C for 4 minutes → 80°C for 4 minutes → 75°C for 4 minutes → 70°C for 10 minutes → 60°C for 4 minutes → 50°C for 10 minutes → 37°C for 20 minutes → 10°C for 10 minutes and finish the run at 4°C for infinity → product is ready for ligation

2. Linearize vector by restriction enzyme digestion
   a. Hind III & Bgl II RE digestion in sequential reaction step:

H_2O	15.8 μL
10X buffer 2	2.0 μL
100X BSA	0.2 μL
pSUPER.retro.puro	1.0 μL (1 μg)
Hind III RE	1.0 μL

Total ---------- 20 µL

b. Incubate at 37°C for 60 minutes
c. Add 2 µl 10X buffer 3.1 and 1.0 µl Bgl II
d. Incubate at 37°C for 2 hours
e. Confirm digestion of pSUPER.retro.puro by gel electrophoresis on 1% agarose gel
    i. Add 4 µL 5X gel loading dye and run whole digested product
    ii. Run circular vector as control
    iii. Purify gel using QIAquick gel extraction kit
    iv. Quantify linear vector using NanoDrop spectrophotometer

3. Ligation of annealed oligonucleotides to linearized vector using NEB quick ligation protocol (M2200)
    a. Combine 50 ng of pSUPER.retro.puro with a 3-fold molar excess of annealed oligonucleotides
        i. NEBioCalculator can be used to calculate molar ratios
        ii. Adjust volume to 10 µl with H_2O
    b. Add 10 µl of 2X Quick Ligation Buffer and mix
    c. Add 1 µl of Quick T4 DNA Ligase and mix thoroughly
    d. Centrifuge briefly and incubate at room temperature (25°C) for 5 minutes
    e. Chill on ice, then transform or store at -20°C
    f. Do not heat inactivate
        i. Heat inactivation dramatically reduces transformation efficiency
4. Reduce background transformants by Bgl II digestion
    a. Vector that contain an insert lack a Bgl II digestion site and will remain intact while vector that lack an insert will be linearized

    Ligated pSUPER.retro.puro vector ---------- 20 µl (From the previous step)
    10X Buffer 3.1 ---------- 2.0 µl
    Bgl II restriction enzyme ---------- 1.0 µl
    Total ---------- 23 µl

    b. Incubate at 37°C for 1 hour (digestion)
    c. Chill on ice
    d. Add 5 µL of reaction to competent DH5α
5. Transformation of competent DH5α
    a. Add 5 µL of product from previous step to 50 µL of competent DH5α
        i. Competent cells should be stored at -80°C
        ii. When handling competent cells ensure they are kept on ice at all times unless indicated for transformation
        iii. Do not pipet competent cells to mix instead use the tip of the pipet to mix the insert and the vector or gently flick the tube

iv. Include two controls
    1. Untransformed DH5α without any insert
    2. DH5α transformed with control vector that underwent all procedures as target vector with the exception that the oligonucleotide insert was not included

b. Incubate mixture on ice of 10 minutes
c. Incubate at 42°C for 30 seconds
d. Immediately place back on ice and incubate for 10 minutes
e. Add 1 mL 37°C LB media without antibiotics and incubate at 37°C in a shaking incubator for 1 hour
f. Pellet cells by spinning at 13,200 rpm for 1 minute
g. Remove supernatant
h. Re-suspend cells in approximately 100 μL of LB
i. Pipet cells onto an LB agar plate with ampicillin (100 μg/mL)
j. Use a glass rod or sterile loop to spread cells well enough to get single colonies
    i. Spread until LB no longer appears wet on the surface of the agar
k. Grow at 37°C overnight

6. Screening transformed DH5α colonies
    a. The untransformed control plate of DH5a should have no colonies
    b. The control vector without insert should have very few colonies or no colonies
    c. The target vector should have multiple colonies to select
        i. The target vector should have at least four times more colonies than the control vector without an insert prior to proceeding with screening
    d. Select individual colonies and grow them overnight in 5 mL LB broth with 100 μg/mL ampicillin
    e. Isolate plasmid DNA using QIAprep Spin Miniprep Kit
    f. Analyze insert by restriction digestion with Bgl II
        i. Uncut plasmid remains supercoiled and will run further down the gel than plasmids with inserts
    g. Once candidates have been identified with restriction digestion, orientation and sequence of inserts should be confirmed by sequencing
        i. Sequencing primers for pSUPER.retro.puro
            1. pMSCV Fwd – 5' –CCC TTG AAC CTC CTC GTT CGA CC– 3'
            2. pMSCV Rvs – 5' –GAG ACG TGC TAC TTC CAT TTG TC– 3'
    h. Upon confirmation of correct sequence and orientation of insert in vector additional plasmid should be produced for use in transfection of mammalian cells

        i. Confirmation of an effective insert is accomplished with biochemical screening in the target cell line
            i. RT-PCR or western blot of target product should show greater than 60% silencing of the target mRNA or protein over a control sample
7. Retrovirus should be produced using pSUPER.retro.puro according to Appendix P retrovirus preparation

Notes:

- Manufacturer's (Oligoengine) protocol was used with modifications

APPENDIX T

RAICHU CDC42 FÖRSTER RESONANCE ENERGY TRANSFER

Materials:

- MDA-MB-231 stably expressing:
  - Scrambled shRNA plus Raichu Cdc42 Förster resonance energy transfer (FRET) probe
  - Nck1 and Nck2 shRNA plus Raichu Cdc42 Förster resonance energy transfer (FRET) probe
- MDA-MB-231 complete media (10% FBS and 1% v/v penicillin streptomycin)
- DPBS (HyClone, ThermoScientific)
- Live Cell Imaging Media (Phenol-red free DMEM High Glucose supplemented with 10% FBS, 1% Pen/Strep and 25 mM HEPES)
- 35-millimeter glass bottom MatTek dishes (MatTek Corporation, Ashland, MA)
- Fibronectin (10 μg/mL in DPBS)
- Zeiss LSM780 Confocal Microscope Plan-Apo 40X/1.40NA oil objective

Procedure:

1. Two days prior to imaging plate $10x10^4$ cells in a 60-millimeter tissue culture plate to synchronize growth at low density
2. One day prior to imaging:
   a. Coat MatTek dishes with 10 μg fibronectin (use 1 mL of 10 μg/mL fibronectin in DPBS for one hour at room temperature)
   b. After one hour aspirate excess DPBS and add 200 μL live cell imaging media to the glass portion of the MatTek for 15 minutes and place in $37^oC/5\%$ CO_2 incubator
   c. Lift cells using 350 μL Trypsin/EDTA for 5 minutes at room temperature
   d. Collect cells in 15 mL Falcon tube and spin for 3 minutes at 800 rpm
   e. Re-suspend cells in 250 μL of Live Cell Imaging Media
   f. Count cells using hemocytometer
   g. Make dilutions of $4x10^4$ cells in 200 μL Live Cell Imaging Media
   h. Remove fibronectin coated plates from incubator and aspirate media
   i. Add $4x10^4$ cells in 200 μL to each fibronectin coated plate and place in $37^oC/5\%$ CO_2 incubator for one hour to allow cells to adhere
   j. After one hour add 2 mL imaging media to each plate and incubate for approximately 20 hours prior to imaging
3. Day of imaging
   a. Place plate on stage and allow 5 to 15 minutes for equilibration
   b. Images of CFP/FRET/YFP were captured every minute for 1 hour
4. Data analysis
   a. Process CFP channel stack and FRET channel stack using a 3x3 median filter

b. Use the median filtered stacks to create a ratio stack of the FRET channel divided by the CFP channel
c. Limit analysis area to individual cells using regions of interest
d. Average the FRET ratio over one hour for each cell

APPENDIX U

MAMMALIAN CELL STABLE PLASMID TRANSFECTION

Materials:

- MDA-MB-231 complete media (10% FBS and 1% v/v penicillin streptomycin)
- MDA-MB-231 complete media without antibiotic (10% FBS)
- Lipofectamine® 2000 Transfection Reagent (Life Technologies Catalog Number: 50470)
- Opti-MEM® Reduced Serum Medium (Life Technologies Catalog Number: 31985-062)
- Plasmid DNA
- 1.5 mL Eppendorf Tubes
- Geneticin

Procedure:

Day 1

1. Plate $20x10^4$ MDA-MB-231 cells with complete media in a 35-millimeter dish and place in a 37°C incubator with 5% CO_2

Day 2

2. Label two Eppendorf tubes and add 250 μL of Opti-MEM media to each tube
    a. Tube 1 - Plasmid DNA
    b. Tube 2 - Lipofectamine 2000
3. Add 2 μg plasmid DNA to tube 1 and mix well by gently pipetting up and down
4. Add 5 μL of Lipofectamine 2000 reagent to tube 2 and mix well by gently pipetting up and down
5. Incubate at room temperature for 5 minutes
6. After 5 minutes take entire volume from Tube 2 and add it to Tube 1
7. Mix well by gently pipetting up and down then incubate at room temperature 20-30 minutes
8. Add 500 μL antibiotic free complete media to the transfection reagent plasmid mixture in Tube 1
9. Remove complete from cells and add entire contents of Tube 1 to the plate then place back in 37°C incubator
10. After one hour replace media with fresh antibiotic free complete media
11. After an additional four hours the media can be replaced with complete media containing antibiotic
12. Grow cells overnight then lift and re-plate with fresh complete media
13. Grow cells for 48 hours
14. After 48 hours lift and re-plate cells in complete media with 800 μg/mL Geneticin
15. During selection process cells were passed as required
16. Cells were selected for 14 days with 800 μg/mL Geneticin

17. Cells were then expanded for 7 days in 500 μg/mL Geneticin
18. After expansion cells were frozen in liquid nitrogen

Notes:

- Adapted from manufacturer's protocol (Life Technologies) for Lipofectamine 2000 and selection conditions adapted from Yu et al. 2012